(12) INTERNATIONAL APPLICATION PUBLISHED UNDER THE PATENT COOPERATION TREATY (PCT)

(19) World Intellectual Property Organization
International Bureau

(43) International Publication Date
07 November 2024 (07.11.2024)

WIPO | PCT

(10) International Publication Number
WO 2024/228904 A2

(51) International Patent Classification:
A61K 39/395 (2006.01) *A61K 35/74* (2015.01)

(21) International Application Number:
PCT/US2024/026253

(22) International Filing Date:
25 April 2024 (25.04.2024)

(25) Filing Language: English

(26) Publication Language: English

(30) Priority Data:
63/499,335 01 May 2023 (01.05.2023) US

(71) Applicant: **WISCONSIN ALUMNI RESEARCH FOUNDATION** [US/US]; 614 Walnut Street, 13th Floor, Madison, Wisconsin 53726 (US).

(72) Inventors: **HU, Quanyin**; 777 Highland Avenue, Rennebohm Hall, Madison, Wisconsin 53705 (US). **LI, Zhaoting**; 919 Eagle Heights, Apartment F, Madison, Wisconsin 53705 (US).

(74) Agent: **LECUYER, Karen A.** et al.; 25 W. Main Street, Suite 800, Madison, Wisconsin 53703 (US).

(81) Designated States *(unless otherwise indicated, for every kind of national protection available)*: AE, AG, AL, AM, AO, AT, AU, AZ, BA, BB, BG, BH, BN, BR, BW, BY, BZ, CA, CH, CL, CN, CO, CR, CU, CV, CZ, DE, DJ, DK, DM, DO, DZ, EC, EE, EG, ES, FI, GB, GD, GE, GH, GM, GT, HN, HR, HU, ID, IL, IN, IQ, IR, IS, IT, JM, JO, JP, KE, KG, KH, KN, KP, KR, KW, KZ, LA, LC, LK, LR, LS, LU, LY, MA, MD, MG, MK, MN, MU, MW, MX, MY, MZ, NA, NG, NI, NO, NZ, OM, PA, PE, PG, PH, PL, PT, QA, RO, RS, RU, RW, SA, SC, SD, SE, SG, SK, SL, ST, SV, SY, TH, TJ, TM, TN, TR, TT, TZ, UA, UG, US, UZ, VC, VN, WS, ZA, ZM, ZW.

(84) Designated States *(unless otherwise indicated, for every kind of regional protection available)*: ARIPO (BW, CV, GH, GM, KE, LR, LS, MW, MZ, NA, RW, SC, SD, SL, ST, SZ, TZ, UG, ZM, ZW), Eurasian (AM, AZ, BY, KG, KZ, RU, TJ, TM), European (AL, AT, BE, BG, CH, CY, CZ, DE, DK, EE, ES, FI, FR, GB, GR, HR, HU, IE, IS, IT, LT, LU, LV, MC, ME, MK, MT, NL, NO, PL, PT, RO, RS, SE, SI, SK, SM, TR), OAPI (BF, BJ, CF, CG, CI, CM, GA, GN, GQ, GW, KM, ML, MR, NE, SN, TD, TG).

Published:
— *without international search report and to be republished upon receipt of that report (Rule 48.2(g))*

WO 2024/228904 A2

(54) Title: COMPOSITIONS AND METHODS TO ENHANCE IMMUNE CHECKPOINT BLOCKADE THERAPY AGAINST HYPOXIC TUMORS

(57) Abstract: Described herein a drug delivery system including protein nanocages, the protein nanocages including collagenase proteins and anti-immune checkpoint inhibitor antibodies. The protein nanocages are conjugated to the surface of a probiotic bacterial carrier. Also described are pharmaceutical compositions including the drug delivery system, methods of making the drug delivery system, and methods of treating a patient with a hypoxic tumor characterized by oncogenic collagen by systemically administering to the patient the composition described above.

COMPOSITIONS AND METHODS TO ENHANCE IMMUNE CHECKPOINT BLOCKADE THERAPY AGAINST HYPOXIC TUMORS

CROSS-REFERENCE TO RELATED APPLICATIONS

This application claims priority to U.S. Provisional Application 63/499,335 filed on May 1, 2023, which is incorporated herein by reference in its entirety.

FIELD OF THE DISCLOSURE

[0001] The present disclosure is related to drug delivery systems for immune checkpoint inhibitors and methods of treating hypoxic tumors.

BACKGROUND

[0002] Pancreatic Ductal Adenocarcinoma (PDAC) is an extremely aggressive gastrointestinal malignancy with less than 6% of patients surviving beyond 5 years. Since less than 20% of PDAC patients can be treated with surgery, chemotherapy is still the standard care for non-surgical patients in the clinic. However, the treatment efficacy of current therapeutics in PDAC is low, and the prognosis of PDAC patients remains dismal due to frequent relapse and metastasis, and high resistance to chemotherapy. Recently, immunotherapy represented by immune checkpoint blockade (ICB) has achieved great success in treating patients with various malignancies and holds promise for the treatment of PDAC. However, the application of immunotherapy for PDAC remains challenging due to the low tumor infiltration of effector T cells that can be re-activated by blocking PD1/PD-L1 pathway. Additional limitations for developing an effective PDAC immunotherapy strategy are a consequence of prominent features of the PDAC tumor microenvironment (TME), both that PDAC is highly desmoplastic and that PDAC is characterized by enriched immunosuppressive cells.

[0003] PDAC is characterized by extremely dense extracellular matrix (ECM) deposition surrounding cancer cells resulting from the desmoplastic reaction. This desmoplasia has been recognized as one of the key factors in initiating and facilitating cancer progression and metastasis, contributing to PDAC biological aggressiveness and treatment resistance. As a hallmark of the PDAC TME, abundant ECM composed of collagen, stroma, and fibronectin results in a high interstitial pressure in PDAC, which could form a compact barrier to impede the permeation of therapeutics toward tumor parenchyma, resulting in dismal treatment outcomes of chemotherapy and immunotherapy in the clinic. Among all the

ECM components, oncogenic collagen has been recently reported to play a significant role in promoting an immunosuppressive TME and inhibiting ICB efficacy. Oncogenic collagen is produced by epigenetic hypermethylation of cancer cells that have silenced the α2 gene, resulting in cancer-specific collagen "homotrimers", consisting of three α1 chains. This oncogenic collagen could attach to the surface of tumor cells and activate downstream FAK/MAPK/AKT signaling by interacting with the integrin α3β1 receptor. Consequently, the activation of FAK promotes the secretion of immunosuppressive factors such as TGFβ and increases the infiltration of immunosuppressive cells such as T regulator cells (Tregs) and myeloid-derived suppressor cells (MDSCs), thereby limiting the activation of CD8 T cells and creating an immunosuppressive environment. Moreover, the activation of MAPK/AKT signaling pathway promotes the proliferation and therapeutic resistance of tumor cells.

[0004] Given the importance of oncogenic collagen in facilitating PDAC carcinogenesis and reducing responses to therapies, regulating its expression could be vital to increase therapeutic efficacy and improve PDAC treatment outcomes. However, current collagen regulation strategies mainly focus on degrading collagen generated by fibroblasts, and little has been reported on targeting oncogenic collagen. One of the major reasons accounting for the difficulty in targeting oncogenic collagen is the limited penetration capability of current drug delivery systems caused by the dense ECM and high interstitial fluid pressure; therefore, these barriers prevent access of collagen-degrading agents to tumor parenchyma and PDAC cells in which the oncogenic collagen is secreted.

[0005] What is needed are novel drug delivery systems to target oncogenic collagen and allow for penetration of anti-cancer agents to treat PDAC and other cancers characterized by oncogenic collagen.

BRIEF SUMMARY

[0006] In an aspect, a drug delivery system comprises protein nanocages comprising collagenase proteins and anti-immune checkpoint inhibitor antibodies, wherein the protein nanocages are conjugated to the surface of a probiotic bacterial carrier.

[0007] In another aspect, a pharmaceutical composition comprises the drug delivery system described above.

[0008] In yet another aspect, a method of making a drug delivery system, comprises preparing protein nanocages by contacting collagenase proteins, anti-immune checkpoint inhibitor antibodies, and a bifunctional linker in a solvent for a time and temperature to

provide the protein nanocages having diameters of 90 to 300 nm; and contacting the protein nanocages with probiotic bacteria in the presence of a crosslinking agent to conjugate the protein nanocages to the surface of the probiotic bacteria.

[0009] In a further aspect, a method of treating a patient with a hypoxic tumor characterized by oncogenic collagen comprises systemically administering to the patient the composition described above.

BRIEF DESCRIPTION OF THE DRAWINGS

[0010] FIGs. 1a-j illustrate the bioinformatic analysis of oncogenic collagen in patient data and schematic illustration of the therapeutic strategy. 1a. Schematic illustration of the clinical data analysis and sample collection and preparation from human PDAC patients. 1b. Clinical data analysis of the integrin α3 expression in the pancreatic tumor tissue and normal tissue. 1c. Disease-free survival of clinical pancreatic patients correlated with integrin α3 expression level. 1d. The correlation analysis between COL1A1 and integrin α3. 1e. Clinical data analysis of the integrin β1 expression in the pancreatic tumor tissue and normal tissue. 1f. Disease-free survival of clinical pancreatic patients correlated with integrin β1 expression level. 1g. The correlation analysis between COL1A1 and integrin β1. 1h. Immune fluorescence assay of oncogenic collagen expression in human pancreatic tumor tissues (Nucleus stained with Hoechst-Blue, tumor cells stained with anti-EpCAM-Green, oncogenic collagen stained with anti-COL1A1-Red). 1i. Immune fluorescence assay of the oncogenic collagen interacting with integrin α3 in human pancreatic tumor tissues (Nucleus stained with Hoechst-Blue, integrin α3 stained with anti-integrin α3-Green, oncogenic collagen stained with anti-COL1A1-Red). 1j. Schematic illustration of Col/aPD-L1@ECN enhancing the anti-PD-L1 immunotherapy by blocking integrin α3-FAK signaling pathway. Col/aPD-L1@ECN penetrates through the ECM barriers and targets the tumor parenchyma because of the hypoxia tropism and superior motility of EcN. Under the trigger of ROS, collagenases were released to degrade the oncogenic collagen and block the interaction of oncogenic collagen with integrin α3β1 receptors on the tumor cells, thus inhibiting the activation of downstream FAK, AKT and MAPK signaling pathway to reduce the immunosuppression and tumor proliferation and cooperate with ICB therapy.

[0011] FIG. 2 shows a bioinformatic analysis of the COL1A1 expression in pancreatic tumor tissues and normal tissues.

[0012] FIG. 3 shows Disease-Free Survival of pancreatic cancer patients with low COL1A1 expression and high COL1A1 expression.

[0013] FIG. 4 shows a correlation analysis between integrin β1 (ITGβ1) and integrin α3 (ITG α3) in pancreatic cancer.

[0014] FIG. 5 shows a Western blot assay of the COL1A1 expression in the pancreatic cancer tissues from PDAC patients.

[0015] FIG. 6 shows a Western blot assay of the Integrin α3 expression in the pancreatic cancer tissues from PDAC patients.

[0016] FIG. 7 shows a Western blot assay of the Integrin β1 expression in the pancreatic cancer tissues from PDAC patients.

[0017] FIG. 8 shows an immune fluorescence assay of the interaction between COL1A1 and integrin β1 in the pancreatic cancer tissues from PDAC patients (scale bar = 100 μm).

[0018] FIGs. 9a-g illustrate the preparation and characterization of Col/aPD-L1@ECN. 9a. Schematic illustration of the preparation of aPD-L1/Col protein cage and the Col/aPD-L1@ECN. 9b. Particle size and representative TEM image of the Col/aPD-L1 protein cages (scale bar = 100 nm). 9c. Zeta potential of different protein cages. Data are presented as mean ± s.d. (n = 3 biologically independent samples). 9d. Representative TEM image of Col/aPD-L1@ECN (scale bar = 1 μm). 9e. Flow cytometry assay of Col/aPD-L1@ECN. aPD-L1 was labeled with FITC, and collagenase was labeled with Rhodamine B. 9f. Confocal assay of the protein cage conjugation on ECN (scale bar = 2 μm). aPD-L1 was labeled with FITC, and collagenase was labeled with Rhodamine B. 9g. Cumulative release of aPD-L1 at determined time points with or without H_2O_2 (0.5 mM) treatment. Data are presented as mean ± s.d. (n = 3 biologically independent samples).

[0019] FIGs. 10a-i show the motility and tumor penetration ability of Col/aPD-L1@ECN. 10a. Schematic illustration of the bacteria migration assay. Col/aPD-L1@ECN was loaded in the alginate scaffold at 0 h, and the migration of Col/aPD-L1@ECN toward the Matrigel-based tissue mimicking gel was observed by confocal microscopy. 10b. Representative images of bacteria migration toward the tissue mimicking gel at selective time points (0 h and 4 h, scale bar = 100 μm). 10c. Schematic illustration of the transwell invasion assay to evaluate the motility of ECN and Col/aPD-L1@ECN. 10d. Percentage of the bacteria penetrated into the lower chamber in the transwell invasion assay. Data are presented as mean ± s.d. (n = 3 biologically independent samples) and analyzed with unpaired t-test, $P^{ns} = 0.6982$. 10e. Representative images of the *in vivo* IVIS® imaging for the biodistribution of the Col/aPD-L1@ECN (labeled with Cy5.5) at 72 h. The white circle indicates the location of orthotopic pancreatic cancer. 10f. *Ex vivo* IVIS® imaging of the

major organs for the biodistribution of the Cy5.5-Col/aPD-L1@ECN and Cy5.5-Col/aPD-L1 at 72 h (n = 3 mice). 10g. *Ex vivo* IVIS® imaging of the tumor biodistribution of the Cy5.5-Col/aPD-L1@ECN and Cy5.5-Col/aPD-L1 at 72 h (n = 3 mice). 10h. Quantitative data analysis of the radiant efficiency of the tumor tissue in Cy5.5-Col/aPD-L1@ECN group and Cy5.5-Col/aPD-L1 group at 72 h. Data are presented as mean ± s.d. (n = 3 mice) and analyzed with unpaired t-test, $P^{**} = 0.0063$. 10i. *In vivo* fluorescence analysis of the biodistribution of the Cy5.5 labeled protein cages in the tumor tissue at 72 h (n = 3 mice, scale bar = 100 μm).

[0020] FIGs. 11a-h show antitumor efficacy of Col/aPD-L1@ECN in the orthotopic pancreatic cancer. 11a. Western blot assay of the oncogenic collagen expression in the supernatant of KPC-Luc cell culture medium. 11b. Oncogenic collagen depletion effect of Col/aPD-L1@ECN in 3D tumor spheroids established from KPC cells. Collagen was stained with red fluorescence, and the cell nucleus was stained with Hoechst (scale bar = 100 μm). 11c. Quantitative data analysis of the average spheroid diameter after treated with PBS and Col/aPD-L1@ECN for 72 hours. Data are presented as mean ± s.d. (n = 3 biologically independent samples) and analyzed with unpaired t-test, $P^{**} = 0.0050$. 11d. Schematic illustration of the experimental design for the orthotopic pancreatic cancer model. 11e. Body weight of the mice after the treatments of PBS, ECN, Col@ECN, Col/aPD-L1, Col/aPD-L1+ECN, aPD-L1@ECN, and Col/aPD-L1@ECN at different timepoints (n = 6 mice). 11f. Representative IVIS® images of the PDAC-bearing mice after the treatments of PBS, ECN, Col@ECN, Col/aPD-L1, Col/aPD-L1+ECN, aPD-L1@ECN, and Col/aPD-L1@ECN on day 0, day 7, day 14 and day 21 (n = 6 mice). 11g. Data analysis of the fold changes of the bioluminescence intensity in the orthotopic PDAC-bearing mice after different treatments on day 0, day 7, day 14 and day 21. Data are presented as mean ± s.d. (n = 6 mice) and analyzed with two-way ANOVA followed by Dunnett's multiple comparisons test. Col/aPD-L1@ECN vs. aPD-L1@ECN: $P^{**} = 0.0030$; Col/aPD-L1@ECN vs. Col/aPD-L1+ECN: $P^{***} = 0.0003$. 11h. Survival curve of the PDAC- bearing mice after different treatments (n = 6 mice). Data are analyzed with Log-rank (Mantel-Cox) test. Col/aPD-L1@ECN vs. aPD-L1@ECN: $P^{**} = 0.0082$.

[0021] FIG. 12 shows H&E staining of different organs, including heart, liver, spleen, lung, and kidney, after the treatments of PBS and Col/aPD-L1@ECN (Scale bar = 100 μm).

[0022] FIGs. 13a-h show immune activation of Col/aPD-L1@ECN in the orthotopic pancreatic cancer. 13a. Flow cytometry assay of $CD8^+$ T cell infiltration in the orthotopic pancreatic cancer after different treatments. 13b. Quantitative $CD8^+$ T cell number per mg

pancreatic tumor tissue after different treatments. Data are presented as mean ± s.d. (n = 5 mice) and analyzed with one-way ANOVA followed by Dunnett's multiple comparisons test. Col/aPD-L1@ECN vs. aPD-L1@ECN: $P^{***} = 0.0006$; Col/aPD-L1@ECN vs. Col/aPD-L1+ECN: $P^{****} < 0.0001$. 13c. Quantitative Granzyme B^+ $CD8^+$ T cell number per mg pancreatic tumor tissue after different treatments. Data are presented as mean ± s.d. (n = 5 mice) and analyzed with one-way ANOVA followed by Dunnett's multiple comparisons test. Col/aPD-L1@ECN vs. aPD-L1@ECN: $P^{****} < 0.0001$; Col/aPD-L1@ECN vs. Col/aPD-L1+ECN: $P^{****} < 0.0001$. 13d, e. IFNγ (13d) and TNFα (13e) expressions in the tumor tissue were detected by ELISA assay after different treatments. Data are presented as mean ± s.d. (n = 5 mice) and analyzed with one-way ANOVA followed by Dunnett's multiple comparisons test. (13d, Col/aPD-L1@ECN vs. aPD-L1@ECN: $P^{**} = 0.0046$; Col/aPD-L1@ECN vs. Col/aPD-L1+ECN: $P^{****} < 0.0001$; 13e, Col/aPD-L1@ECN vs. aPD-L1@ECN: $P^{**} = 0.0045$; Col/aPD-L1@ECN vs. Col/aPD-L1+ECN: $P^{****} < 0.0001$). 13f. Luminex®-based quantification of cytokines and chemokines, including IL-1α, IL-1β, IL-3, IL-12, IL-27, GM-CSF, IFN-γ, TNF-α. (n = 5 mice). 13g. Immune fluorescence assay of $CD8^+$ T cell infiltration in the tumor tissues after PBS or Col/aPD-L1@ECN treatment. 13h. Schematic illustration of the underlying mechanism of immune activation.

[0023] FIGs. 14a-h show Col/aPD-L1@ECN depletes oncogenic collagen and modulates integrin α3β1-FAK-related signaling pathway. 14a. Schematic illustration of the downstream signaling pathways after blocking the interaction between oncogenic collagen and integrin α3β1. 14b. Oncogenic collagen expression on day 7 in the pancreatic tumor tissue after the treatments of PBS and Col/aPD-L1@ECN on day 0, day 2, and day 4 (scale bar = 50 μm). 14c, d, e. Immune fluorescence assay of the p-FAK (14c), p-AKT (14d), and p-MAPK (14e) signaling pathways in the pancreatic tumor tissues on day 7 (scale bar = 100 μm) after the treatments of PBS and Col/aPD-L1@ECN on day 0, day 2, and day 4. 14f, g, h. Normalized expression of the p-FAK (14f), p-AKT (14g), and p-MAPK (14h) signaling pathways in the pancreatic tumor tissues. Data are presented as mean ± s.d. (n = 3 mice) and analyzed with an unpaired t-test. (14f: $P^* = 0.0254$; 14g: $P^* = 0.0363$; 14h: $P^* = 0.0161$).

[0024] FIG. 15 shows a Western blot assay of the oncogenic collagen expression in the supernatant of 4T1 cell culture medium.

[0025] FIGs. 16a-h show antitumor efficacy of Col/aPD-L1@ECN in the metastatic breast cancer. 16a. Schematic illustration of the experimental design in the orthotopic breast cancer model. 16b. Representative image of the tumor tissues collected from the mice on day 20 (scale bar = 1 cm). 16c. Tumor growth curve of the 4T1 tumor model after the treatments

of PBS, ECN, Col@ECN, Col@aPD-L1, Col@aPD-L1+ECN, aPD-L1@ECN, and Col/aPD-L1@ECN. Data are presented as mean ± s.d. (n = 6 mice) and analyzed with two-way ANOVA followed by Dunnett's multiple comparisons test. Col/aPD-L1@ECN vs. aPD-L1@ECN: $P^{**} = 0.0038$; Col/aPD-L1@ECN vs. Col/aPD-L1+ECN: $P^{***} = 0.0004$. 16d. Body weight change of the mice after different treatments during the treatment course. 16e. Survival curve of the 4T1 tumor-bearing mice after different treatments of PBS, ECN, Col@ECN, Col@aPD-L1, Col@aPD-L1+ECN, aPD-L1@ECN, and Col/aPD-L1@ECN. Data are analyzed with Log-rank (Mantel-Cox) test. Col/aPD-L1@ECN vs. aPD-L1@ECN: $P^{**} = 0.0065$. 16f. Schematic illustration of the experimental design in the metastatic breast cancer model. 16g. Representative images of the lung tissues collected from the mice and subsequent H&E staining after different treatments, including PBS, Col@ECN, Col@aPD-L1+ECN, aPD-L1@ECN, and Col/aPD-L1@ECN (Scale bar = 2 mm for the whole lung picture, Scale bar = 200 μm for the H&E staining). 16h. Data analysis of the number of metastatic nodules on the surface of the collected lung tissues after different treatments on Day 21. Data are presented as mean ± s.d. (n = 5 mice) and analyzed with one-way ANOVA followed by Dunnett's multiple comparisons test. Col/aPD-L1@ECN vs. aPD-L1@ECN: $P^{**} = 0.0075$; Col/aPD-L1@ECN vs. PBS: $P^{****} < 0.0001$.

[0026] The above-described and other features will be appreciated and understood by those skilled in the art from the following detailed description, drawings, and appended claims.

DETAILED DESCRIPTION

[0027] Traditional treatment approaches for PDAC in the clinic, including chemotherapy, surgery, and radiotherapy, often achieve unsatisfactory efficacy due to factors including late diagnosis from lack of specific markers and early screening methods; less than 20% of PDAC patients eligible for surgery; poor response and drug resistance to chemotherapy and radiotherapy; and frequent relapse and early metastasis. Immunotherapy, represented, for example, by CAR-T cells recognizing tumor-associated antigens and immune checkpoint inhibitors reinvigorating T cell activity by blocking PD1/PDL1 pathway, brings new hopes for PDAC patients. However, PDAC is characterized by the immune desert TME which significantly impedes immunotherapy efficacy. The immune desert TME of PDAC is composed of several unique biological features, including immunosuppressive microenvironment due to infiltration of various immunosuppressive cells, such as TAMs, MDSCs, and Treg cells; and strong desmoplasia due to dense ECM deposition resulting from

the desmoplastic reaction. These microenvironments in PDAC collectively result in impaired T cell infiltration and poor immunotherapy efficacy.

[0028] To address above-mentioned challenges in PDAC immunotherapy, efforts have focused on regulating immunosuppressive TME to facilitate T cell infiltration and immune response. One typical and effective strategy is to destroy the extracellular physical barrier by degrading the extracellular matrix. Type I collagen (Col1), as a major component of ECM, has been identified with a critical role in promoting PDAC development and metastasis, besides the primary function in constructing a biophysically "stiff" TME to prevent drug access to PDAC cells. In addition to the well-understood Col1 heterotrimer ($\alpha1/\alpha2/\alpha1$) generated by cancer-associated fibroblasts, a recent study has identified a new type of Col1 homotrimer ($\alpha1/\alpha1/\alpha1$), referred to as oncogenic collagen, that is specifically produced by PDAC cells. Using a genetically modified mouse model with the deletion of Col1 homotrimer, the critical role of Col1 homotrimer in promoting PDAC cell proliferation and carcinogenesis was confirmed through binding to $\alpha3\beta1$ integrin and activating downstream oncogenic signaling. Besides the identification of the biological function of oncogenic Col1, the potential therapeutic impact has also been validated through combining the deletion of Col1 homotrimer and ICB. However, despite the fact that oncogenic Col1 could serve as a promising target to synergize with current ICB for PDAC immunotherapy, the targeted depletion of oncogenic Col1 is still challenging due to the dense ECM barrier and high interstitial pressure prevent the access of collagen-degrading agents to PDAC cells; and lack of therapeutics that can selectively deplete oncogenic Col1.

[0029] Described herein is a probiotic EcN-based oncogenic Col1 degrader (Col/aPD-L1@ECN) to enhance ICB-mediated PDAC immunotherapy. As a historically recognized sterile organ, the pancreas has been recently found infiltrated with diverse bacteria, and a much higher density of bacteria is found in PDAC tumor samples than in normal pancreatic tissues. The reasons accounting for this include the hypoxic and immunosuppressive TME in PDAC creating a favorable environment for bacteria proliferation and the easy migration of bacteria residing in the intestine. By taking advantage of the unique biological features of PDAC, the developed EcN-based oncogenic Col1 degraders could preferentially home to and accumulate at the PDAC site. Furthermore, the excellent motility of EcN could add the selectivity of collagenases in degrading oncogenic Col1 through penetrating the tumor parenchyma rather than residing at the margin of PDAC that is often seen in traditional delivery systems. Besides, the ROS responsiveness of Col/aPD-L1@ECN also contributes to the oncogenic Col1 selectivity, given the higher ROS levels in the tumor parenchyma than

that in the edge of the tumor. Collectively, even though the collagen degrading agent – collagenases used herein– cannot distinguish oncogenic collagen from the collagen in the ECM, the EcN-based delivery system design described herein could penetrate the dense ECM and substantially deliver the collagenases to the PDAC cells. In addition, the compositions and methods described herein can be applied to hypoxic tumors in cancers other than PDAC.

[0030] In an aspect, described herein is a bacteria-based protein drug delivery system for deep PDAC penetration to target and deplete oncogenic collagen, which further blocked the integrin α3β1 signaling pathway to inhibit PDAC cell proliferation and facilitate the efficacy of ICB. Utilizing a ROS-responsive linker, a protein cage formulation was constructed comprising collagenase and anti-PD-L1 antibodies (aPD-L1). The protein cages were then conjugated to the surface of probiotic *Escherichia coli* strain Nissle 1917 (EcN) to form Col/aPD-L1@ECN. Given the highly hypoxic TME of PDAC, Col/aPD-L1 protein cages could be delivered to the PDAC site driven by the bacteria's hypoxic tropism after systemic administration. In addition, the strong motility of EcN promoted deep tumor penetration and released collagenase and aPD-L1 under the trigger of elevated ROS inside the tumor tissue. Collagenase then degraded the oncogenic collagen secreted by tumor cells and blocked the downstream FAK signaling pathway, thereby reducing the infiltration of immunosuppressive cells and increasing the abundance of effector T cells, thus paving the way for improving the response rate of aPD-L1 therapy.

[0031] In an aspect, a drug delivery system comprises protein nanocages comprising collagenase proteins and anti-immune checkpoint inhibitor antibodies conjugated to the surface of a probiotic bacterial carrier.

[0032] As used herein, a protein nanocage is a protein assembly prepared by crosslinking proteins using bifunctional linkers such as ROS linkers. The protein nanocages comprise a collagenase and an anti-immune checkpoint inhibitor antibody.

[0033] A collagenase is an enzyme that breaks down the peptide bonds in collagen. Collagenases belong to the matrix metalloproteinase (MMPs) family that digest collagens in the extracellular matrix (ECM). Exemplary collagenases include collagenase type I from *Clostridium histolyticum*. In an aspect, the collagenase is a commercially available collagenase such as Sigma-Aldrich, C1-22-1G. Collagenases can also be prepared from *C. perfringens*, *Vibrio alginolyticus*, *Streptomyces* sp., *Pseudomonas* sp. such as *Pseudomonas* aeruginosa, and *Achromobacter iophagus*. Combinations of collagenases may be employed.

[0034] Exemplary anti-immune checkpoint inhibitor antibodies comprise anti-PD-L1 antibodies, anti-CTLA-4 antibodies, anti-PD-1 antibodies, anti-TIM-3 antibodies, anti-LAG-3 antibodies, or a combination thereof.

[0035] Exemplary anti-PD-L1 antibodies include atezolizumab, avelumab and durvalumab.

[0036] Exemplary anti-CTLA-4 antibodies include ipilimumab and tremelimumab.

[0037] Exemplary anti-PD-1 antibodies include cemiplimab, pembrolizumab, nivolumab, cemiplimab, retifanlimab, and dostarlimab.

[0038] Exemplary anti-TIM-3 antibodies include LY3321367, LY3300054, Sym023, BMS-986258. ICAGN02390, RO7121661, BGBA425, TSR-022, and MGB453.

[0039] Exemplary anti-LAG-3 antibodies include relatlimab, fianlimab, Sym022, GSK2831781, INCAGN02385, TSR-033, ieramilimab, and favezelimab.

[0040] Exemplary bifunctional linkers include reactive oxygen species (ROS)-responsive linkers, glutathione (GSH)-responsive linkers, pH-responsive linkers, enzyme-responsive linkers, and the like, and combinations thereof. Exemplary ROS-responsive linkers include thioether-containing polymers, diselenide, thioketal, arylboronic ester, aminoacrylate, oligoproline, peroxalate ester, and mesoporous silicon. GSH-responsive linkers can react with an amino group in a protein and release the protein under GSH trigger. Exemplary pH-responsive linkers include pH-sensitive hydrazone linkers, orthoester linkers, weak acid labile linkers, and the like. Exemplary enzyme-responsive linkers include matrix metalloproteinase (MMP)-degradable peptide linkers.

[0041] An exemplary ROS-responsive linker is 2,2′-[propane-2,2-diylbis(thio)] diacetic acid.

[0042] In an aspect, the protein nanocages have diameters of 90 to 300 nm.

[0043] The protein nanocages can be assembled by incubating the collagenase, the anti-immune checkpoint inhibitor antibody and the bifunctional linker under assembly conditions, such as dissolution in a solvent such as DMSO at room temperature to about 40°C for about 35 min.

[0044] Optionally, after preparing the nanocages, any unreacted linkers may be removed, for example, by dialysis or centrifugal filter tube.

[0045] A preferred ratio of the antibody to the collagenase in the protein nanocages is about 1:1, although deviations from this ratio are possible.

[0046] The protein nanocages are conjugated to the surface of a probiotic bacterial carrier.

[0047] Certain bacterial species such as *Clostridium*, *Bifidobacterium*, *Listeria*, *Escherichia coli*, and *Salmonella* species, possess inherent tumor-targeting and tumor-killing activities. Exemplary probiotic bacteria for the drug delivery system include *S. typhimurium* strains VNP20009, A1-R, SHJ2037, SL3261, SL7207, BRD509, YB, LH430, VNP (*PhoQ*-), MvP728, YB1, ST8, c4550, SF200, S364, RE88, SB824, ST8, SF200, and MPO378; *Listeria monocytogenes* strains DP-L4027, DP-L4029, DP-L4017, DP-L4042, DP-L4097, DP-L4364, DP-L4405, DP-L4406, CS-L0001, CS-L0002, CS-L0003, DP-L4038, and DP-L4384; Clostridium novyi; and *E. coli* Nissle 1917, MG1655, SYNB1020, and SYNB1891.

[0048] In a preferred embodiment, the probiotic bacteria is *E. coli* Nissle 1917.

[0049] In an aspect, the ratio of protein nanocages to probiotic bacterial carrier is 10 to 100 pg proteins per probiotic bacterium, specifically 30 pg proteins per *E. coli* Nissle 1917.

[0050] The protein nanocages are conjugated to the surface of the probiotic bacteria with a crosslinking agent, such as 1-ethyl-3-(-3-dimethylaminopropyl) carbodiimide hydrochloride (EDC)/ *N*-hydroxysuccinimide (NHS) or ECD/Sulfo-NHS. Other crosslinking agents known in the art may also be employed.

[0051] Without being held to theory, it is believed that the COOH groups on the protein nanocages can react with the NH_2 group on the ECN under the catalysis of EDC/NHS, thus crosslinking the protein nanocages to the surface of the probiotic bacteria.

[0052] Also included herein are pharmaceutical compositions comprising the drug delivery vehicles and a pharmaceutically acceptable excipient.

[0053] Compositions for systemic administration include compositions for oral administration or injection such as intravenous injection, intramuscular injection, intraperitoneal injection, subcutaneous injection, and the like.

[0054] The drug delivery system described herein is particularly useful to treat hypoxic tumors characterized by oncogenic collagen. A method of treating a patient with a hypoxic tumor characterized by oncogenic collagen comprises systemically administering to the patient the drug delivery vehicle described herein.

[0055] As used herein, a hypoxic tumor is a tumor wherein the tumor cells are deprived of oxygen. Hypoxia can occur due to rapid tumor growth and/or impaired blood vessel formation. Solid tumors are subject to hypoxia, with head and neck, breast, pancreatic, skin, prostate, liver, cervical or brain cancer tumors being particularly subject to hypoxia. In an aspect, the patent has pancreatic ductal adenocarcinoma (PDAC) or locally advanced breast cancer.

[0056] For example, in the treatment of PDAC, the hypoxia tropism and excellent motility of EcN will provide delivery of the drug delivery vehicle to hypoxic tumors. The elevated levels of Reactive Oxygen Species (ROS) in the microenvironment of PDAC can cause the breakdown of ROS-responsive linkers in the protein nanocages that respond to ROS, thereby releasing collagenases and anti-immune checkpoint inhibitor antibodies from the protein nanocages. The released collagenases degrade the oncogenic collagen, blocking the integrin α3β1-FAK signaling pathway, thereby overcoming immunosuppression and reducing the proliferation of tumor cells. The activity of the collagenases will then synergize with anti-PD-L1 antibodies, resulting in the activation of infiltrating T cells for enhanced PDAC immunotherapy.

[0057] The invention is further illustrated by the following non-limiting examples.

EXAMPLES

METHODS

[0058] Cell lines and antibodies: HEK293T and 4T1 cells were purchased from ATCC. KPC cells were gifted by the Ronnekleiv-Kelly lab. Escherichia coli Nissle 1917 (EcN) was purchased from Mutaflor, Canada. Cells were cultured in the CO_2 incubator at 37°C with 5% CO_2 and 90% relative humidity. The antibodies used in this study were summarized as follows (company, clone, category number): Ultra-LEAF™ purified anti-mouse CD274 (B7-H1, PD-L1) antibody (BioLegend, 10F.9G2, 124338), Fluorescein isothiocyanate (FITC)-anti-mouse CD45 (BioLegend, 30-F11, 103108), APC-anti-mouse CD3 (BioLegend, 17A2, 100236), FITC-anti-mouse CD4 (BioLegend, GK1.5, 100406), PE-anti-mouse CD8a (BioLegend, 53-6.7, 100708), PerCP/Cy5.5-anti-human/mouse Granzyme B (BioLegend, QA16A02, 372212), PE-anti-mouse CD45 (BioLegend, 30-F11, 103106), Alexa Fluor® 594 anti-mouse CD8a (BioLegend, 53-6.7, 100758), anti-Collagen I (Cell signaling technology, E8F4L, 72026), HRP-anti-beta actin antibody (abcam, AC-15, ab49900), anti-Phospho-Akt (Ser473) (Cell signaling technology, D9E, 4060), anti-Phospho-p44/42 MAPK (Erk1/2) (Thr202/Tyr204) (Cell signaling technology, D13.14.4E, 4370), anti-Phospho-FAK (Tyr397) (Thermo Fisher Scientific, 31H5L17, 700255), anti-CD326 (EpCAM) (Thermo Fisher Scientific, 1B7, 14-9326-82), anti-CD49c (integrin alpha 3) (Thermo Fisher Scientific, ASC-1, MA5-28565), anti-CD29 (integrin β1) (BioLegend, TS2/16, 303001), anti-Mouse IgG (H+L, Alexa Fluor® 488) (Thermo Fisher Scientific, A28175SAMPLE), anti-rabbit IgG (H+L, Alexa Fluor® 59) (Cell signaling technology,

8889), anti-Rabbit IgG (H+L) Secondary Antibody-HRP (Thermo Fisher Scientific, 31460), Precision Count Beads™ (BioLegend, 424902). All antibody dilutions were performed following the manufacturer's guidance (for flow cytometry assay and immune fluorescence: diluted by approximately 200 times for use; for western blot assay: diluted approximately 1000 times for use).

[0059] To generate the luciferase-expressing KPC cell line, the firefly luciferase fragment was amplified and inserted into the EcoRI and XbaI digested pLVX-IRES-Neo vector; the newly constructed plasmids were named pLVX-Luc-IRES-Neo. Clones were verified by Sanger sequencing. The plasmids psPAX2 and pMD2.G were obtained from Addgene.

[0060] Lentiviruses were produced by co-transfecting the pLVX-Luc-IRES-Neo, psPAX2, and pMD2.G into HEK293T cells using lipofectamine™ 3000 reagent (Thermo Fisher). The lentivirus supernatant was harvested 48h post-transfection. Viral transduction was conducted according to the Broad Institute's lentiviral production guidelines. Briefly, KPC cells were spin transfected with lentivirus supernatant at 32°C for 1 h at 1000g, then incubated for 48 h, and transduction efficiency was checked with a luciferase assay. Transduced cells were then placed into 96-well plates with the goal of obtaining one cell per well. Cell clones will grow under G418 selection for 1 week. Clones derived from single cells were expanded to obtain sufficient cell numbers over a few days. All selected clones were verified using luciferase assay. Briefly, freshly transduced cell lines were lysed in cell culture lysis buffer (Promega) and mixed with luciferase assay reagent (Promega); the relative light units (RLU) were detected using the Centro LB 960 Microplate Luminometer (Berthold Technologies). RLU was normalized based on total protein (Pierce).

[0061] Analysis of the prognosis of pancreatic cancer patients: For the scatter map of the correlation between two genes, correlations were carried out using Spearman's method, and plots were generated using the ggplot2 (v.3.3.6) package in R (v.4.2.1). These correlations were validated using a linear model in the R base library. For data that were not normally distributed, log transformation was carried out. Overall survival and disease-free survival were analyzed by the Gene Expression Profiling Interactive Analysis (GEPIA) tool based on the TCGA database. Moreover, Kaplan-Meier survival analysis and Logrank analysis were performed to reveal the significant difference between the disease-free survival (DFS) of patients with high gene expression and low gene expression. In addition, the median gene expression in the GEPIA database is utilized to divide the high and low gene expression.

[0062] Synthesis of ROS-responsive linkers: To synthesize the ROS-responsive linker, 2,2′-[propane-2,2-diylbis(thio)] diacetic acid (1 equiv), EDC (2.5 equiv), and NHS (2.5 equiv) were mixed in dimethyl sulfoxide (DMSO) and stirred for 6 h at room temperature. The reaction mixture was slowly dripped into cold water. After the white solid was precipitated, the product was obtained by filtration and analyzed with NMR and mass spectrometry.

[0063] Preparation and characterization of Col/aPD-L1@ECN: To prepare the protein cage, aPD-L1 (0.5 equiv) and collagenase (Sigma-Aldrich, C1-22-1G, 0.5 equiv) were dissolved in the PBS solution, and then the ROS-responsive linker (20 equiv) dissolved in the DMSO was added into the solution for about 35 min reaction at room temperature to form the protein cages. The particle size and zeta potential of the protein cages were detected by the Malvern Zetasizer instrument. TEM imaging (FEI Tecnai T-12 Cryo TEM system) was performed to observe the morphology of the protein cages. The obtained protein cages were conjugated onto the surface of EcN (10^8 CFU·ml^{-1}) by reaction for one hour at a 37°C shaker incubator under the catalysis of EDC/NHS. The reaction mixture was centrifuged (4000 rpm, 5 min) to obtain the Col/aPD-L1@ECN. TEM imaging was performed to demonstrate the successful preparation of the Col/aPD-L1@ECN. Furthermore, aPD-L1 was labeled with FITC, and collagenase was labeled with Rhodamine B. The conjugation of the protein cages on EcN was verified by the flow cytometry assay (Thermo Fisher Attune™) and confocal assay (Leica SP8 Confocal WLL STED Microscope). Next, the protein release assay at different time points was performed with or without H_2O_2 (0.5 mM) by collecting the supernatant and detecting it with the ELISA kit according to the instructions.

[0064] Motility of Col/aPD-L1@ECN: Col/aPD-L1@ECN was prepared accordingly and further washed with PBS before mixed with 200μl alginate solution (10 mg/ml). Then, 10 μl of $CaCl_2$ solution (100 mg/ml) was added to form the inner gel. The Matrigel™ was prepared by diluting Corning™ Matrigel™ Matrix with double distilled water in a proportion of 1:1. Then, the gel was put in the 37°C incubator for gelation. After gelation of both gels, the Col/aPD-L1@ECN containing alginate gel was abutted to the Matrigel™. The Col/aPD-L1@ECN distribution near the boundary of the two gels was observed under the microscope at 0 hour and 4 hours for migration assay. For the transwell invasion assay, first, the Matrigel™ was diluted with double distilled bacteria-free water and then added into the transwell inserts preloaded in the 24 wells plates. Bacteria-free PBS was added into the 24-well plate, and Col/aPD-L1@ECN solution in PBS was added into the upper transwell

inserts. The numbers and penetration ratios of Col/aPD-L1@ECN were calculated after 8 h incubation.

[0065] Western blot assay: For the verification of the oncogenic collagen expression in the KPC-Luc and 4T1 cells, the cells were seeded in 6-well plates and the supernatant was collected after 72 hours of culture. The related protein concentration was detected by the BCA analysis according to the instruction. Next, the extracted proteins were mixed with loading buffers and boiled for further use. For the verification of the collagen and integrins α3 and β1 expression in pancreatic cancer, human pancreatic tumor tissues were collected and made into western blot samples. To perform the western blot assay, the running buffer was prepared, and protein markers and samples were loaded accordingly into the gel grooves. SDS-PAGE was performed at 120 V for approximately 70 min and then the proteins were transferred onto the PVDF membrane (350 mA, 120 min). After blocking with 5% skim milk for 2 hours at room temperature, the PVDF membranes were incubated with the related primary rabbit antibodies (anti-COL1A1, anti-integrin α3, anti-integrin β1 and anti-β-actin respectively) at 4°C cold room overnight. Then the membranes were washed with PBST buffer and incubated with the secondary antibody (Anti-rabbit IgG, HRP-linked) for 1 hour. After washing with PBST buffer, western blot imaging was performed with the iBright™ Imaging Systems.

[0066] Immunofluorescence assay: The frozen slides were fixed in the pre-cooled acetone for 10 minutes. After drying the slides at room temperature for 20 minutes, the sections were washed with PBS three times (5 minutes each time). The samples were incubated in 0.3% H_2O_2 for 10 minutes and later washed with PBS three times (5 minutes each time). 10% Goat Serum was added to the tissue, and the section was incubated for 1h in the humidified environment. Then, the tissues were incubated with the primary antibody that was diluted with 0.5% BSA-PBS in the proper proportion (1: 200) for 1 hour. Later, the sections were washed with PBS 3 times and incubated in the secondary antibody (1: 2000) for another 1 hour in the dark. After washing with PBS 3 times, the Hoechst (1: 1000) was added to the sectioned tissue for 15-minute staining in the dark, and the section was washed with PBS 3 times for 7 to 10 minutes each time. The sections were later washed with 100% ethanol twice for 7 to 10 minutes each time and dried out for 5 minutes. After all the alcohol was volatilized, the sealing liquid was dropped on the tissue, and then the cover glass was slowly covered over the tissue for further confocal assay.

[0067] Oncogenic collagen depletion in 3D tumor spheroids: To establish the 3D tumor spheroids of pancreatic cancer, a 1.5% agarose gel (18 mL DMEM without FBS, 270

mg agarose, dissolved in 80°C water bath for 30 min) was prepared. Then the gel was sterilized before added to the 24-well plates (500 μl each well). Next, the plate was left on a flat platform for 1 hour for gelation. Meanwhile, the KPC-Luc cells were digested and added to the 24-well plates (approximately 800 cells, 2 ml DEME containing 10% FBS per well). The cells were cultured for about one week in 37°C incubator (5% CO_2). Then the formed tumor spheroids were treated with PBS or Col/aPD-L1@ECN for 72 hours and then washed with PBS and transferred into the confocal dishes carefully. Next, the tumor spheroids were incubated with anti-COL1A1 antibody (dilution: 1: 1000) for 1 hour at room temperature. Then the tumor spheroids were washed with PBS and incubated with the anti-rabbit IgG-Alexa Fluor® 594 (dilution: 1: 1000). PBS wash was performed again, and the tumor spheroids were stained with Hoechst for 15 min. After washed with PBS, the tumor spheroids were observed and analyzed with a confocal assay.

[0068] In vivo tumor targeting verification: To verify the tumor-targeting ability of Col/aPD-L1@ECN, first, the orthotopic pancreatic adenocarcinoma (PDAC) model was established according to the previously reported procedures. Specifically, before the operation, hair removal cream was used to remove the hair on the left abdomen of male C57BL/6 mice. KPC-Luc cells in the logarithmic growth phase were collected and dispersed with PBS containing 20% Matrigel to prepare a cell suspension (10^7 cells/mL) and placed on ice for later use. Then each mouse was anesthetized and fixed on the operating table in the right-lying position with adhesive tape. After disinfection with iodine, an approximately 1 cm incision was cut at the left rectus abdominis muscle. After blunt separation of the subcutaneous radius of 0.5 cm, the muscle layer was cut. It was observed that the pancreas was close to the spleen and covered by the stomach. The pancreas can be fully exposed by gently pulling the spleen out of the incision and slightly everting it. Aspirate the spare cell suspension with an insulin needle, gently insert the needle from the pancreas tail to the head of the pancreas and fix it with ophthalmic forceps. At this time, gently rotate and pull out the needle to avoid exposing the cell suspension. Then the pancreas was pushed back to the abdominal cavity, and the muscle layer and cortex were intermittently sutured with 4-0 medical sutures, respectively. Finally, an iodine solution was used to disinfect the wound. The mice were placed under the near-infrared thermotherapy apparatus and then recovered to the cage for culture after awakening. The activity of mice was observed every day, and the wound was disinfected with iodine until healing. After 14 days of tumor implantation, Col/aPD-L1 protein cages were constructed and labeled with Cy5.5 before being conjugated to the ECN (Col/aPD-L1@ECN). The Cy5.5-labeled protein cages and Col/aPD-L1@ECN

were administered to the mice bearing orthotopic pancreatic tumors by intravenous injection. IVIS imaging was performed at determined time points. At 72 hours post-injection, the mice were euthanized, and major organs and tumor tissue were collected to perform the ex vivo IVIS imaging. Next, the tumors were sectioned and made into frozen tissue slides, and immunofluorescence assays were performed to observe the distribution of the protein cages in the tumor tissue.

[0069] Antitumor efficacy in vivo: C57BL/6 mice (Male, aged 6-8 weeks) and Balb/c mice (Female, aged 6-8 weeks) were purchased from Jackson laboratory. The animal study protocol was approved by the Institutional Animal Care and Use Committee at the University of Wisconsin-Madison. Mice were euthanized at humane endpoints if any of the following criteria were met: (i) weight loss or gain of >20%, (ii) moribund, (iii) severe abdominal swelling, (iv) jaundice, or (v) tumor volume >2000 mm^3. To verify the antitumor efficacy of Col/aPD-L1@ECN in vivo, we first established the orthotopic pancreatic tumor model as described above. The tumor-bearing mice were weighed and randomly divided into seven groups (n = 6) after 14 days of tumor implantation. The mice were treated with PBS, ECN, Col@ECN, Col/aPD-L1, Col/aPD-L1+ECN, aPD-L1@ECN, and Col/aPD-L1@ECN respectively, on day 0, day 2, and day 4 (ECN: 5×10^6 CFU per mice, aPD-L1: 2.5 mg/kg, Col: 5mg/kg). D-Luciferin potassium salt was dissolved in PBS solution and injected into the mice by intraperitoneal administration (3 mg dissolved in 100 μL for each mouse). IVIS® imaging was performed to monitor tumor growth, and body weight was detected every day. The survival of the tumor-bearing mice after different treatments was monitored until day 71. To further verify the antitumor efficacy of the therapeutic strategies in breast cancer, the 4T1 breast cancer model was established, and 10 days later, different treatments, including PBS, ECN, Col@ECN, Col/aPD-L1, Col/aPD-L1+ECN, aPD-L1@ECN, and Col/aPD-L1@ECN (ECN: 5×10^6 CFU per mice, aPD-L1: 2.5 mg/kg, Col: 5mg/kg) were performed on day 0, day 2, and day 4. The tumor volume, body weights, and survival of the tumor-bearing mice were monitored accordingly. On day 20, tumors were collected to evaluate the therapeutic efficacy. Moreover, to further verify the potential anti-metastasis effect of the therapeutic strategy, the metastatic breast cancer model was established. Briefly, first tumor inoculation was performed on Balb/c mice on day -10, then on day 0, day 2 and day 4, different therapeutic strategies (PBS, Col@ECN, Col/aPD-L1+ECN, aPD-L1@ECN, and Col/aPD-L1@ECN, ECN: 5×10^6 CFU per mice, aPD-L1: 2.5 mg/kg, Col: 5mg/kg) were performed. On day 7, 5×10^5 4T1 cells were injected into the mice, and on day 21, the lung tissues of the mice were harvested and fixed with Bouin's solution. The number of surface lung metastatic

nodules was counted, and the H&E assay was performed by the UWCCC Experimental Animal Pathology Laboratory.

[0070] Immune activation in vivo: To evaluate immune activation in vivo, the pancreatic cancer model was established. Then, after different treatments on day 0, day 2, and day 4 (PBS, ECN, Col@ECN, Col/aPD-L1, Col/aPD-L1+ECN, aPD-L1@ECN, Col/aPD-L1@ECN, ECN: 5×10^6 CFU per mice, aPD-L1: 2.5 mg/kg, Col: 5mg/kg), the pancreatic tumors were harvested and homogenized in the PBS solution. Then the cell suspensions were stained with anti-mouse CD3, anti-mouse CD8a, and anti-mouse Granzyme B antibodies for 50 min and analyzed with the flow cytometry assay (Thermo Fisher Attune). Moreover, the cytokines expression in the tumor tissues was analyzed with the LEGENDplex™ Multi-Analyte Flow Assay Kit according to the instructions. In addition, representative immune activation markers IFNγ and TNFα were detected by the related ELISA kits (BioLegend) according to the instructions.

[0071] Statistics: All the results are shown as mean ± s.d. The GraphPad Prism software was used to perform statistical analysis. Unpaired Student-*t* test was used to compare two groups and analysis of variance (ANOVA) was used to compare multiple groups (> two groups) statistically. Log-rank test was performed for the statistical analysis of the survival study. A P value lower than 0.05 ($^*P < 0.05$) was considered the threshold for statistical significance among control groups and experimental groups.

EXAMPLE 1: ONCOGENIC COLLAGEN EXPRESSION NEGATIVELY IMPACTS THE PROGNOSIS OF PANCREATIC CANCER PATIENTS

[0072] To validate that oncogenic collagen can serve as a therapeutic target for pancreatic cancer, a bioinformatic analysis was applied to characterize the correlation between oncogenic collagen and PDAC patients' prognosis (Fig. 1a). As shown in Fig. 2, there are significant differences in the expression of collagen (designated COL1A1) between PDAC tissues and normal pancreas, substantiating that PDAC can generate more collagen. The survival time of PDAC patients who are characterized by high COL1A1 expression is substantially shorter than those patients with low COL1A1 expression, even though the difference is not statistically significant, where the reason for this is that there are technical challenges in the bioinformatic analysis to distinguish the oncogenic COL1A1 derived from pancreatic cancer cells and COL1A1 derived from fibroblast that accounts for the most collagen in the tumor microenvironment (Fig. 3). Since the oncogenic COL1A1 has been demonstrated to bind to the integrin α3β1 on the cancer cells, in order to highlight the critical

role of oncogenic COL1A1 in determining the poor prognosis of PDAC patients, the correlation of integrin α3β1 and oncogenic COL1A1, and the association with PDAC patient survival were analyzed. As shown in Fig. 1b-g, both integrins α3 and β1 displayed elevated expressions in PDAC tissues compared to normal pancreas. PDAC patients with high expressions of both integrins α3 and β1 showed significantly shorter survival time compared to those patients with low expressions. Notably, there was a positive correlation in the expression of integrins α3 and β1 (Fig. 4), and positive correlations between the expression levels of COL1A1 and integrins α3 and β1, which suggests the critical role of oncogenic COL1A1 binding to integrin α3β1 in determining the poor prognosis of PDAC patients.

[0073] To substantiate the key role of oncogenic COL1A1 in PDAC, as suggested by the bioinformatic analysis of clinical data, PDAC tissues were collected from patients and the expression and binding of COL1A1 and integrins α3 and β1 were investigated. First, the expression of COL1A1 and integrins α3 and β1 was found in the human PDAC tissues by western blot assay (Figs. 5-7). Furthermore, to identify the oncogenic COL1A1 in the human PDAC tissues, EpCAM that was overexpressed on pancreatic tumor cells but not on normal cells was applied to differentiate the pancreatic cancer cells from fibroblasts. As shown in Fig. 1h, oncogenic COL1A1 was adjacent/bound to the pancreatic cancer cells labeled by EpCAM. Additionally, the expression of oncogenic COL1A1 in the human PDAC tissues was substantiated by investigating the binding of COL1A1 to integrin α3 and β1. As shown in Fig. 1i and Fig. 8, there was clear overlapping between oncogenic COL1A1 and both integrins α3 and β1.

[0074] Collectively, both bioinformatic analysis and human PDAC tissue characterization demonstrated the expression of oncogenic COL1A1 and highlighted its role in negatively impacting the treatment efficacy of PDAC, suggesting that it can potentially serve as a therapeutic target. Thus, in this study, to target the oncogenic collagen to improve PDAC immunotherapy, an engineered bacteria delivery system was developed to shuttle collagenases to the tumor site to deplete the oncogenic collagen and block the related integrin α3β1-FAK signaling pathway, which holds the promise to synergize with immune checkpoint inhibitors for enhanced PDAC treatment efficacy. Given the extremely dense ECM deposition that blocks the access of therapeutics to the cancer cells, *Escherichia coli* Nissle 1917 (designated EcN) was used as it has a great biosafety profile as the drug delivery carrier (Fig. 1j). EcN has been demonstrated to actively target the tumor site by homing to the hypoxic tumor region. Furthermore, the mobility of EcN could increase the permeability of therapeutics and enable the effective delivery of drugs toward tumor parenchyma instead of

only accumulating at the margins of PDAC by traditional delivery systems. Besides, the collagenases and aPD-L1 antibodies were crosslinked together through a ROS-responsive linker to assemble into a protein cage, which was further conjugated on the surface of EcN. Mechanistically, the EcN-based delivery systems could penetrate through the ECM barriers into the deep tumor tissue, and then under the trigger of the ROS at the PDAC site, the collagenase was released to degrade the oncogenic collagen and block the integrin α3β1-FAK signaling pathway. FAK signaling inhibition could decrease the infiltration of immunosuppressive cells such as MDSCs, and AKT/MAPK signaling inhibition could reduce tumor cell proliferation and survival. Moreover, the released anti-PD-L1 could block the PD-L1 on the surface of tumor cells to prevent immune escape and reestablish immune surveillance, synergizing with the oncogenic collagen depletion to enhance the efficacy of PDAC immunotherapy.

EXAMPLE 2: PREPARATION AND CHARACTERIZATION OF Col/aPD-L1@ECN

[0075] The ROS-sensitive linker (ROS-L), which was characterized by nuclear magnetic resonance (NRM) and mass spectroscopy (data not shown), was first synthesized. ROS-sensitive linkers were utilized to prepare the Col/aPD-L1 protein cage by crosslinking with the amino groups in the collagenase and aPD-L1 (Fig. 9a). The Col/aPD-L1 protein cage showed a uniform spherical morphology under TEM observation, with a particle size around 160 nm (Fig. 9b). As shown in Fig. 9c, the zeta potential of the Col/aPD-L1 protein cage was about -8 mV. After the successful preparation of Col/aPD-L1 protein cages, they were conjugated onto the surface of EcN by an amidation reaction. The existence of Col/aPD-L1 protein cages on the EcN was characterized by the transmission electron microscopy (TEM) observation, as shown in Fig. 9d. Moreover, the aPD-L1 was labeled with FITC and collagenase with Rhodamine B and conjugation of Col/aPD-L1 protein cages on EcN was verified by detecting the distinct fluorescence from collagenases and aPD-L1 in the final formulation through flow cytometry (Fig. 9e). Based on the confocal assay (Fig. 9f), the FITC-labeled aPD-L1 and Rhodamine B-labeled collagenase were merged together with the Hoechst 3342-labeled EcN, further proving that the protein cages were successfully conjugated on the surface of EcN. Furthermore, the aPD-L1 release was verified by the ELISA assay, and the addition of H_2O_2 representing elevated ROS levels could substantially increase the aPD-L1 release rate with over 70% of aPD-L1 released within 72 hours, while without ROS, only less than 10% of aPD-L1 release was detected (Fig. 9g).

EXAMPLE 3: THE *IN VITRO* MOBILITY AND *IN VIVO* PDAC-SELECTIVE ACCUMULATION OF Col/aPD-L1@ECN

[0076] EcN is a facultative anaerobe with flagella, which endows it with movement and penetration ability, particularly towards the hypoxic tumor area. To investigate the *in vitro* mobility of Col/aPD-L1@ECN, a tissue-mimetic gel made from commercial Matrigel® was applied to simulate the ECM in the TME and the migration and penetration of Col/aPD-L1@EcN that was embedded in an alginate scaffold was evaluated (Fig. 10a). As shown in Fig. 10b, there was a substantial amount of Col/aPD-L1@ECN in the tissue-mimetic gel after 4 h. Notably, the Col/aPD-L1@ECN actively migrated to the tissue-mimetic gel with the farthest migration depth of over 200 μm, indicating the potent mobility of Col/aPD-L1@ECN. To quantitatively evaluate the impact of Col/aPD-L1 on the tissue penetration capability of EcN, we further established a transwell device to compare the ECM invasion ability between EcN and Col/aPD-L1@ECN. As shown in Fig. 10c, the Matrigel® was added to the top chamber to set up a dense ECM layer to mimic the strong desmoplasia in PDAC, and the number of bacteria penetrating the Matrigel® layer was used as the indicator to reflect their tissue penetration capability. As shown in Fig. 10d, after 8 h, more than 30% of both initially seeded EcN and Col/aPD-L1@ECN penetrated into the bottom chamber, and there was no significant difference in the bacteria amount between EcN and Col/aPD-L1@ECN, suggesting that the decoration of Col/aPD-L1 on the surface of EcN in the experimental setting did not substantially impact the mobility and penetration capability of EcN.

[0077] The development of desmoplasia shields PDAC from traditional treatments, including chemotherapy, and imposes significant barriers to drug penetration. Intratumoral pressure, dysfunctional vasculature and strong hypoxia caused by the intratumoral desmoplastic reaction during PDAC development contribute to the poor treatment efficacy. EcN has been well demonstrated with potent tumor hypoxia targeting preference in many cancers, including PDAC. To demonstrate the PDAC-selective accumulation of Col/aPD-L1@ECN, an orthotopic PDAC model was established by injecting KPC (*Kras*$^{G12D/+}$; *Trp53*$^{-/-}$; *Pdx1-Cre*) tumor cells into the pancreas of syngeneic C57BL/6J mice. This orthotopic KPC model recapitulates histopathological features of human PDAC, including extensive desmoplasia, a strong immunosuppressive microenvironment with extremely limited infiltrating T cells, robust resistance to the gemcitabine-based chemotherapy, and immunotherapy such as aPDL1 antibodies and CD40 agonists. As shown in Fig. 10e, f, systemic injection of Col/aPD-L1@ECN preferentially accumulated at the PDAC, while

Col/aPD-L1 only showed limited abundance at the tumor site. Besides, the fluorescence intensity of protein cages distributed in the tumor tissue in Col/aPD-L1@ECN group was about three times higher than that in Col/aPD-L1 group, demonstrating the superior tumor-selective accumulation ability of the Col/aPD-L1@ECN (Fig. 10g, h). Moreover, the existence and tumor penetration capability of Col/aPD-L1@ECN was further substantiated by fluorescent imaging, in which more Col/aPD-L1@ECN was found in the PDAC parenchyma compared to Col/aPD-L1(Fig. 10i).

EXAMPLE 4: ANTITUMOR EFFICACY OF Col/aPD-L1@ECN IN AN ORTHOTOPIC PANCREATIC CANCER MODEL

[0078] To demonstrate the direct secretion of oncogenic collagen from pancreatic cancer cells, the supernatant of cultured KPC cells was collected and a western-blot assay was performed to assess for collagen protein. As shown in Fig. 11a, collagen expression was observed in the supernatant of pancreatic cancer cells. Furthermore, to explore the impact of oncogenic collagen depletion on the PDAC cells, 3D PDAC tumor spheroids were established as shown in Fig. 11b. Oncogenic collagen expression was observed in the tumor spheroid and more importantly, the Col/aPD-L1@ECN therapeutic strategy could deplete the oncogenic collagen and reduce the spheroid volume, demonstrating that oncogenic collagen-based depletion strategy could decrease the proliferation and survival of the tumor cells (Fig. 11c).

[0079] To evaluate the antitumor efficacy of Col/aPD-L1@ECN against PDAC, an orthotopic PDAC cancer model was established and treated with different regimens, as illustrated in Fig. 11d. During the treatment course, the body weight of the mice was monitored, and there were no significant differences among different therapeutic groups (Fig. 11e). Moreover, the hematoxylin and eosin staining (H&E) assay of the major organs further demonstrated the good biosafety of Col/aPD-L1@ECN, as evidenced by negligible pathological damage in the Col/aPD-L1@ECN group compared to PBS group (Fig. 12). In addition, the orthotopic PDAC growth was monitored by IVIS imaging based on the bioluminescence signals from luciferase-expressing KPC cells, and we found that after 14 days, there were strong bioluminescence signals observed in the pancreas of mice indicating the successful establishment of the orthotopic PDAC model. For the PBS group, as shown in Fig. 11f, the bioluminescence intensity increased more than 13-fold on day 21 compared with day 0, and EcN showed a similar trend in the increase of bioluminescence signals, indicating negligible antitumor effects. Col@ECN, Col/aPD-L1, Col/aPD-L1+ECN, and aPD-L1@ECN

exhibited moderate antitumor effects with relatively strong bioluminescence intensities on day 21 (Fig. 11g). Notably, the PDAC bearing mice treated with Col/aPD-L1@ECN displayed the weakest bioluminescence intensity demonstrating its most potent antitumor efficacy among all therapeutic groups. More importantly, Col/aPD-L1@ECN prolonged the median survival of PDAC-bearing mice from 24.5 days (PBS) to 56 days, which was significantly longer than that of aPD-L1@ECN (41 days), Col/aPD-L1+ECN (35 days), Col/aPD-L1 (33.5 days), Col@ECN (33.5 days) and ECN (26 days), further substantiating the synergistic effects between oncogenic collagen depletion and immune checkpoint blockade (Fig. 11h).

EXAMPLE 5: IMMUNE ACTIVATION OF Col/aPD-L1@ECN IN AN ORTHOTOPIC PDAC MODEL

[0080] PDAC is notorious for the immune desert TME and extremely limited infiltration of effector T cells. To verify if the Col/aPD-L1@ECN-based therapeutic strategy could generate robust immune activation by increasing infiltrating effector immune cells and reactivating exhausted T cells, the functional immune cell profiles in PDAC were evaluated. The $CD8^+$ T cell infiltration was first evaluated by flow cytometry assay. About 32.7% of $CD8^+$ T cells were observed in the Col/aPD-L1@ECN treatment group, significantly higher than that in the aPD-L1@ECN (23.7%) group, Col/aPD-L1+ECN group (15.5%), and Col@ECN group (13.4%) (Fig.13a). Moreover, as shown in Fig. 13b, quantitatively, Col/aPD-L1@ECN therapeutic strategy showed the highest number of infiltrated $CD8^+$ T cell in the tumor tissue compared with other treatment groups, indicating Col/aPD-L1@ECN could increase the infiltration of $CD8^+$ T cells that could be attributed to the modulation of the immunosuppressive TME through depletion of oncogenic collagen. In addition, the Granzyme B^- $CD8^+$ T cell infiltration was enhanced after Col/aPD-L1@ECN treatment compared to other treatments, demonstrating that Col/aPD-L1@ECN treatment could activate and promote an effector phenotype in the infiltrating $CD8^+$ cells (Fig. 13c). As shown in Fig. 13d, e, ELISA assays were further utilized to detect the IFNγ and TNFα expression levels in PDAC tissues, and we found that Col/aPD-L1@ECN promoted the IFNγ expression. Also, compared with the aPD-L1@ECN group and Col/aPD-L1+ECN group, the higher TNFα expression level in the Col/aPD-L1@ECN group further substantiated the strong immune activation ability of the Col/aPD-L1@ECN therapeutic strategy. Furthermore, the expression levels of various chemokines and cytokines were evaluated. As shown in Fig. 13f, the expression of immune activation chemokines and cytokines significantly increased in the

Col/aPD-L1@ECN group compared to that in other groups, indicating the activated immune status in the PDAC. To further validate the CD8 T cell infiltration, an immune fluorescence assay was performed to visualize the CD8 T cell infiltration in the tumor tissue. As shown in Fig. 13g, there was more CD8 T cell infiltration in the Col/aPD-L1@ECN group compared to the PBS group. Collectively, the Col/aPD-L1@ECN therapeutic strategy could degrade the oncogenic collagen to block the integrin α3β1 signaling pathway, thus enhancing the T cell infiltration to cooperate with the anti-PD-L1 to arouse strong antitumor immune response (Fig. 13h).

EXAMPLE 6: Col/aPD-L1@ECN DEPLETES ONCOGENIC COLLAGEN AND MODULATES INTEGRIN α3β1-RELATED SIGNALING PATHWAYS

[0081] As shown in Fig. 14a, the modulating effect of Col/aPD-L1@ECN for the oncogenic collagen and the downstream signaling pathways was explored, including FAK, AKT, and MAPK. First, the oncogenic collagen expression was verified in pancreatic tumor tissue *in vivo* and it was found that Col/aPD-L1@ECN significantly decreased the oncogenic collagen expression compared with the PBS group (Fig. 14b). Moreover, FAK is a non-receptor tyrosine kinase and a connexin that mainly regulates adhesion signaling and cell migration. Besides, FAK can also promote cell survival in stress response, in which overexpression of FAK can help tumor cells escape from immune surveillance. Therefore, FAK inhibition is considered a potentially promising strategy to overcome adaptive resistance to tumor microenvironment-targeted immunotherapy. As shown in Figs. 14c and Fig. 14f, the activated FAK is overexpressed in the pancreatic tumor tissue, which could contribute to the highly immunosuppressive TME in PDAC. Encouragingly, after the treatment of Col/aPD-L1@ECN, the activated FAK expression was significantly reduced, only showing about 26.7% of expression level compared to the PBS group. Successful FAK inhibition could cooperate with the immune checkpoint blockade therapy to effectively activate the immune system and overcome the immune suppression in PDAC. Additionally, MAPK is a group of serine-threonine protein kinases that can be activated by different extracellular stimuli, such as cytokines, neurotransmitters, hormones, cell stress, and cell adhesion. The MAPK pathway is one of the common intersection points of signal transduction pathways such as cell proliferation, stress, inflammation, differentiation, functional synchronization, transformation, and apoptosis. In addition, the AKT signaling pathway plays an important role in regulating the growth and proliferation of tumor cells, promoting cell invasion and metastasis, accelerating angiogenesis, and enhancing the

tolerance of tumor cells to chemotherapy and radiotherapy. Recent clinical results showed that regardless of the level of PD-L1 expression, the AKT inhibitor ipatasertib combined with PD-L1 monoclonal antibodies atezolizumab and Taxol® had an overall response rate of 73% in the treatment of triple-negative breast cancer (TNBC). In the therapeutic strategy, Col/aPD-L1@ECN significantly decreased the phosphorylated AKT (p-AKT) and phosphorylated MAPK (p-MAPK) expression from the immunofluorescence assay (Fig. 14d and Fig. 14e). In the Col/aPD-L1@ECN group, the expression of activated AKT decreased by about 80%, and activated MAPK decreased about 66.7% compared to those in the PBS group (Fig. 14g and Fig. 14h), demonstrating that oncogenic collagen depletion could regulate the AKT and MAPK signaling pathway to enhance the cancer immunotherapy efficacy.

EXAMPLE 7: ANTITUMOR EFFICACY OF Col/aPD-L1@ECN IN A METASTATIC BREAST CANCER MODEL

[0082] To further validate the applicability of the oncogenic collagen-depleting approach, the treatment efficacy was tested on a 4T1 metastatic breast cancer, which is characterized by abundant collagen expression. First, the oncogenic collagen secretion from 4T1 cells was demonstrated by western blot assay (Fig. 15). Next, as shown in Fig. 16a, the orthotopic metastatic breast cancer model was established to evaluate if our therapeutic strategy could facilitate metastatic breast cancer immunotherapy. Col/aPD-L1@ECN treatment significantly inhibited tumor growth with all tumor volumes less than 400 mm^3 on day 20, and 4T1 tumor-bearing mice in Col/aPD-L1@ECN group exhibited slower tumor growth than that in the Col@ECN group, Col/aPD-L1+ECN group, and aPD-L1@ECN group (Fig. 16b, 7c). In addition, as shown in Fig. 16d, the body weight of mice in different treatment groups showed negligible differences during the treatment course, demonstrating the great biosafety profiles of the therapeutic strategies. Moreover, the survival of the 4T1 tumor-bearing mice was monitored, and Col/aPD-L1@ECN treatment prolonged the median survival of the mice from 27.5 days (PBS) to 58 days, with half of the mice still alive on day 60, significantly longer than that in Col@ECN group (35.5 days), Col/aPD-L1+ECN group (42 days) and aPD-L1@ECN group (46 days) (Fig. 16e). To further validate the therapeutic efficacy of Col/aPD-L1@ECN in treating breast cancer metastasis, we established a metastatic breast cancer model by i.v. injecting 4T1 cells (Fig. 16f). On day 21, the lung tissue was collected, and it was found that Col/aPD-L1@ECN could potently prevent the

lung metastasis as evidenced by the significantly decreased number and size of the lung metastatic nodules (Fig. 16g, 7h).

[0083] The use of the terms "a" and "an" and "the" and similar referents (especially in the context of the following claims) are to be construed to cover both the singular and the plural, unless otherwise indicated herein or clearly contradicted by context. The terms first, second etc. as used herein are not meant to denote any particular ordering, but simply for convenience to denote a plurality of, for example, layers. The terms "comprising", "having", "including", and "containing" are to be construed as open-ended terms (i.e., meaning "including, but not limited to") unless otherwise noted. Recitation of ranges of values are merely intended to serve as a shorthand method of referring individually to each separate value falling within the range, unless otherwise indicated herein, and each separate value is incorporated into the specification as if it were individually recited herein. The endpoints of all ranges are included within the range and independently combinable. All methods described herein can be performed in a suitable order unless otherwise indicated herein or otherwise clearly contradicted by context. The use of any and all examples, or exemplary language (e.g., "such as"), is intended merely to better illustrate the invention and does not pose a limitation on the scope of the invention unless otherwise claimed. No language in the specification should be construed as indicating any non-claimed element as essential to the practice of the invention as used herein.

[0084] While the invention has been described with reference to an exemplary embodiment, it will be understood by those skilled in the art that various changes may be made and equivalents may be substituted for elements thereof without departing from the scope of the invention. In addition, many modifications may be made to adapt a particular situation or material to the teachings of the invention without departing from the essential scope thereof. Therefore, it is intended that the invention not be limited to the particular embodiment disclosed as the best mode contemplated for carrying out this invention, but that the invention will include all embodiments falling within the scope of the appended claims. Any combination of the above-described elements in all possible variations thereof is encompassed by the invention unless otherwise indicated herein or otherwise clearly contradicted by context.

CLAIMS

1. A drug delivery system, comprising

protein nanocages comprising collagenase proteins and anti-immune checkpoint inhibitor antibodies,

wherein the protein nanocages are conjugated to the surface of a probiotic bacterial carrier.

2. The drug delivery system of claim 1, wherein the anti-immune checkpoint inhibitor antibodies comprise anti-PD-L1 antibodies, anti-CTLA-4 antibodies, anti-PD-1 antibodies, anti-TIM-3 antibodies, anti-LAG-3 antibodies, or a combination thereof.

3. The drug delivery system of claim 1, wherein the anti-immune checkpoint inhibitor antibodies comprise atezolizumab, avelumab, durvalumab, ipilimumab, tremelimumab, cemiplimab, pembrolizumab, nivolumab, cemiplimab, retifanlimab, dostarlimab, LY3321367, LY3300054, Sym023, BMS-986258. ICAGN02390, RO7121661, BGBA425, TSR-022, MGB453, relatlimab, fianlimab, Sym022, GSK2831781, INCAGN02385, TSR-033, ieramilimab, favezelimab, or a combination thereof.

4. The drug delivery system of any of the foregoing claims, wherein the collagenase comprises collagenase from *Clostridium histolyticum*, *C. perfringens*, *Vibrio alginolyticus*, a *Streptomyces* sp., a *Pseudomonas* sp., or a combination thereof.

5. The drug delivery system of any of the foregoing claims, wherein the collagenase comprises Type 1 collagenase from *Clostridium histolyticum*.

6. The drug delivery system of any of the foregoing claims, wherein the collagenase proteins and anti-immune checkpoint inhibitor antibodies are assembled into the protein nanocage with a bifunctional linker, wherein the bifunctional linker comprises a reactive oxygen species (ROS)-responsive linker, a glutathione (GSH)-responsive linker, a pH-responsive linker, an enzyme-responsive linker, or a combination thereof.

7. The drug delivery system of any of the foregoing claims, wherein the collagenase proteins and anti-immune checkpoint inhibitor antibodies are assembled into the protein nanocage with a reactive oxygen species (ROS)-responsive linker.

8. The drug delivery system of any of the foregoing claims, wherein the protein nanocages have diameters of 90 to 300 nm.

9. The drug delivery system of any of the foregoing claims, wherein the probiotic bacterial carrier comprises a *Clostridium*, *Bifidobacterium*, *Listeria*, *Escherichia coli*, or *Salmonella* species.

10. The drug delivery system of any of the foregoing claims, wherein the probiotic bacterial carrier comprises *Escherichia coli* strain Nissle 1917.

11. The drug delivery system of any of the foregoing claims, wherein the ratio of protein nanocages to probiotic bacterial carrier is 10 to 100 pg proteins per ECN1917.

12. A pharmaceutical composition comprising the drug delivery system of any of claims 1-11 and a pharmaceutically acceptable excipient.

13. A method of making a drug delivery system, comprising

preparing protein nanocages by contacting collagenase proteins, anti-immune checkpoint inhibitor antibodies, and a bifunctional linker in a solvent for a time and temperature to provide the protein nanocages having diameters of 90 to 300 nm, and

contacting the protein nanocages with probiotic bacteria in the presence of a crosslinking agent to conjugate the protein nanocages to the surface of the probiotic bacteria.

14. The method of claim 13, wherein the crosslinking agent is 1-ethyl-3-(-3-dimethylaminopropyl) carbodiimide hydrochloride (EDC)/ *N*-hydroxysuccinimide (NHS) or ECD/Sulfo-NHS.

15. A method of treating a patient with a hypoxic tumor characterized by oncogenic collagen, comprising systemically administering to the patient the composition of claim 12.

16. The method of claim 15, wherein the patient has head and neck, breast, pancreatic, skin, prostate, liver, cervical or brain cancer.

17. The method of claim 15, wherein the patent has pancreatic ductal adenocarcinoma (PDAC) or locally advanced breast cancer.

18. The method of claim 15, wherein the composition is administered by intravenous injection, by intramuscular injection, by intraperitoneal injection, or by subcutaneous injection.

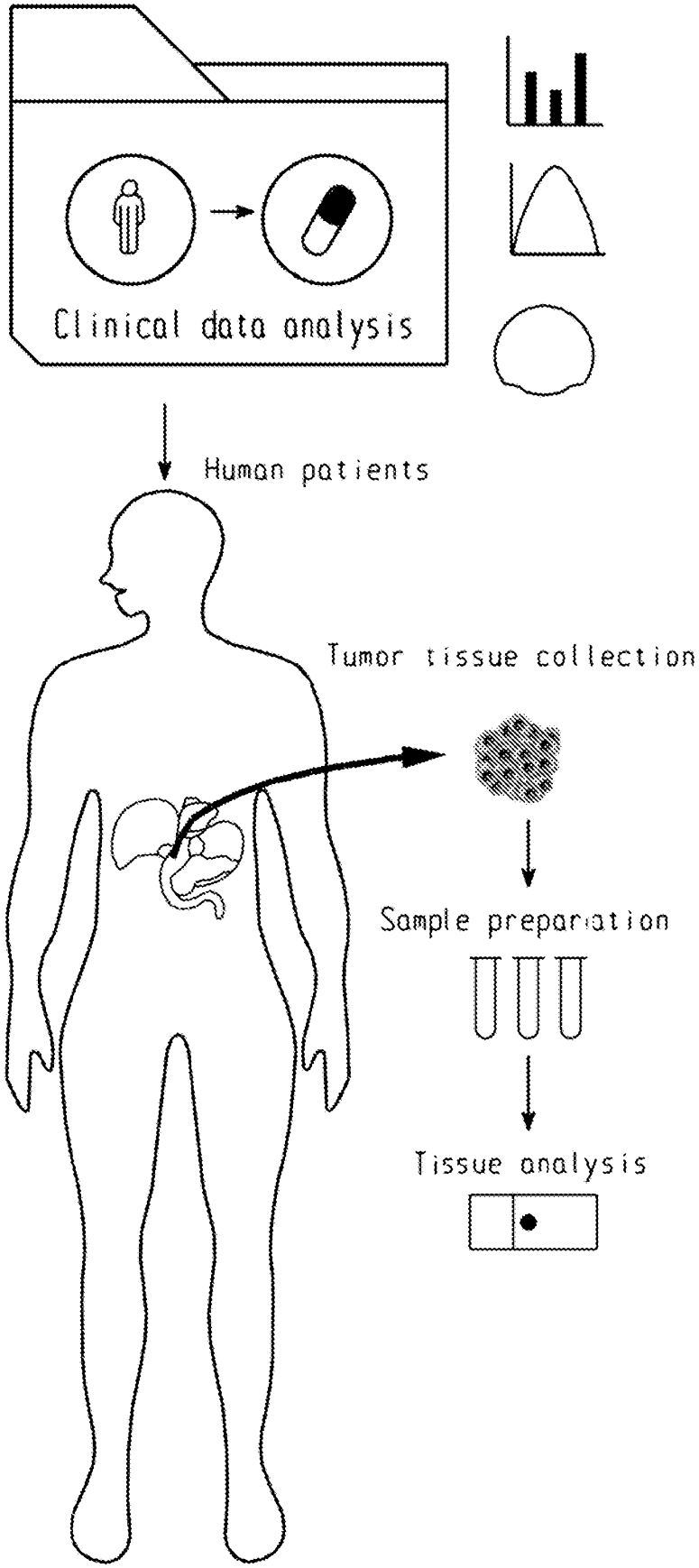
Clinical data analysis
Human patients
Tumor tissue collection
Sample preparation
Tissue analysis

Fig. 1A

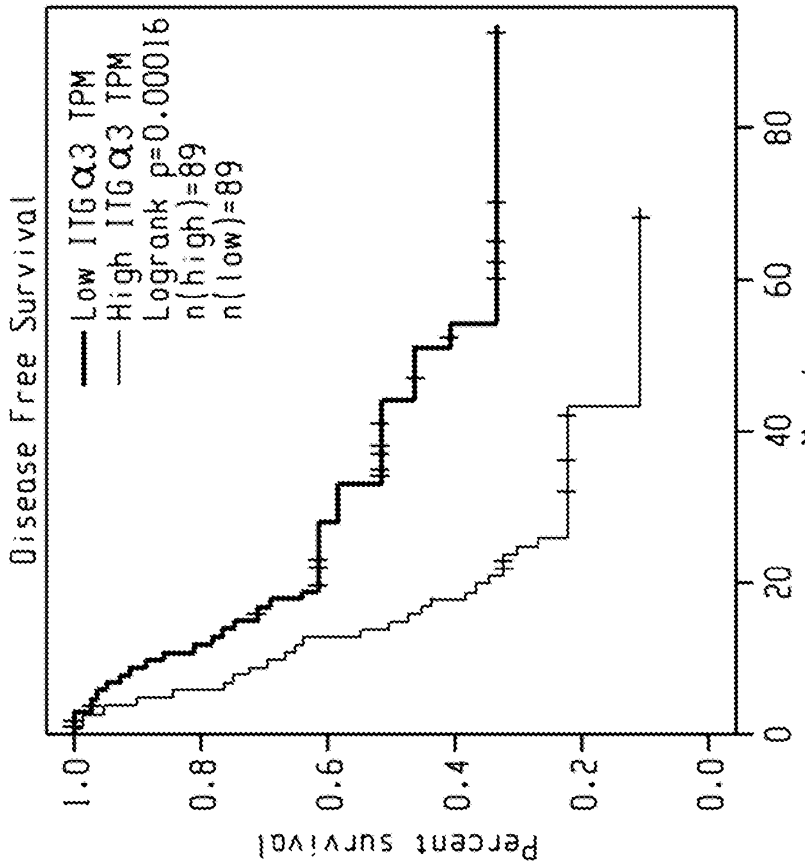
Disease Free Survival
Low ITGα3 TPM
High ITGα3 TPM
Logrank p=0.00016
n(high)=89
n(low)=89
Percent survival
1.0
0.8
0.6
0.4
0.2
0.0
0
20
40
60
80
Months

Fig. 1C

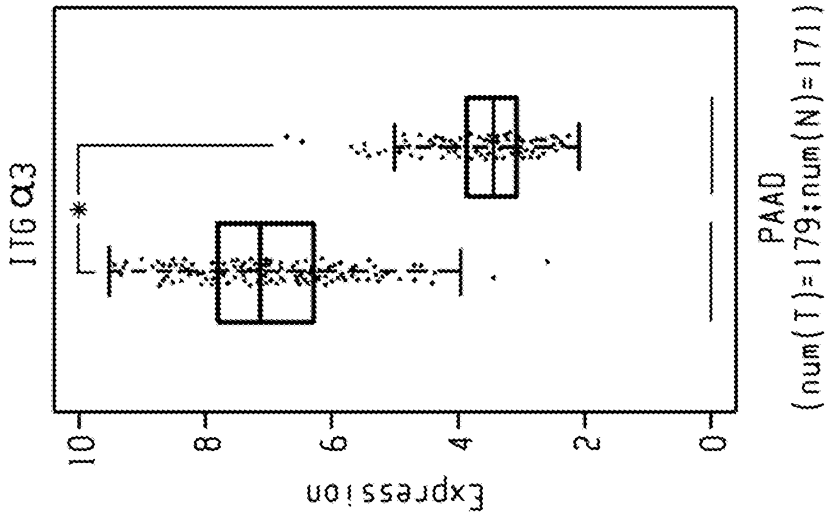
ITGα3
Expression
10
8
6
4
2
0
PAAD
(num(T)=179;num(N)=171)

Fig. 1B

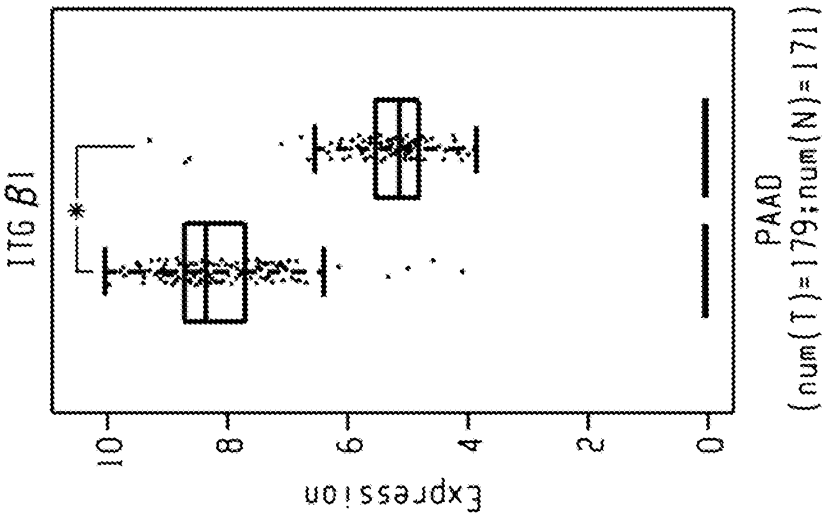
ITG B1
Expression
10
8
6
4
2
0
PAAD
(num(T)=179;num(N)=171)

Fig. 1E

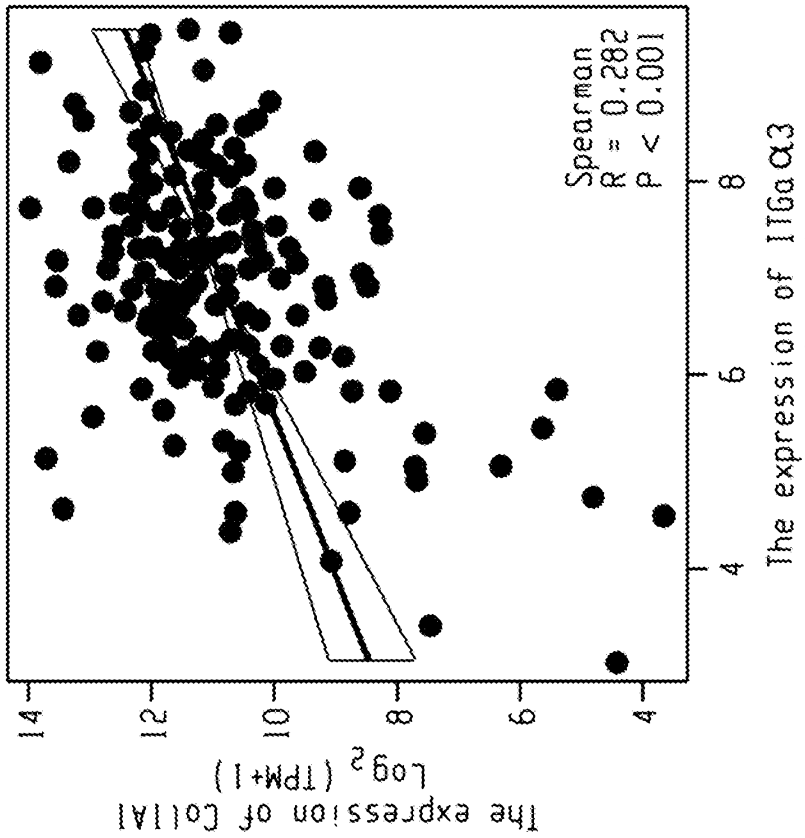
The expression of COL1A1
Log2 (TPM+1)
14
12
10
8
6
4
Spearman
R = 0.282
P < 0.001
4
6
8
The expression of ITGa3
Log2 (TPM+1)

Fig. 1D

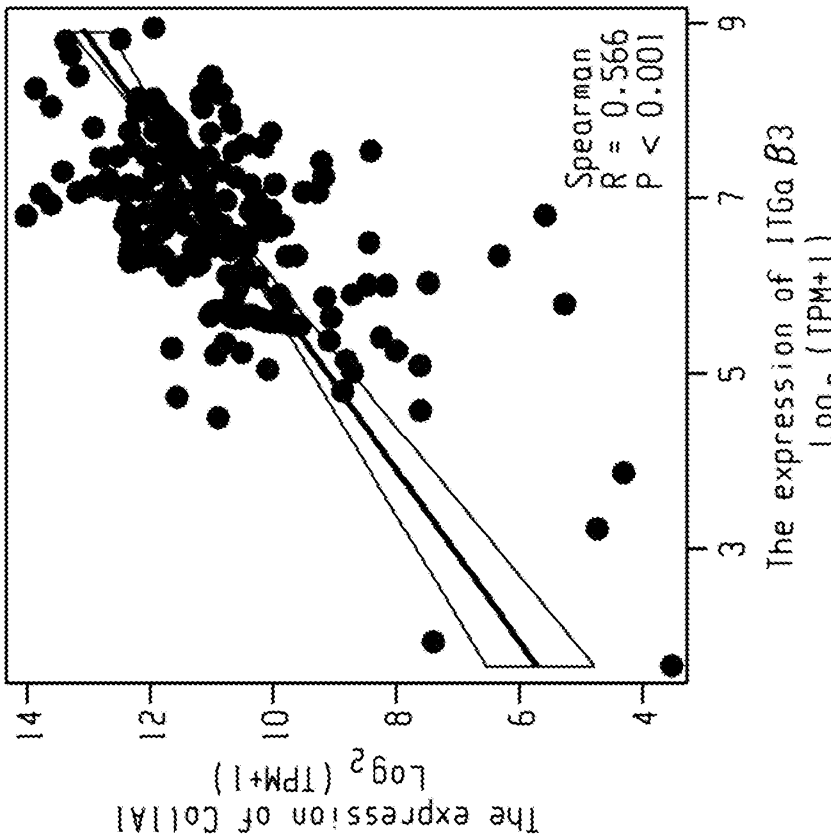
The expression of COL1A1
Log2 (TPM+1)
14
12
10
8
6
4
Spearman
R = 0.566
P < 0.001
3
5
7
9
The expression of ITGα β3
Log2 (TPM+1)

Fig. 1D

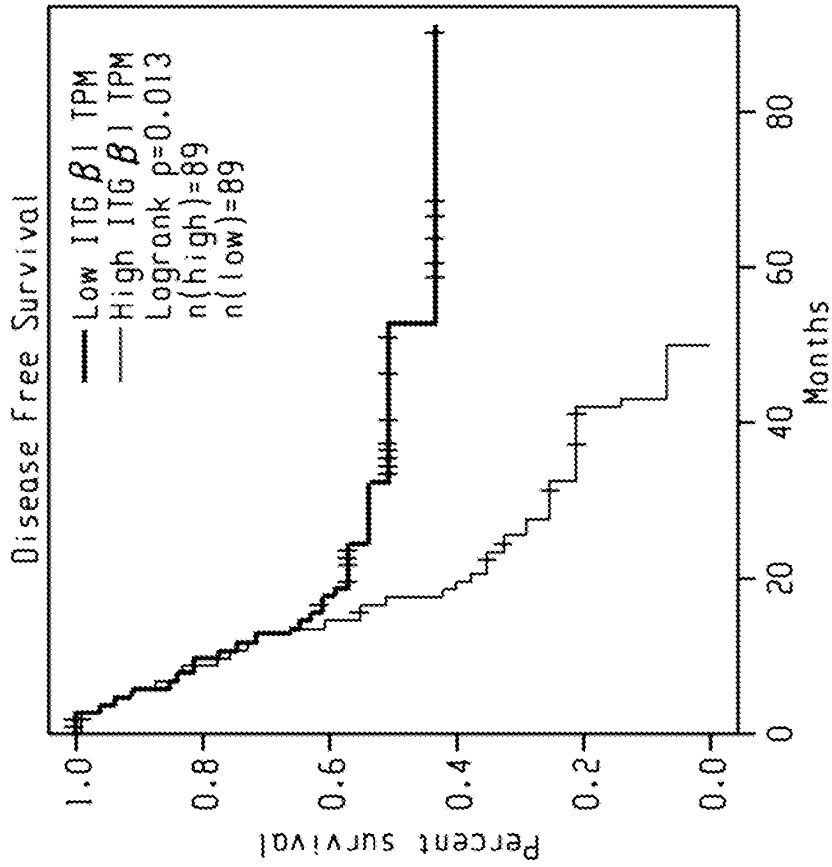
Disease Free Survival
Low ITGβ1 TPM
High ITGβ1 TPM
Logrank p=0.013
n(high)=89
n(low)=89
Percent survival
1.0
0.8
0.6
0.4
0.2
0.0
0
20
40
60
80
Months

Fig. 1F

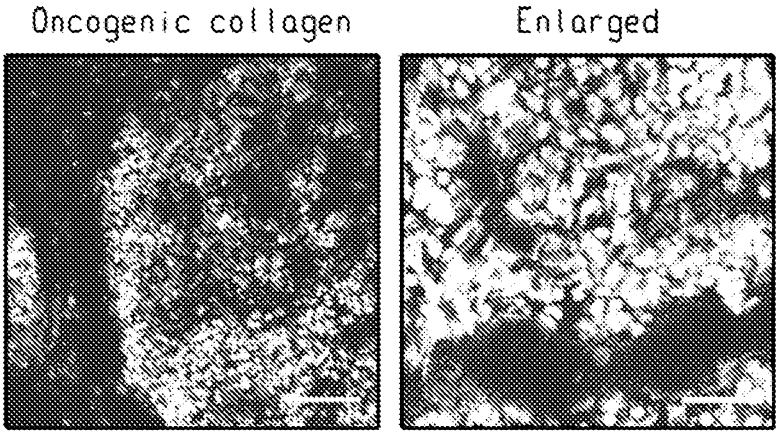

Fig. 1H

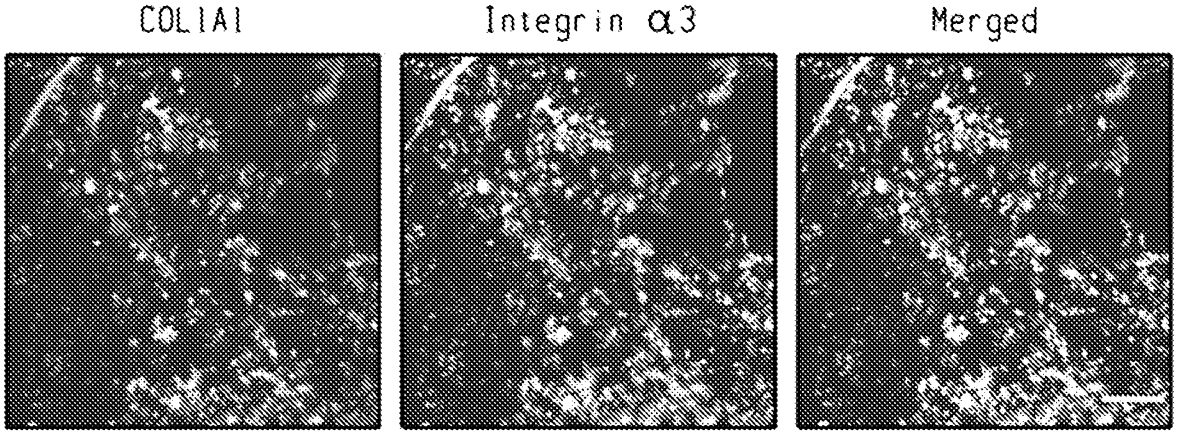

Fig. 1I

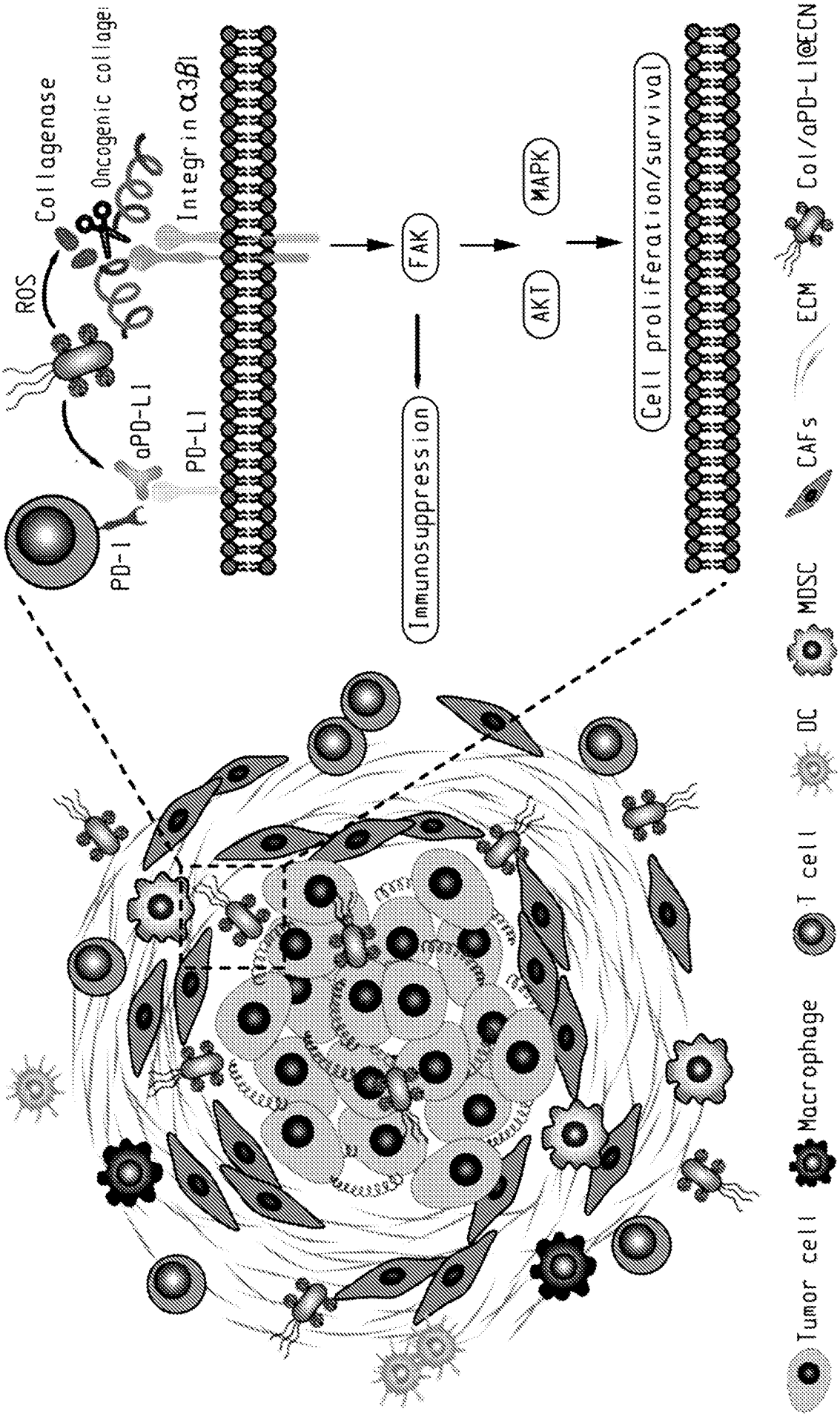
ROS
Collagenase
Oncogenic collage
Integrin α3β1
aPD-L1
PD-L1
PD-1
FAK
AKT
MAPK
Immunosuppression
Cell proliferation/survival
Tumor cell
Macrophage
T cell
DC
MDSC
CAFs
ECM
Col/aPD-L1@ECN

Fig. 1J

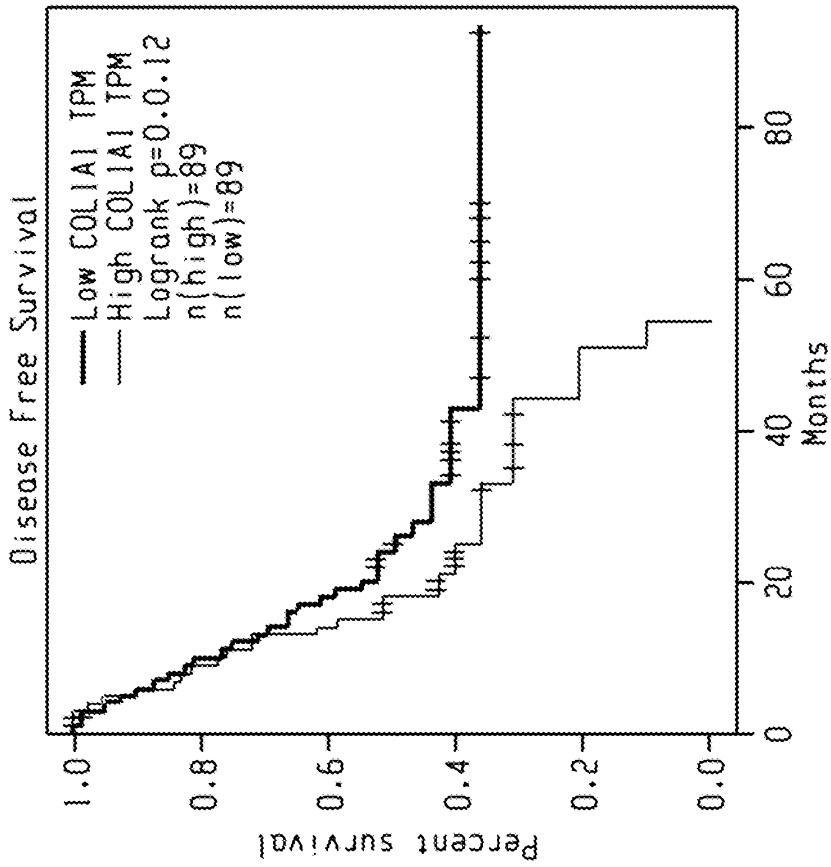
Disease Free Survival
Low COL1A1 TPM
High COL1A1 TPM
Logrank p=0.012
n(high)=89
n(low)=89
Percent survival
1.0
0.8
0.6
0.4
0.2
0.0
0
20
40
60
80
Months

Fig. 3

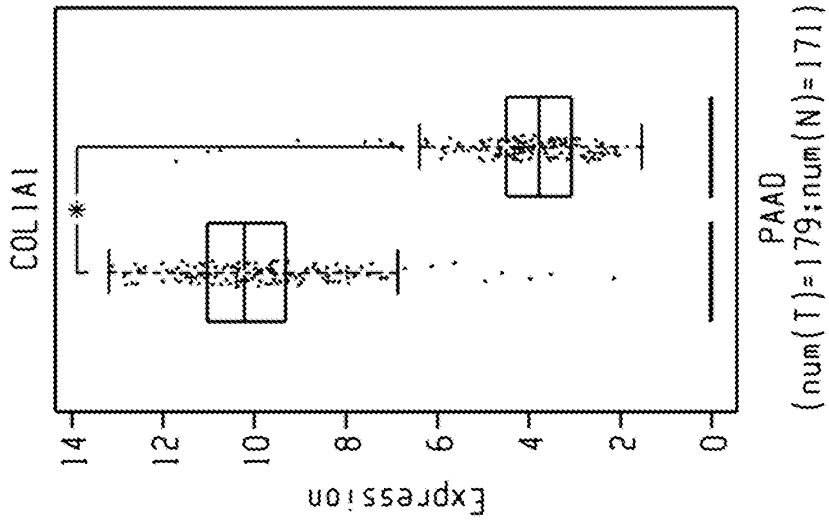
COL1A1
Expression
14
12
10
8
6
4
2
0
PAAD
(num(T)=179;num(N)=171)

Fig. 2

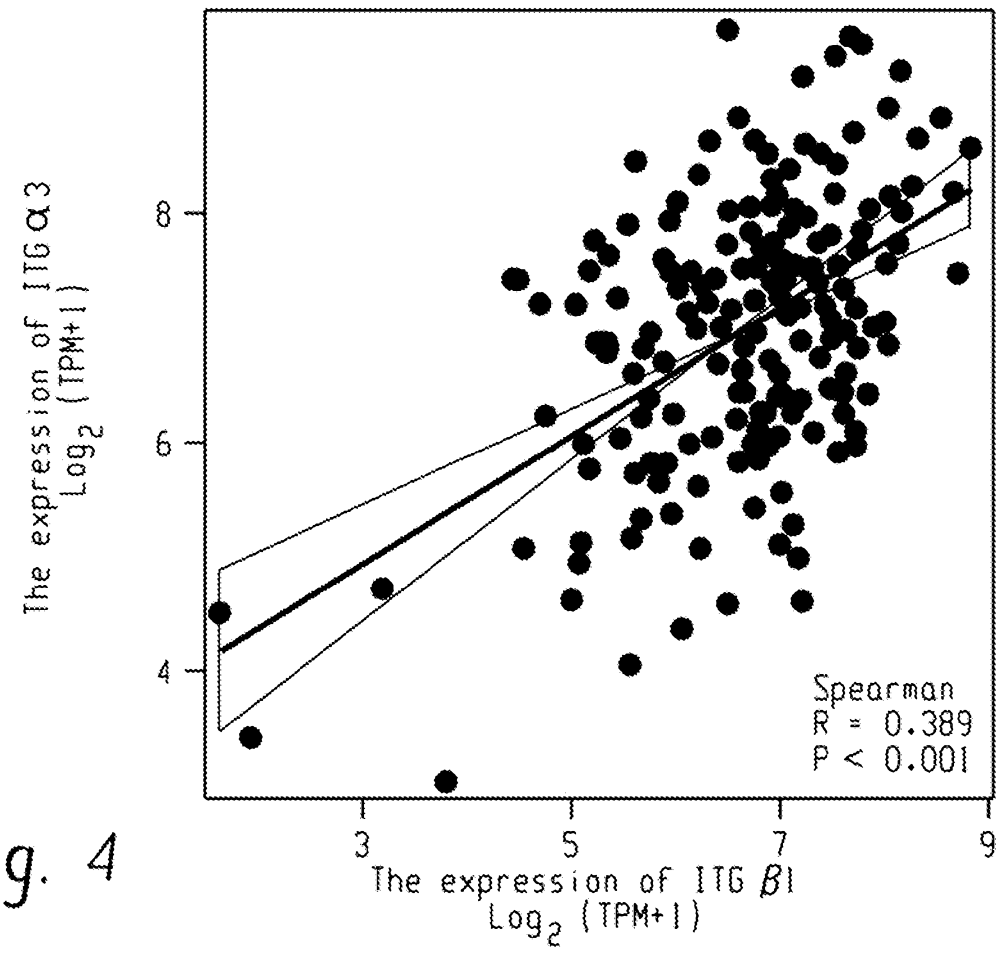
The expression of ITG α3
Log2 (TPM+1)
8
6
4
3
5
7
9
The expression of ITG β1
Log2 (TPM+1)
Spearman
R = 0.389
P < 0.001

Fig. 4

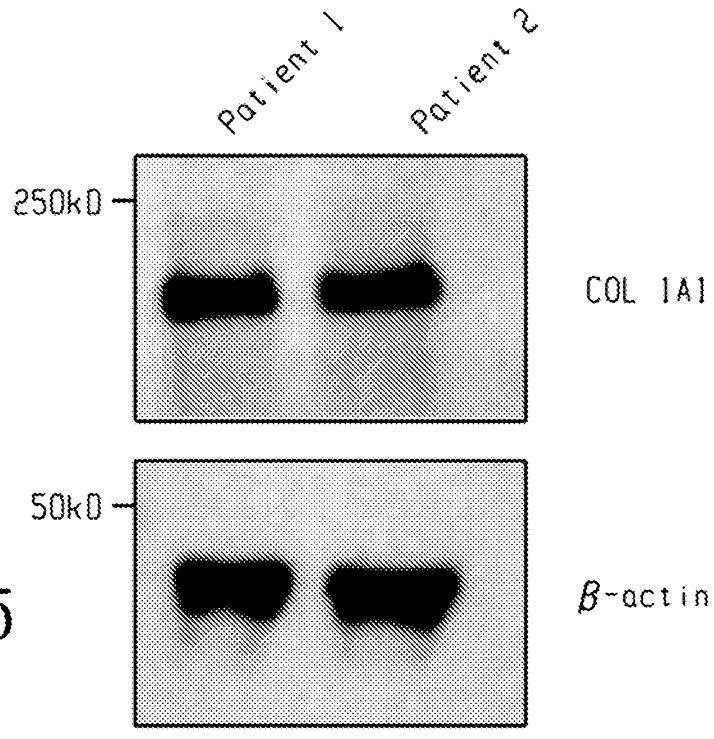
Patient 1
Patient 2
250kD
COL 1A1
50kD
β-actin

Fig. 5

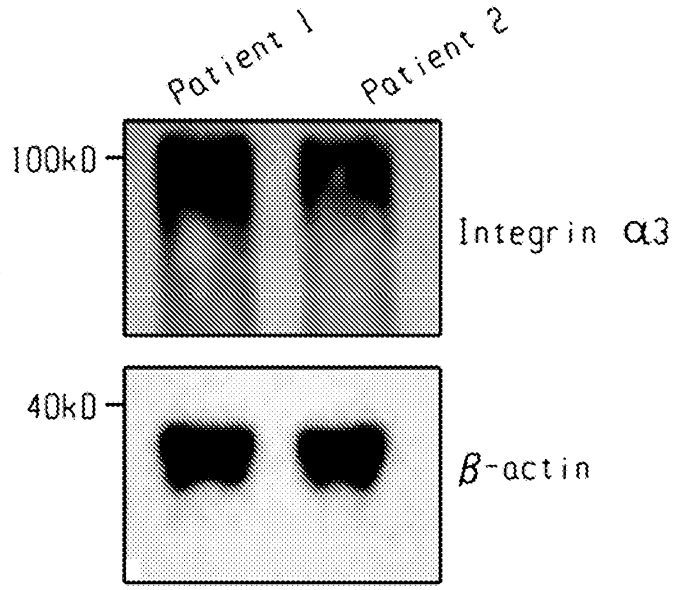

Fig. 6

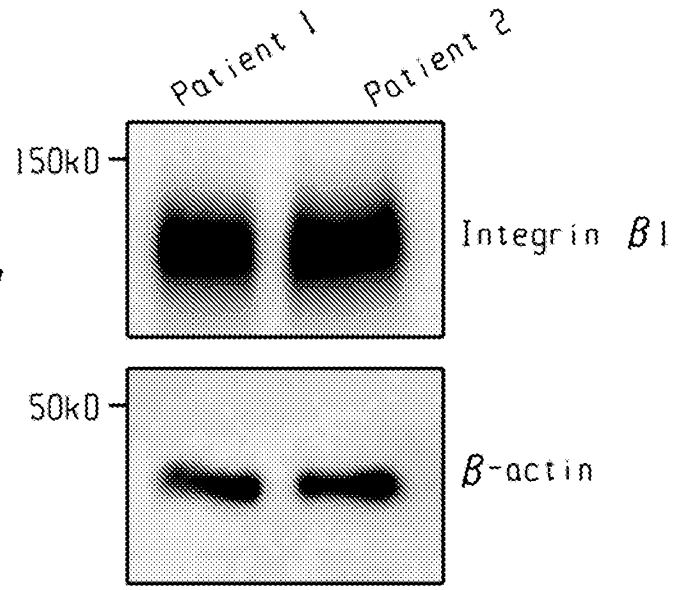

Fig. 7

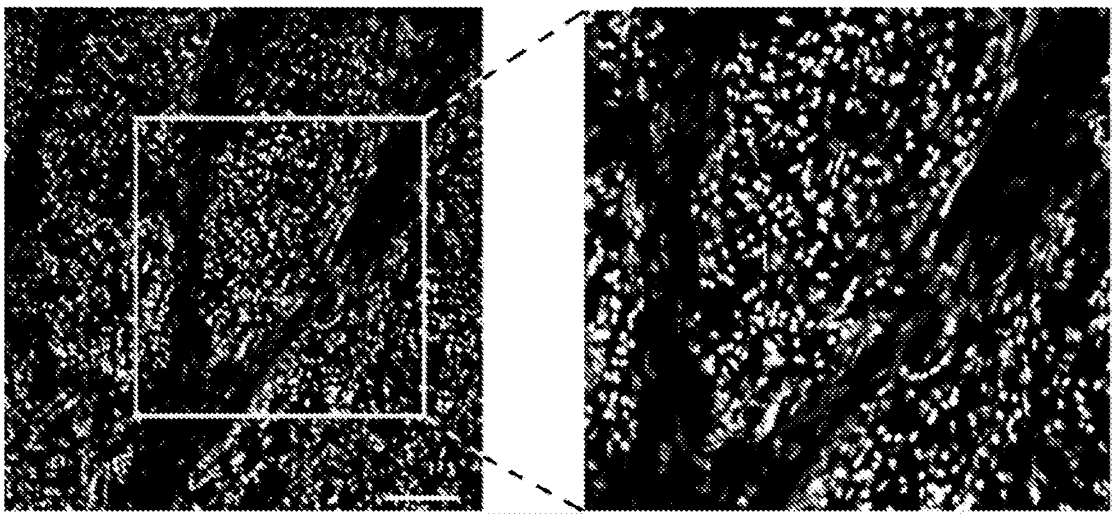

Fig. 8

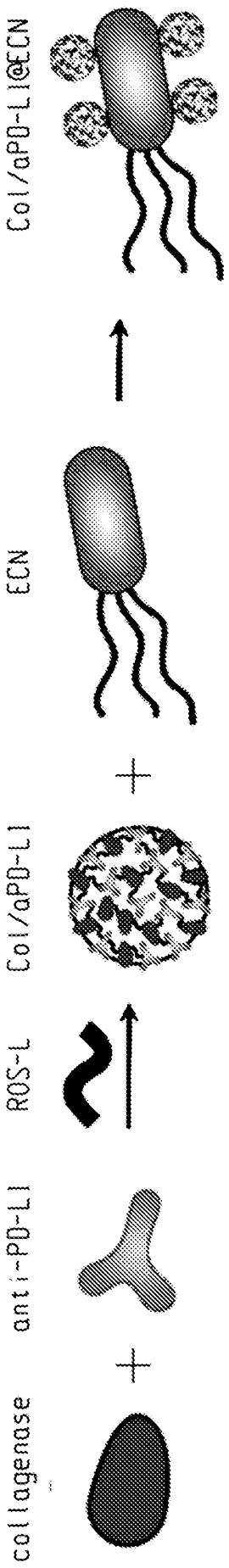

Fig. 9A

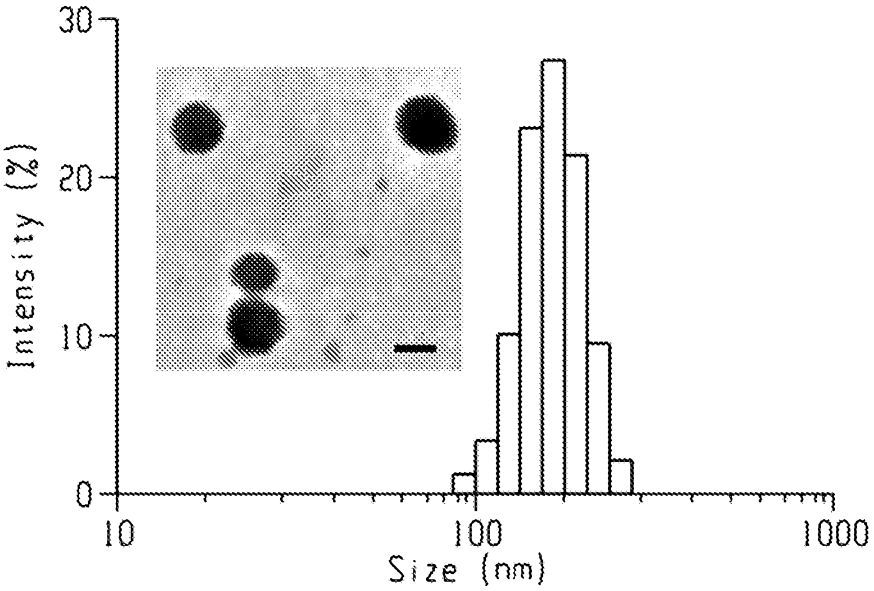

Fig. 9B

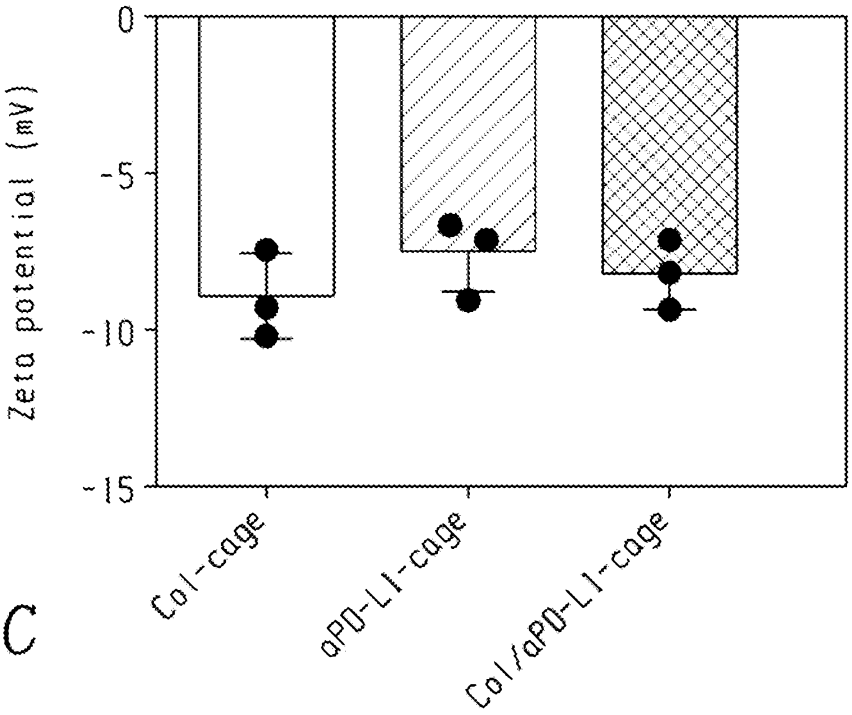

Fig. 9C

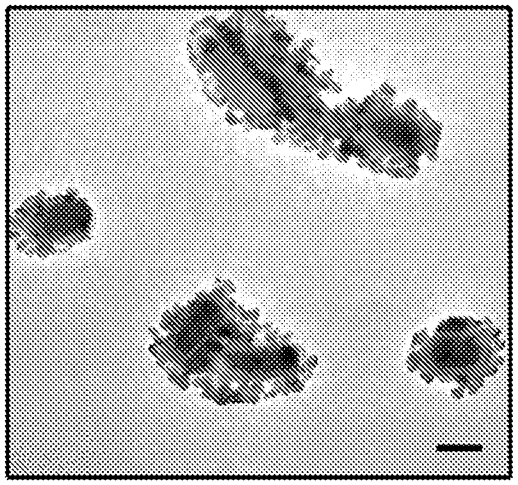

Fig. 9D

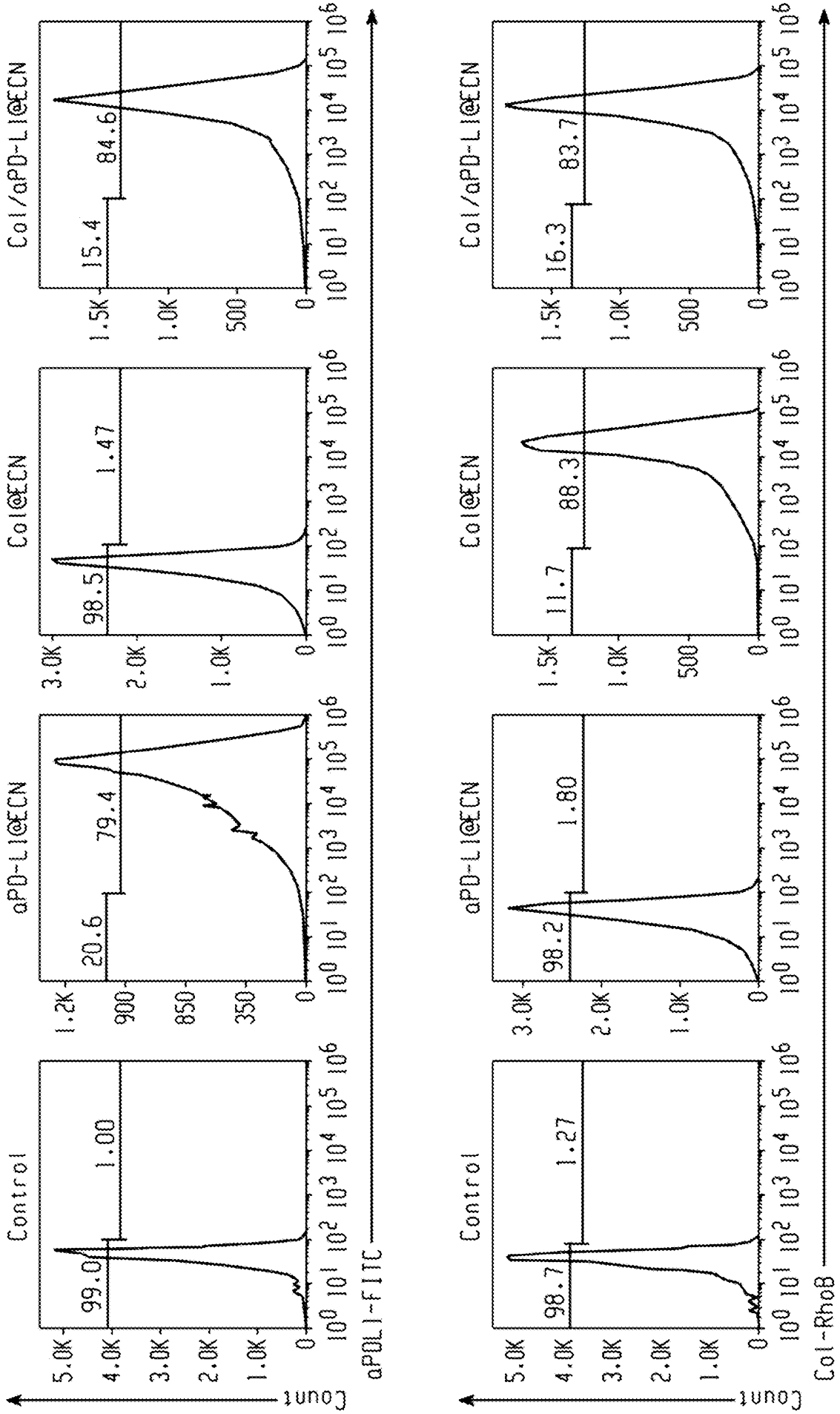
Control
aPD-L1@ECN
Col@ECN
Col/aPD-L1@ECN
Count
aPDL1-FITC
Col-RhoB
99.0
1.00
20.6
79.4
98.5
1.47
15.4
84.6
98.7
1.27
98.2
1.80
11.7
88.3
16.3
83.7

Fig. 9E

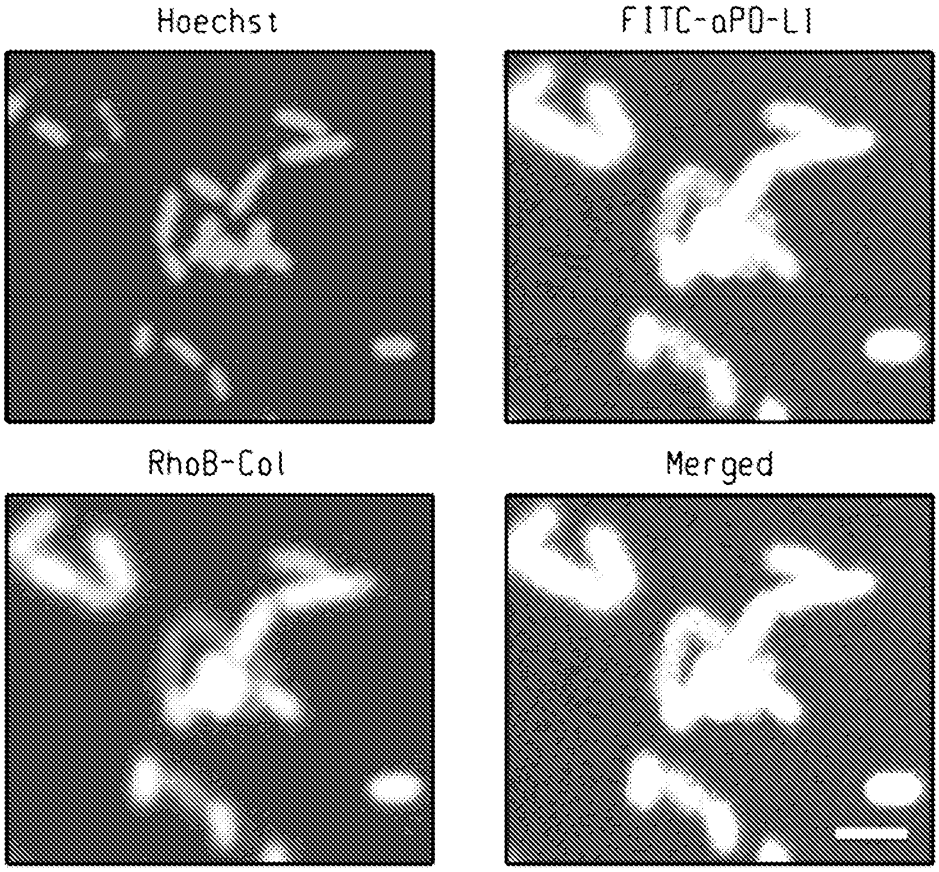
Hoechst
FITC-αPD-L1
RhoB-Col
Merged

Fig. 9F

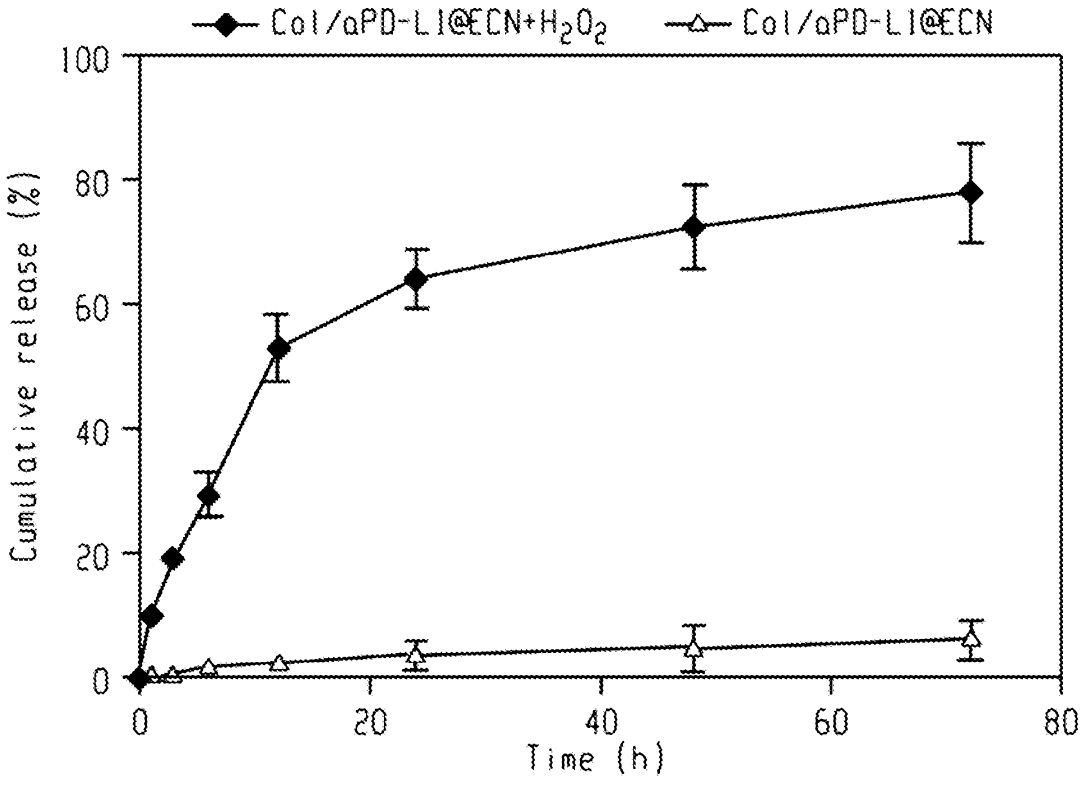
Col/αPD-L1@ECN+H2O2
Col/αPD-L1@ECN
Cumulative release (%)
Time (h)
0
20
40
60
80
100

Fig. 9G

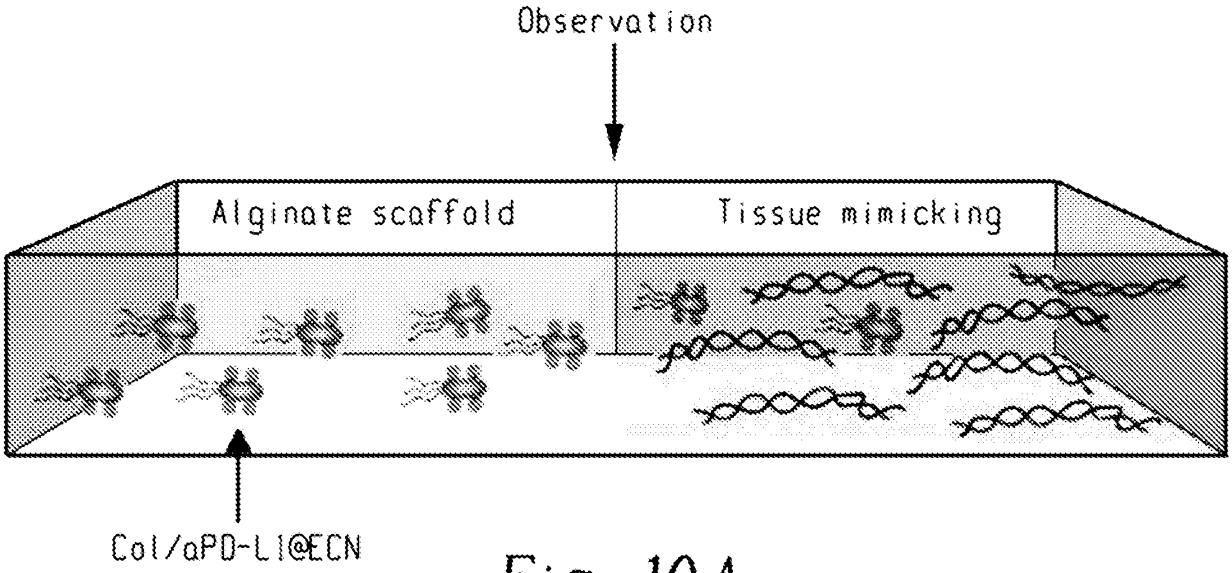

Fig. 10A

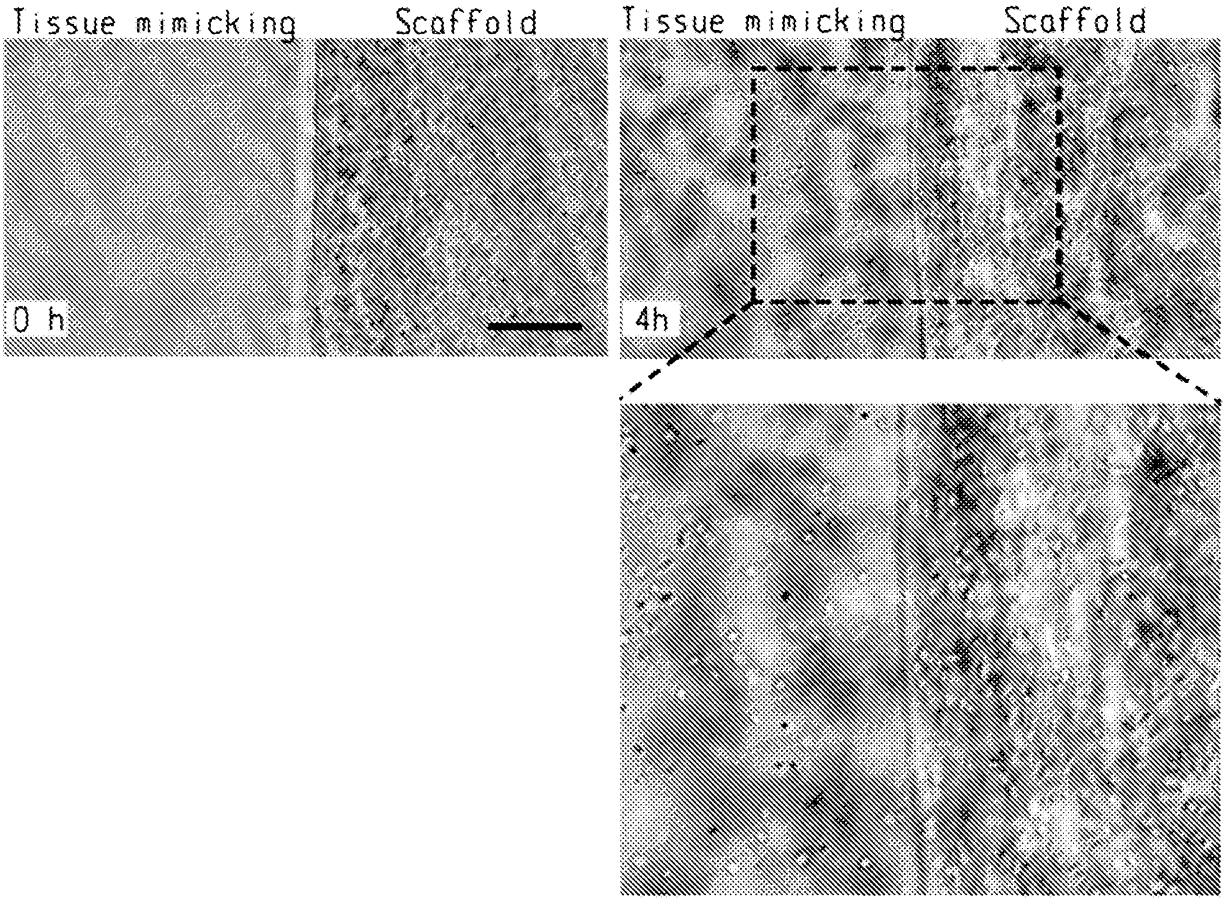

Fig. 10B

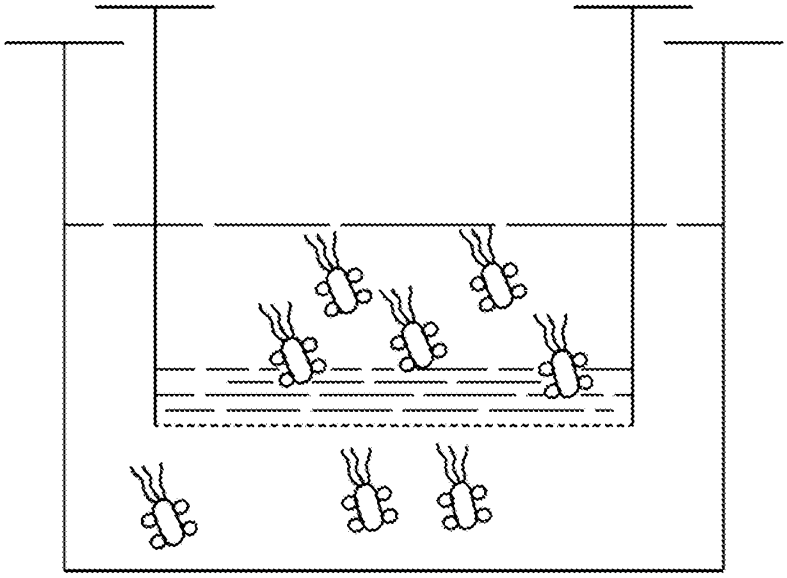

Fig. 10C

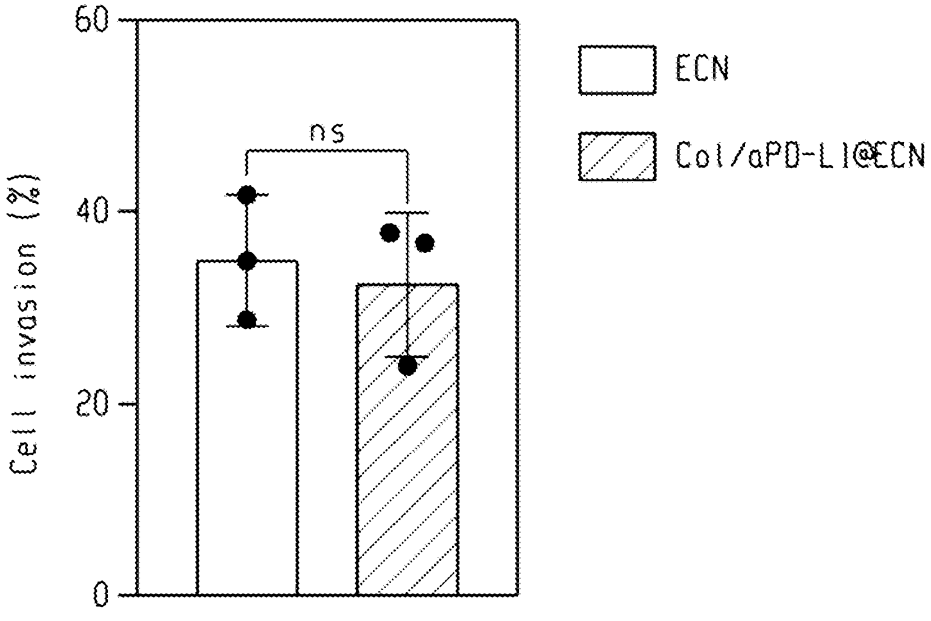

Fig. 10D

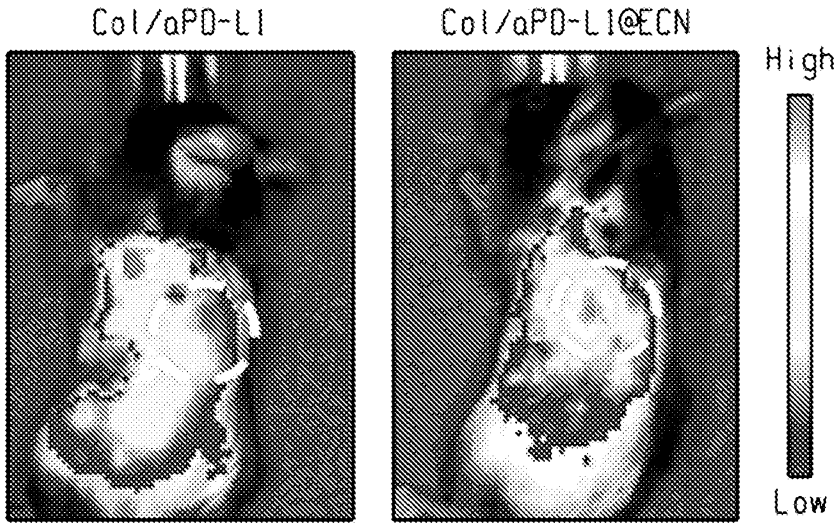

Fig. 10E

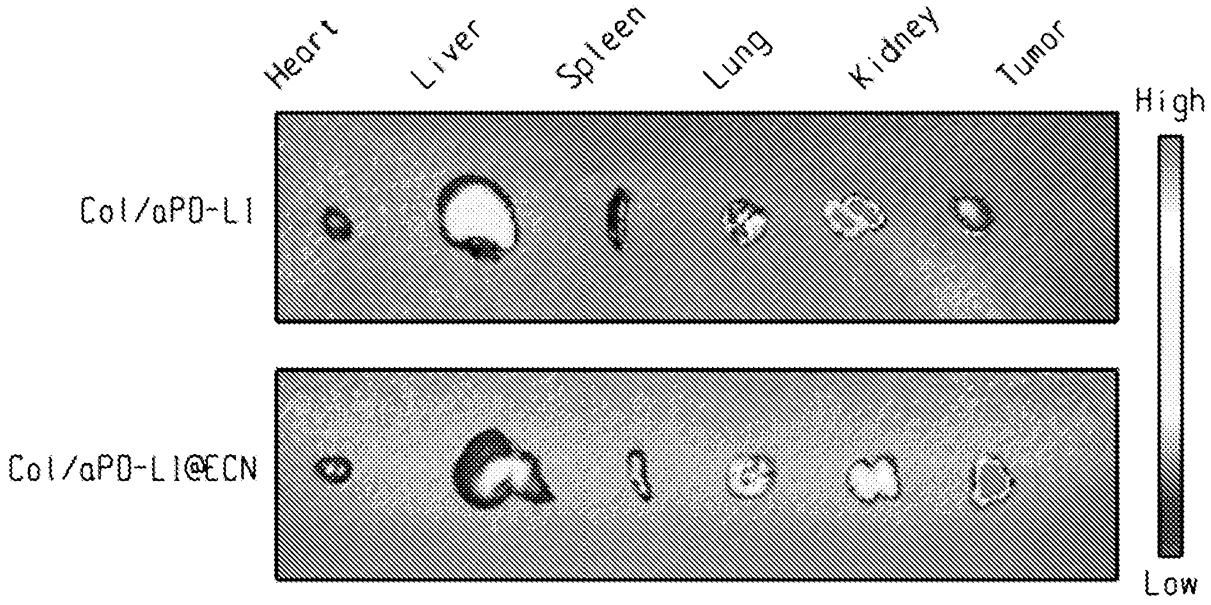

Fig. 10F

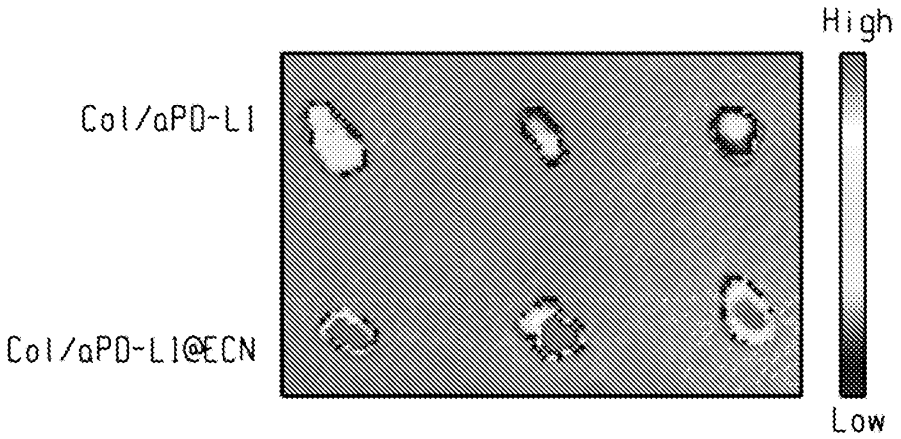

Fig. 10G

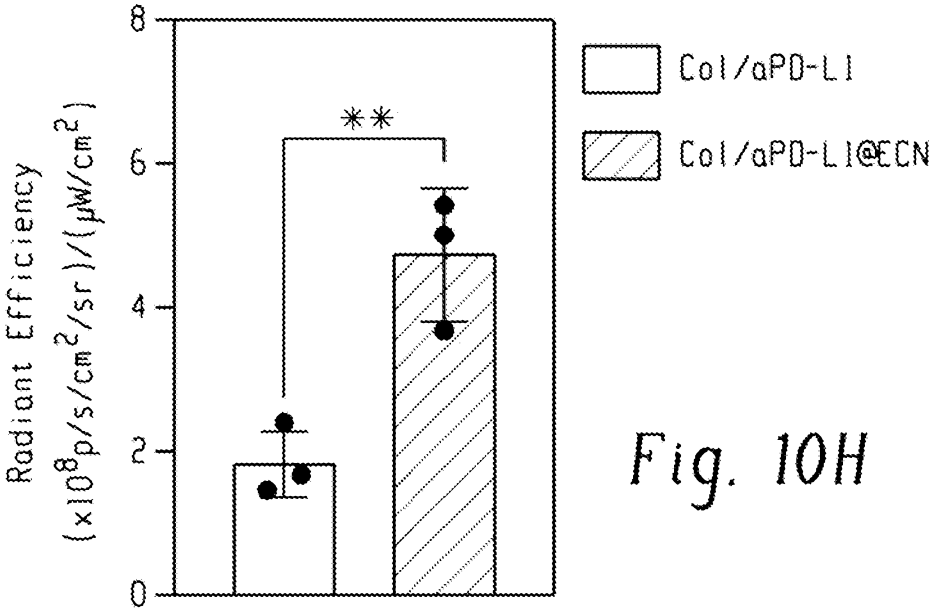

Fig. 10H

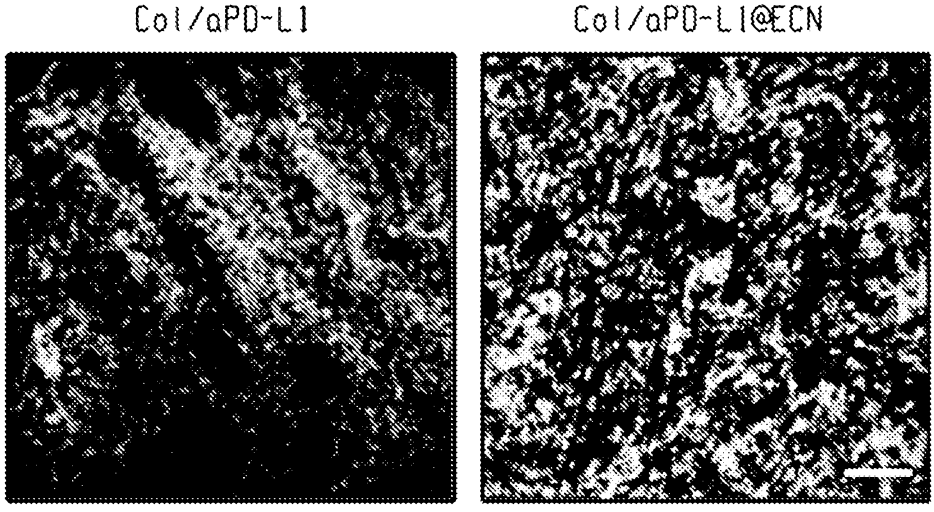

Fig. 10I

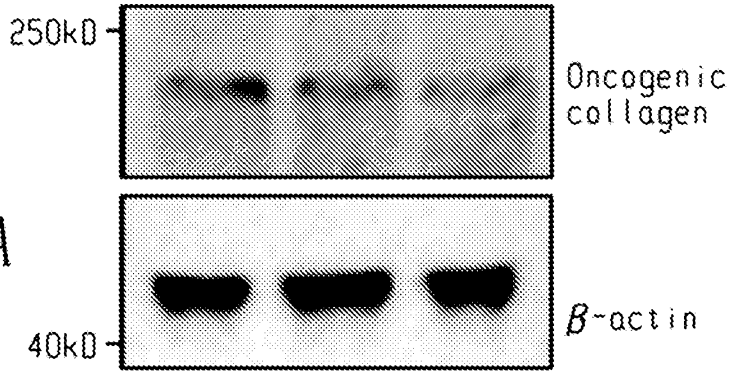

Fig. 11A

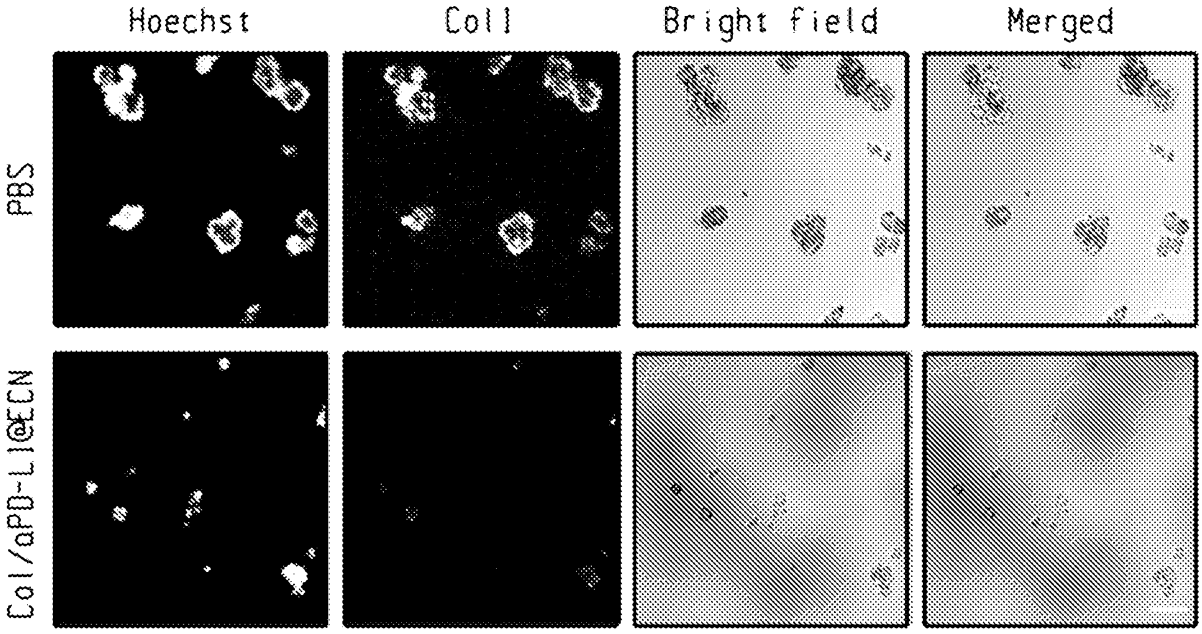

Fig. 11B

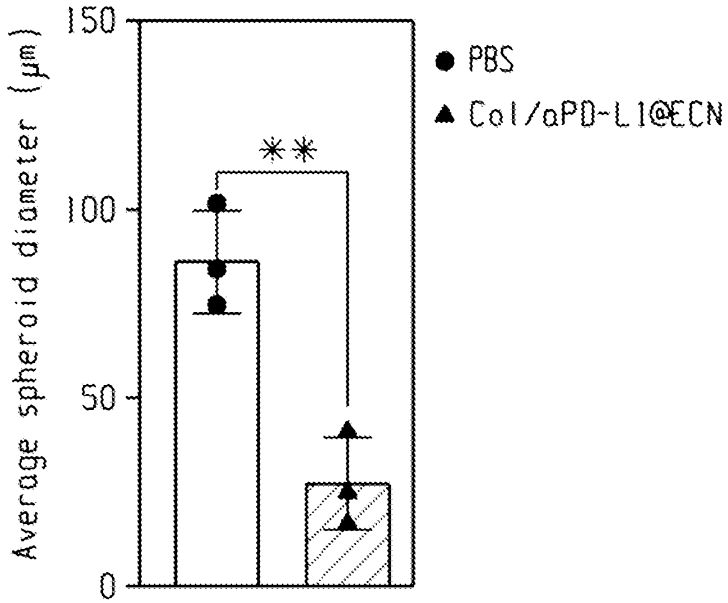

Fig. 11C

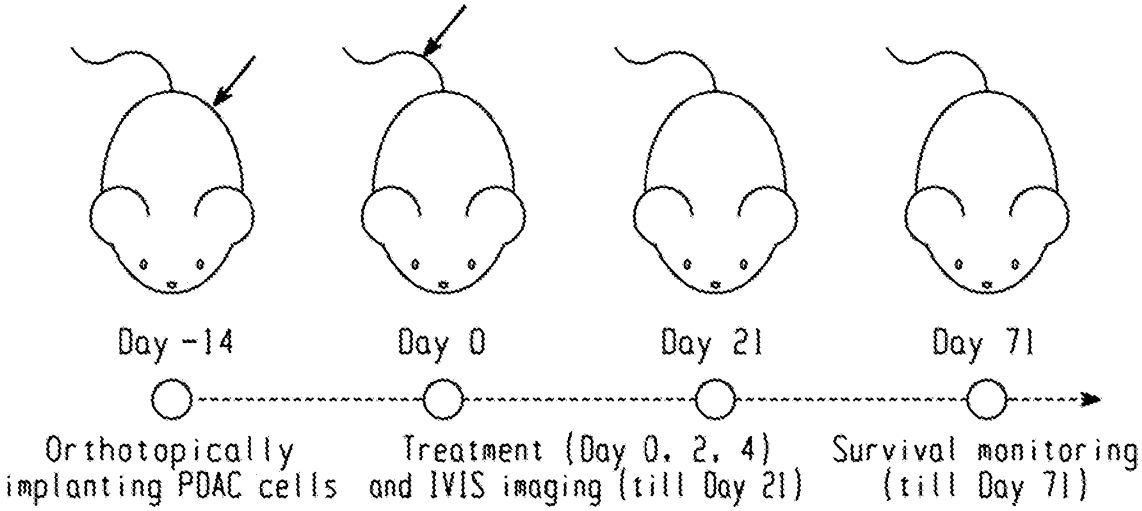

Fig. 11D

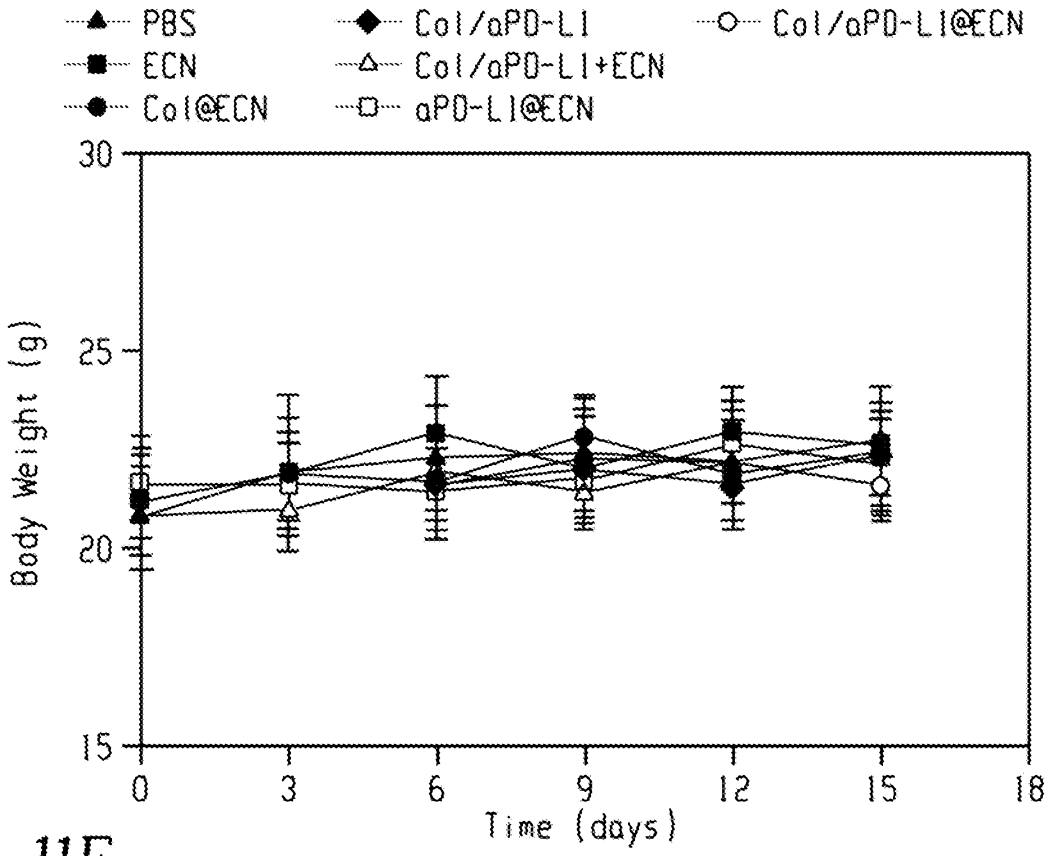

Fig. 11E

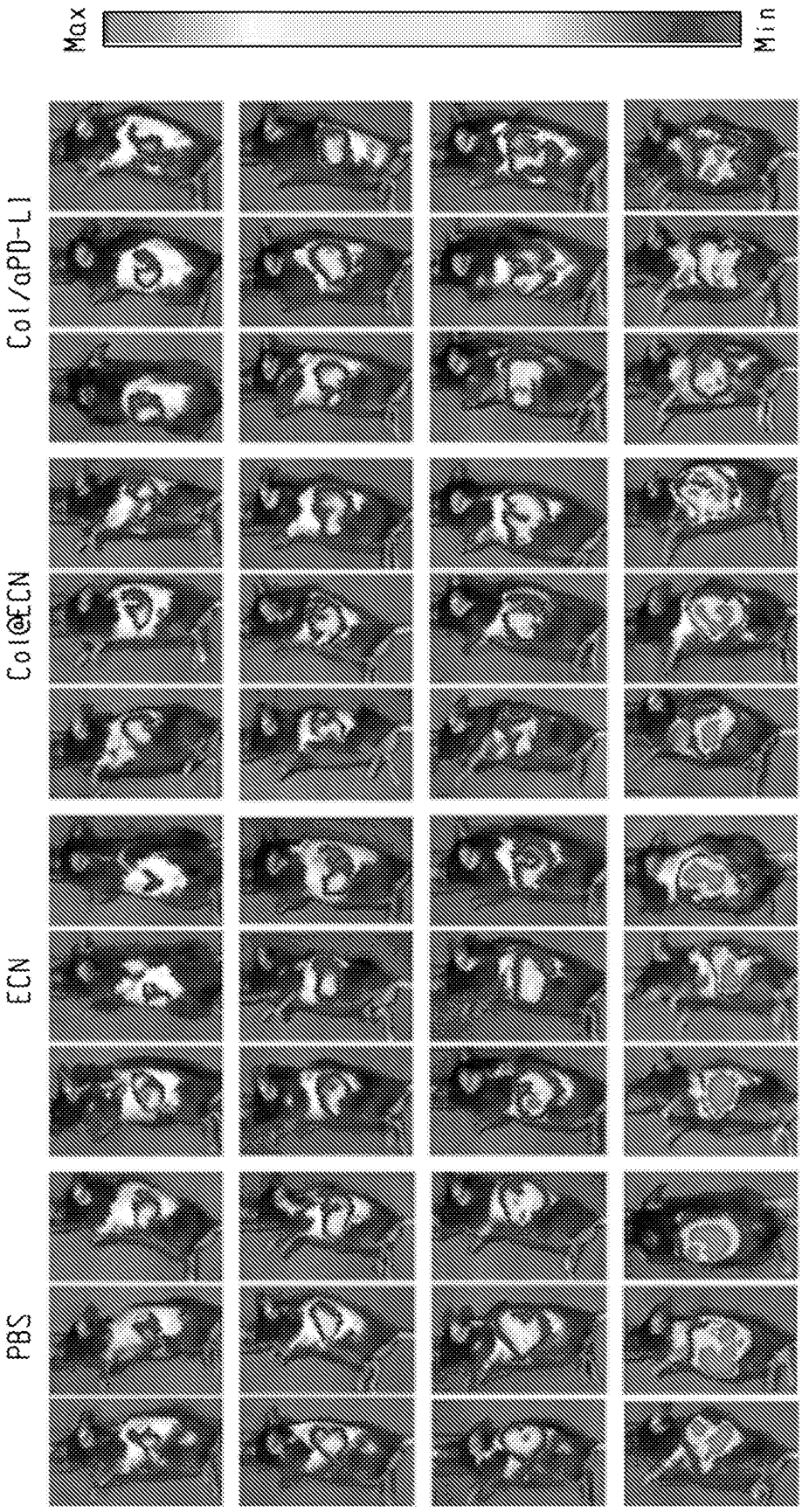

Fig. 11F

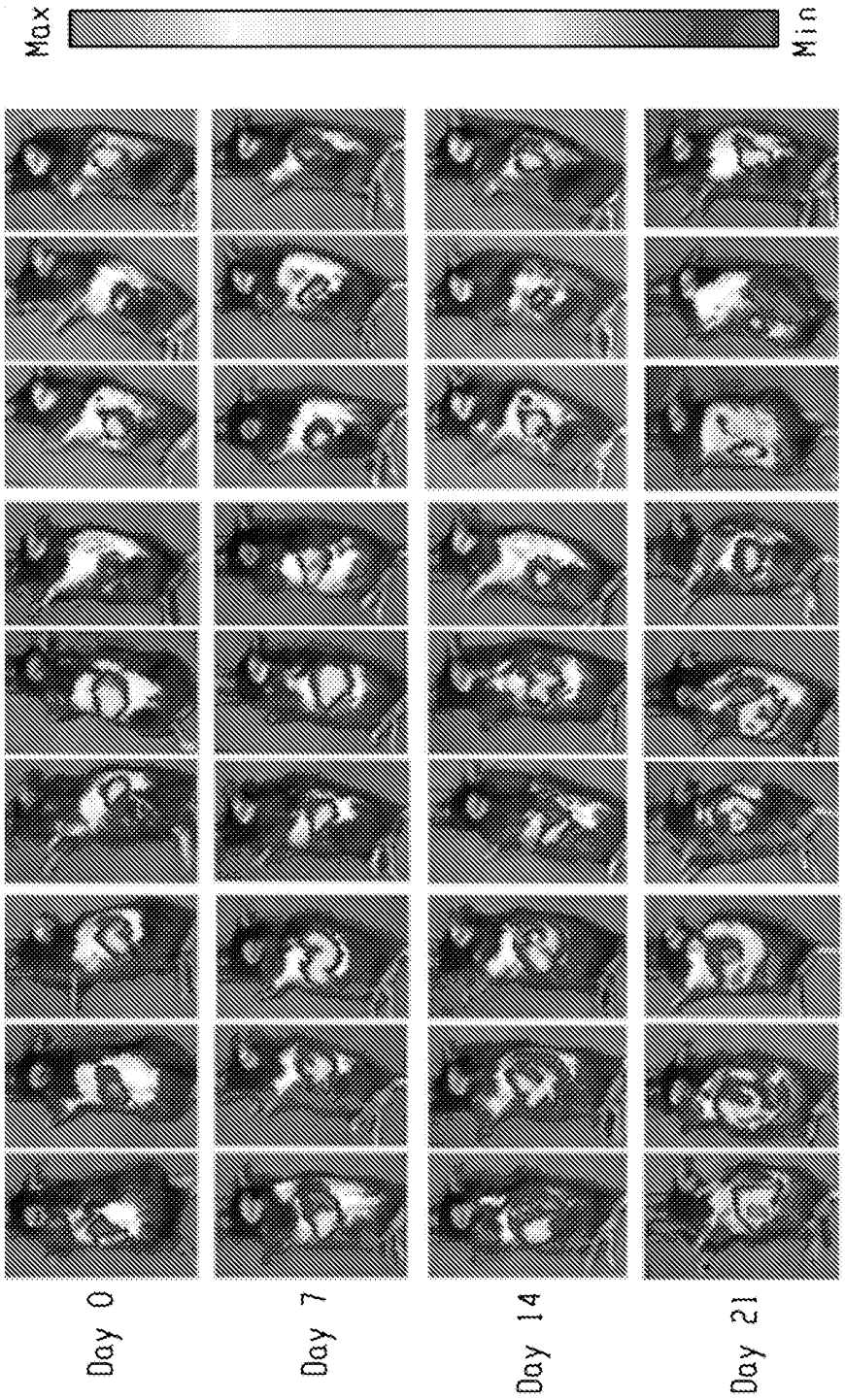

Fig. 11F (cont'd.)

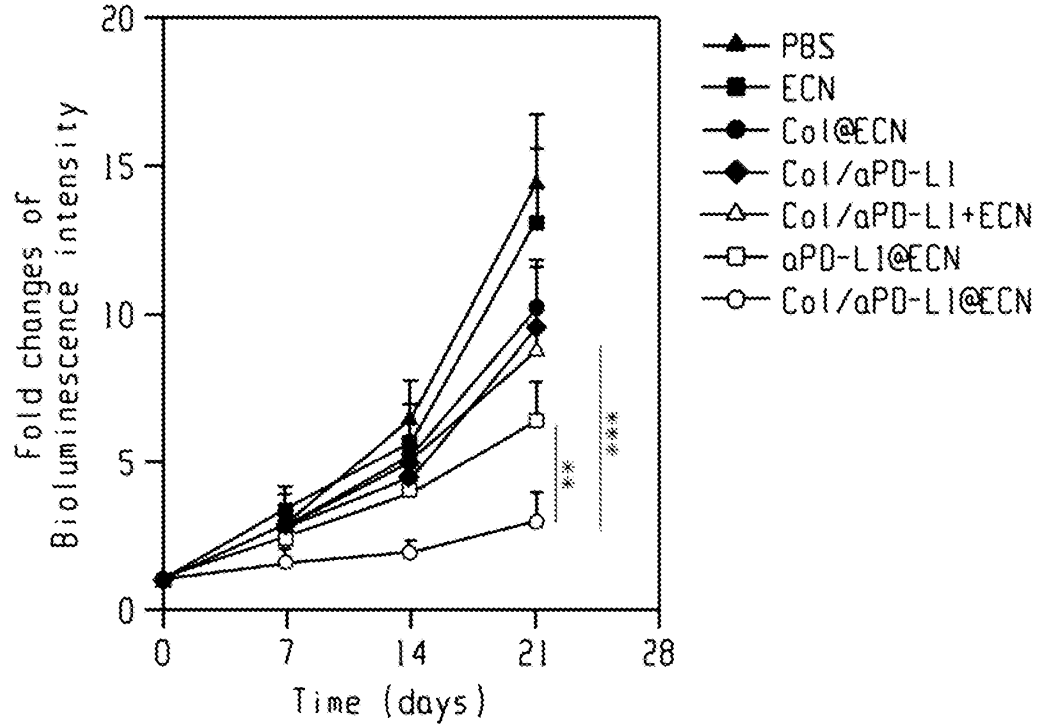

Fig. 11G

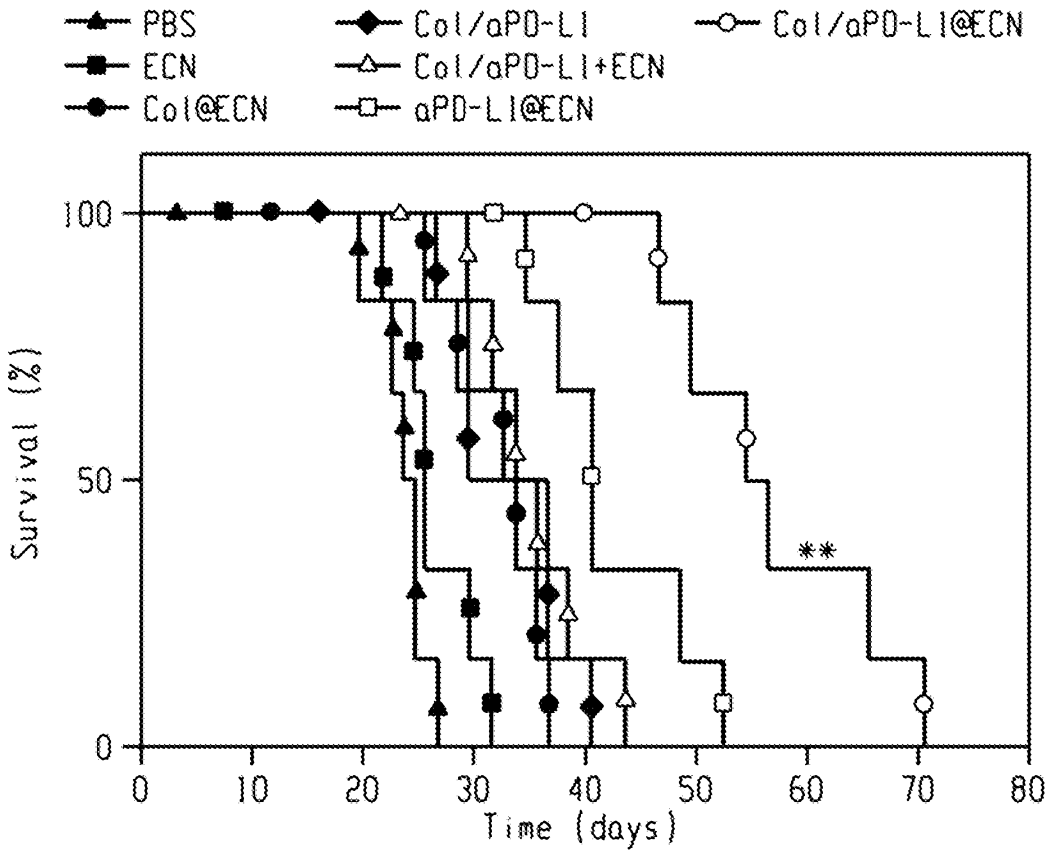

Fig. 11H

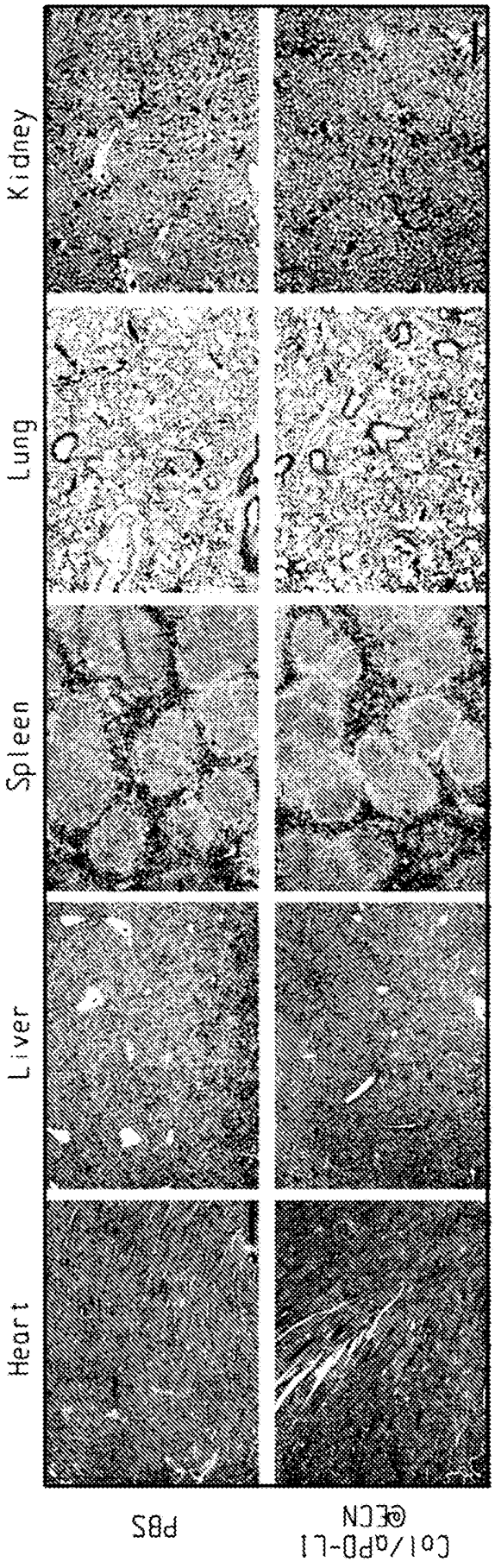

Fig. 12

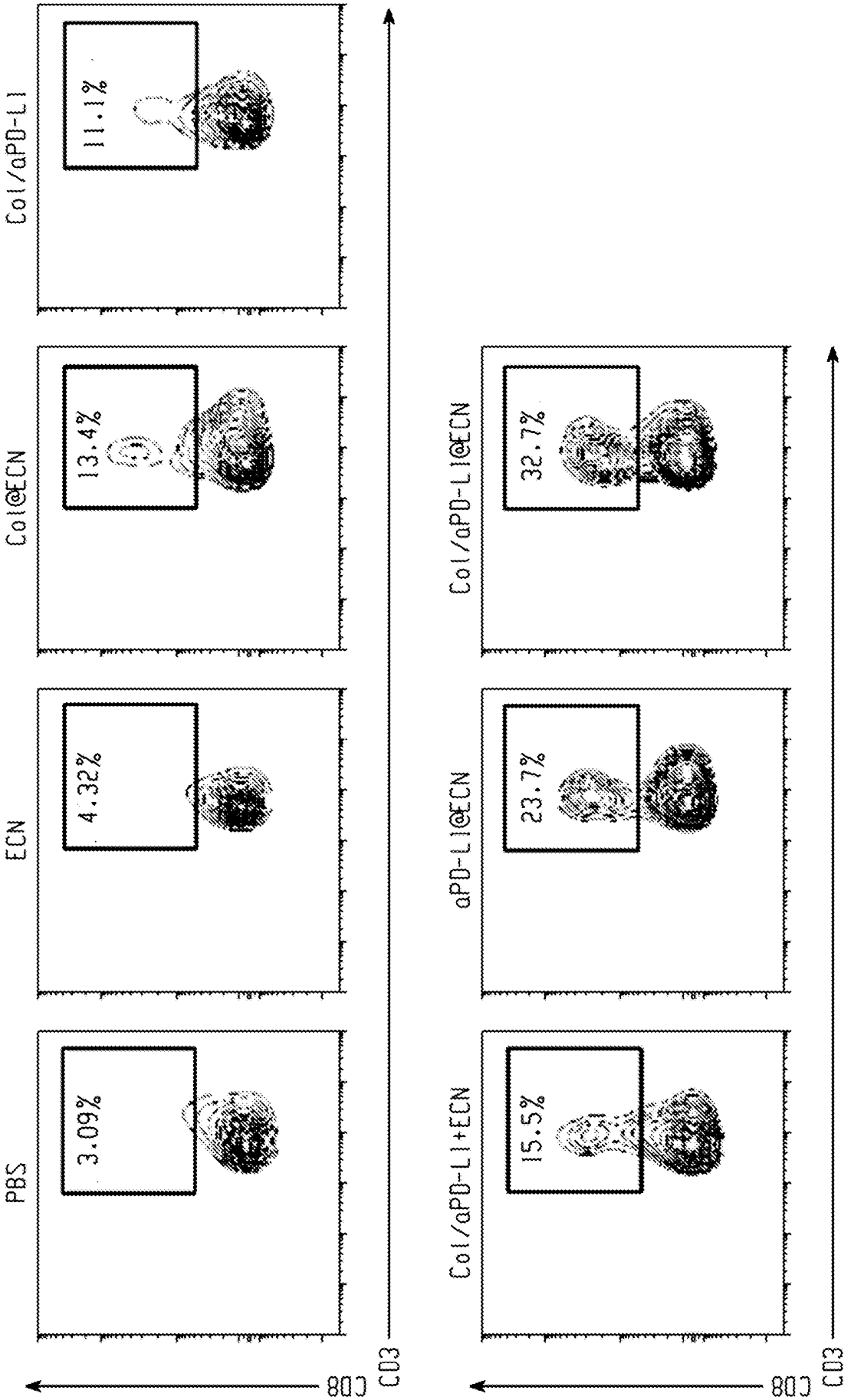
PBS
3.09%
ECN
4.32%
Col@ECN
13.4%
Col/aPD-L1
11.1%
Col/aPD-L1+ECN
15.5%
aPD-L1@ECN
23.7%
Col/aPD-L1@ECN
32.7%
CD8
CD3

Fig. 13A

Fig. 13C

Fig. 13B

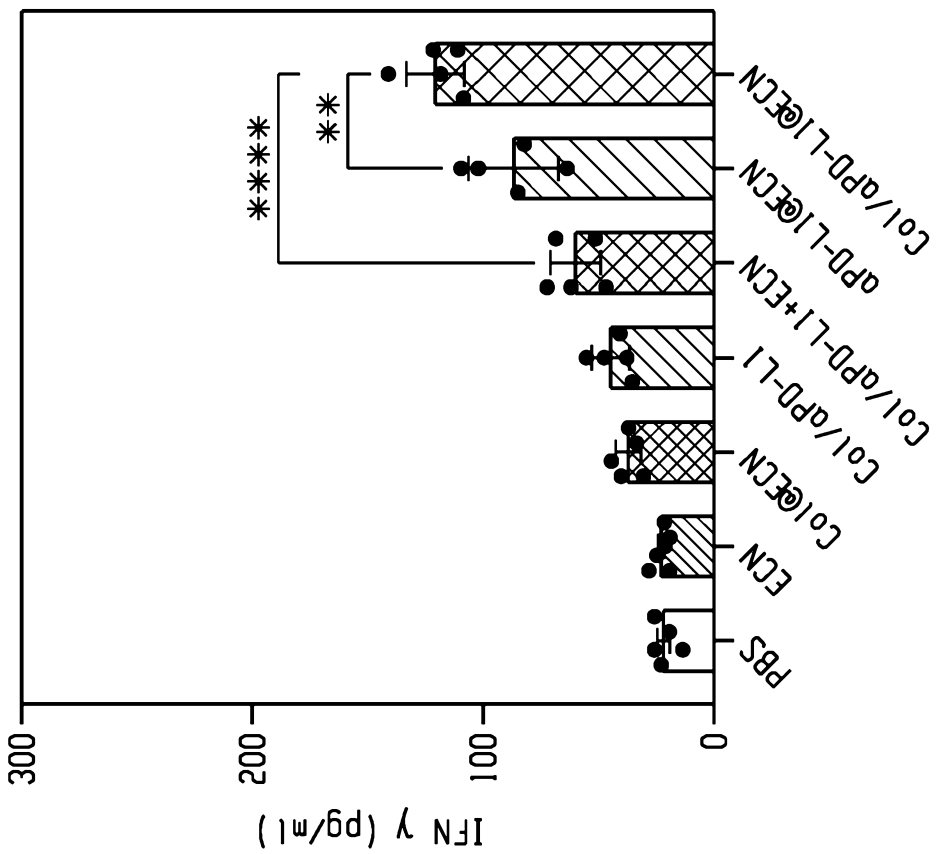

Fig. 13E

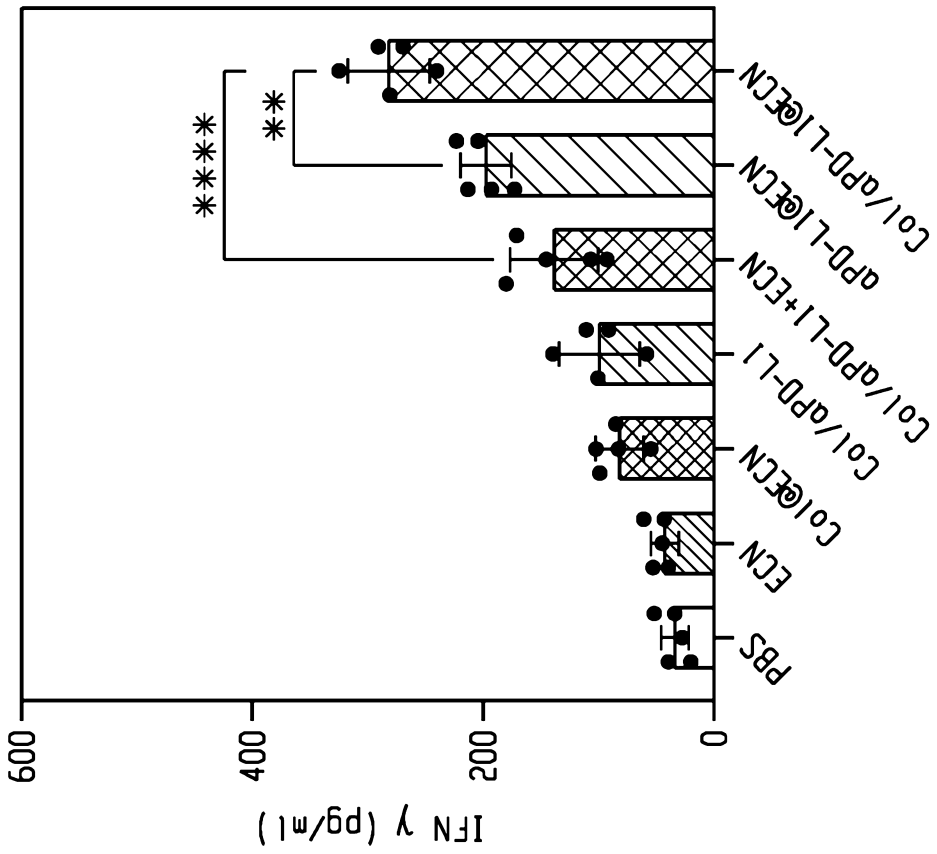

Fig. 13D

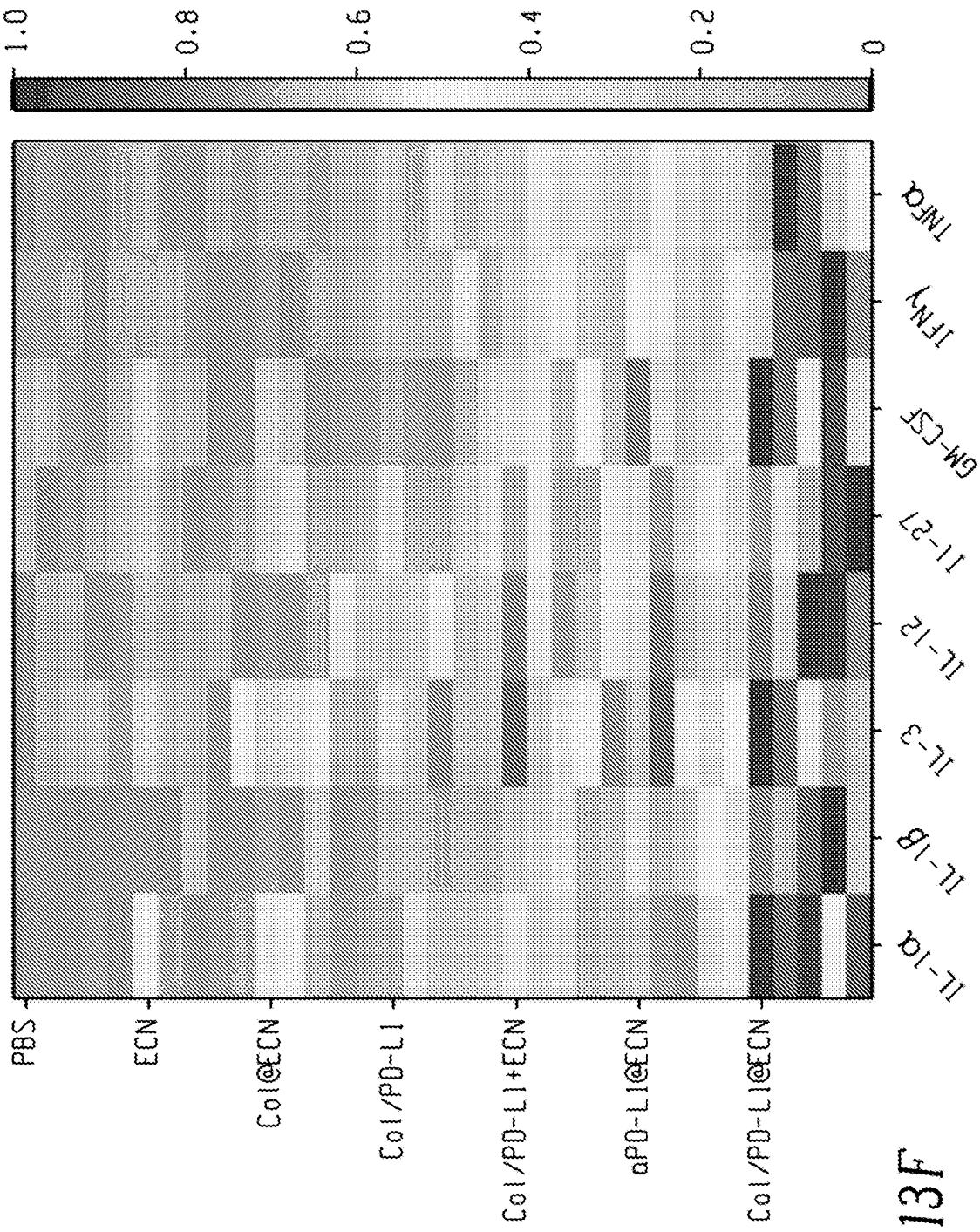
1.0
0.8
0.6
0.4
0.2
0
PBS
ECN
Col@ECN
Col/PD-L1
Col/PD-L1+ECN
aPD-L1@ECN
Col/PD-L1@ECN
IL-1α
IL-1β
IL-3
IL-12
IL-21
GM-CSF
IFNγ
TNFα

Fig. 13F

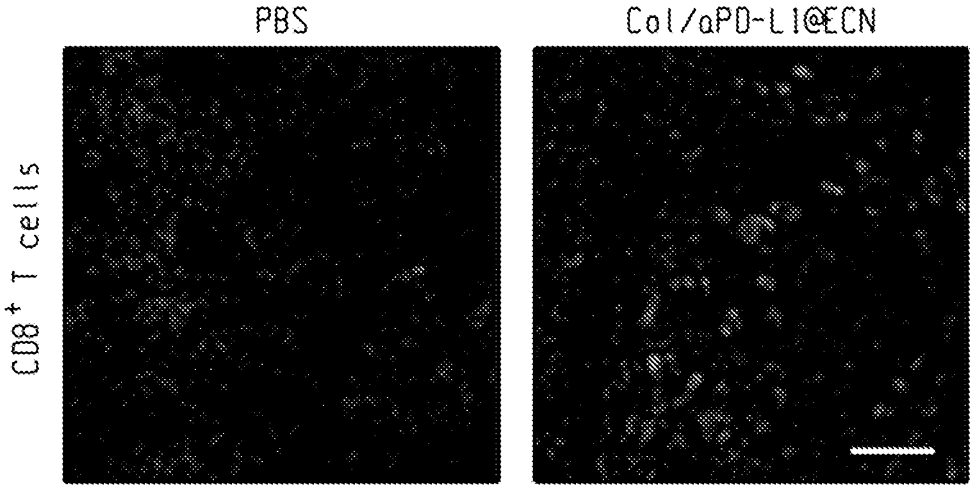

Fig. 13G

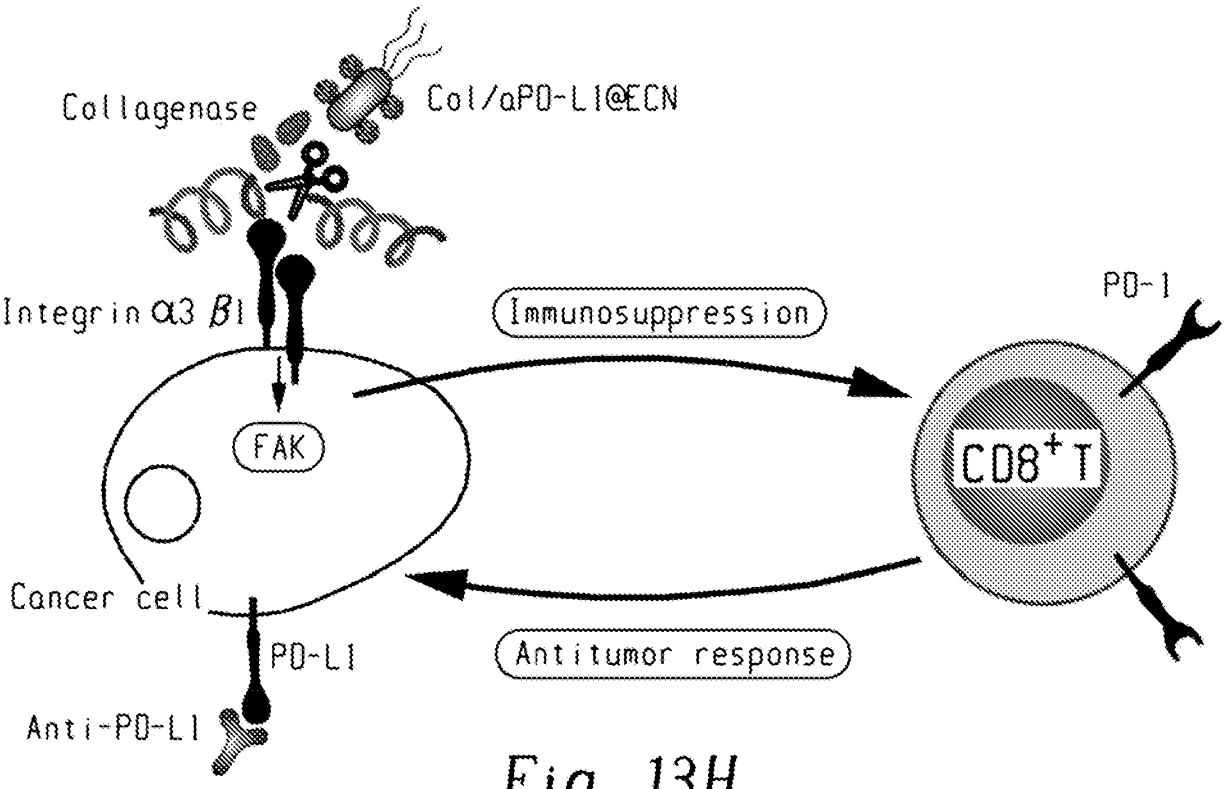

Fig. 13H

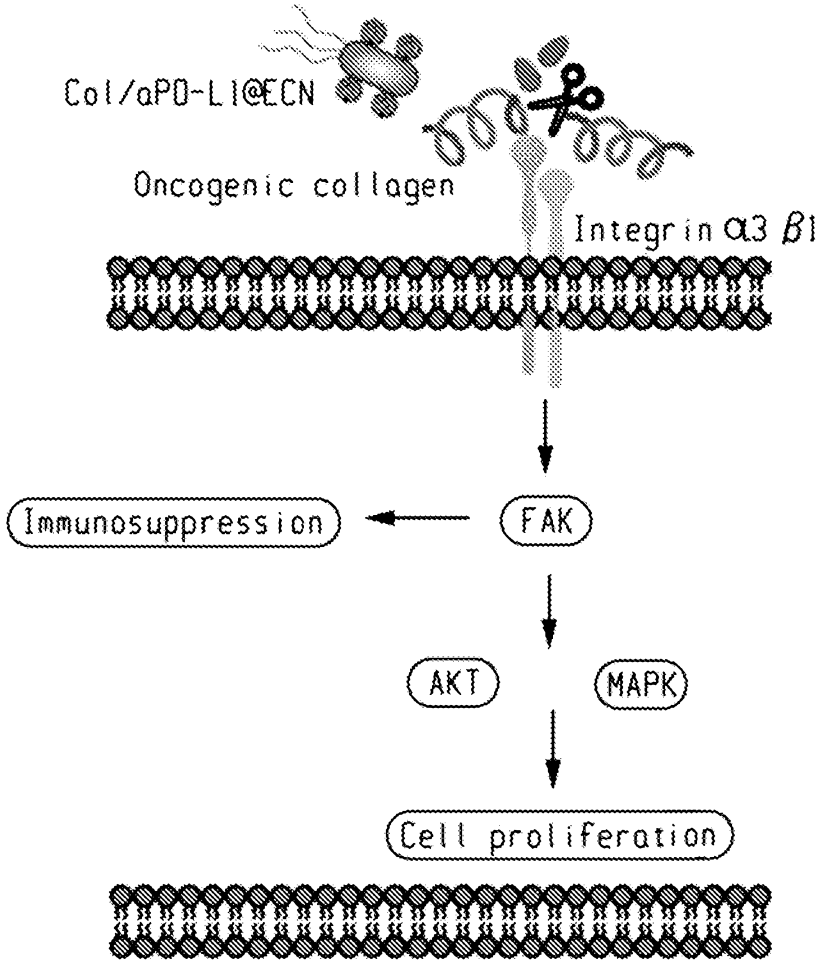

Fig. 14A

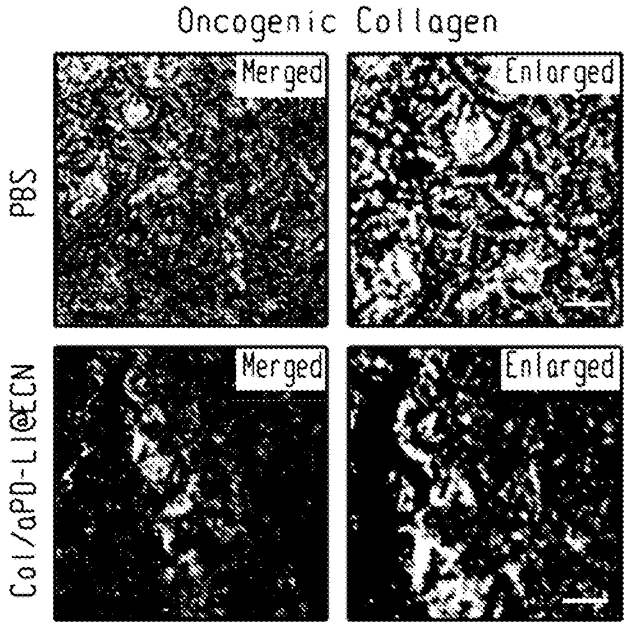

Fig. 14B

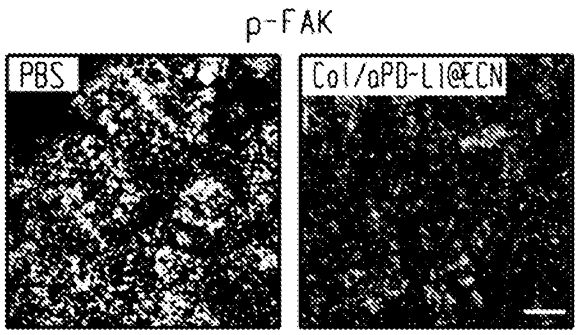

Fig. 14C

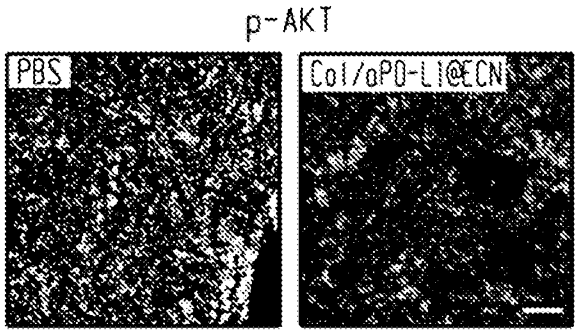

Fig. 14D

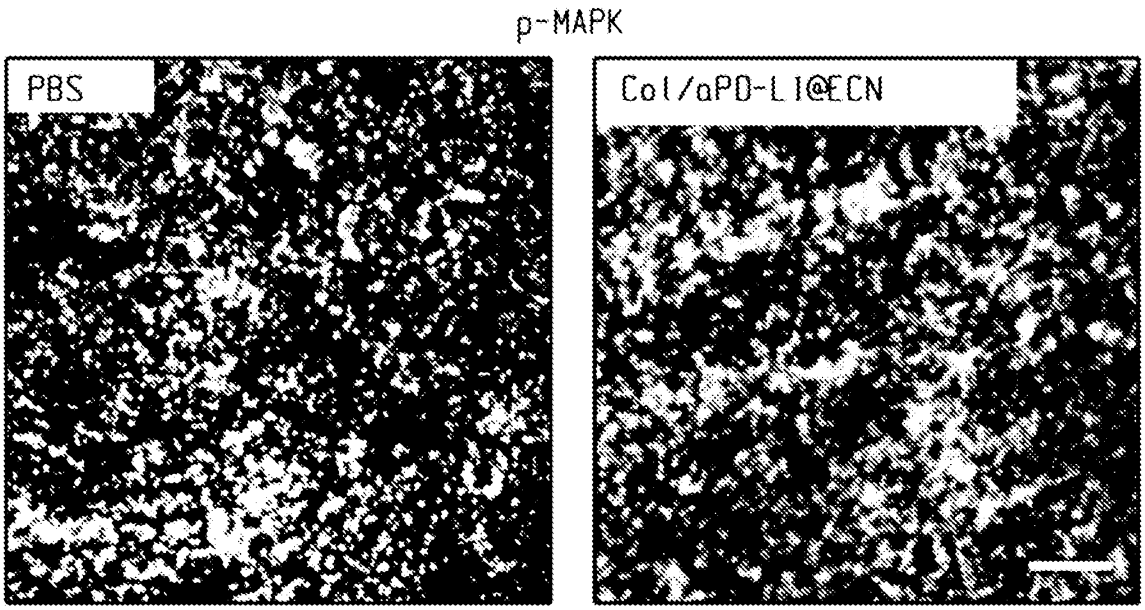

Fig. 14E

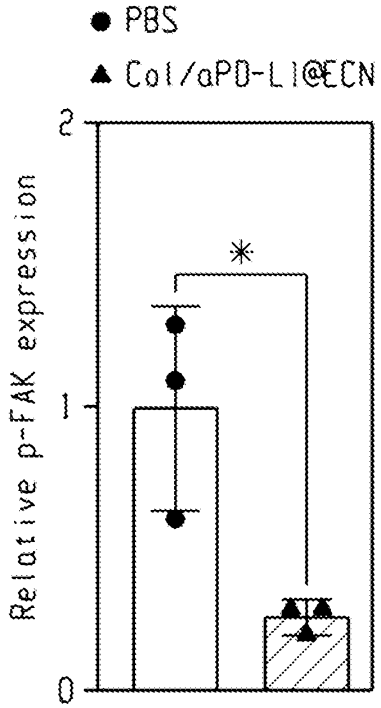

Fig. 14F

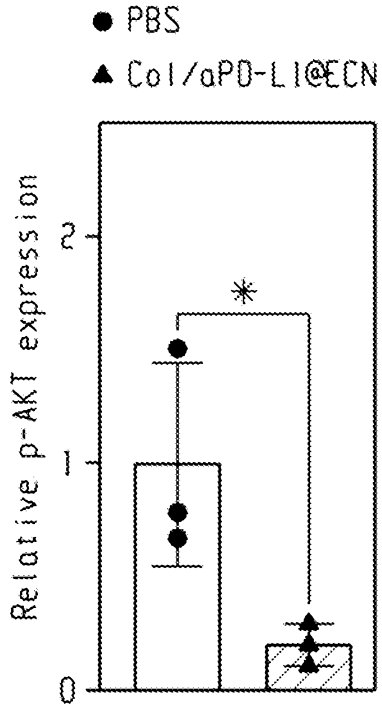

Fig. 14G

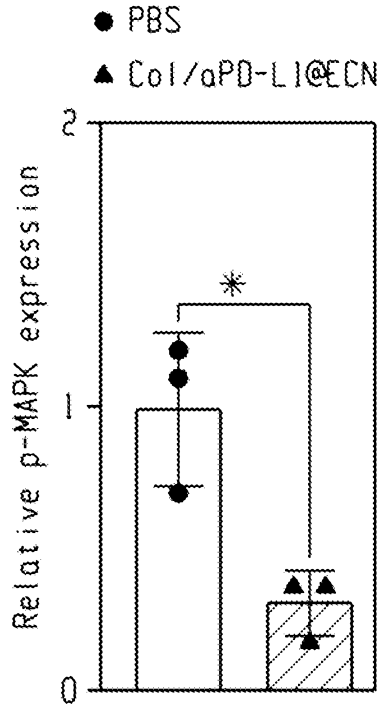

Fig. 14H

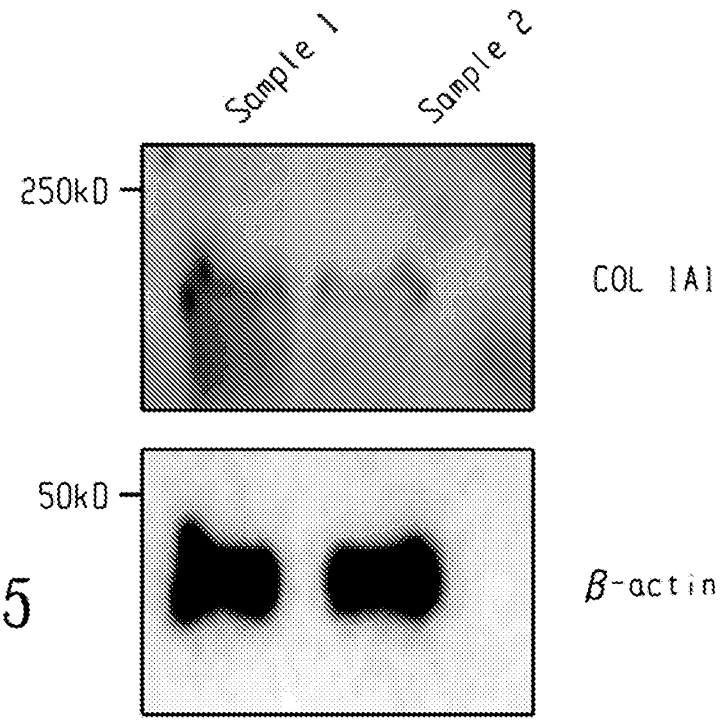

Fig. 15

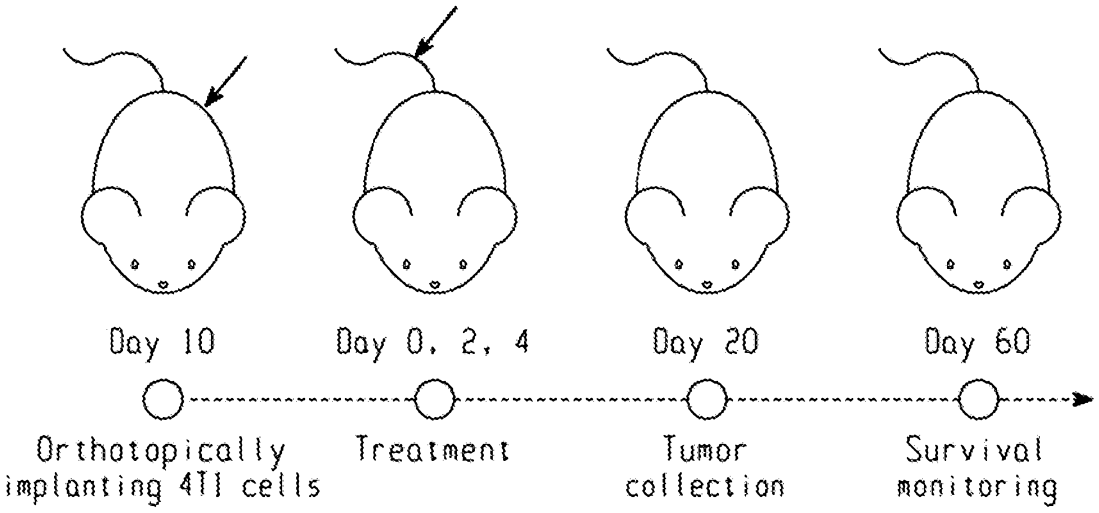

Fig. 16A

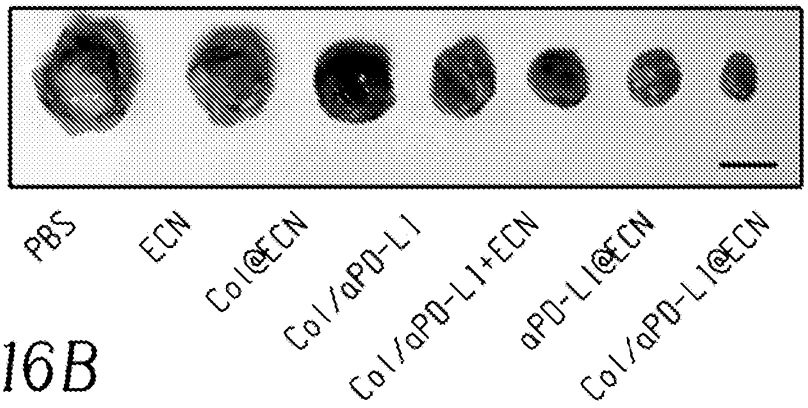

Fig. 16B

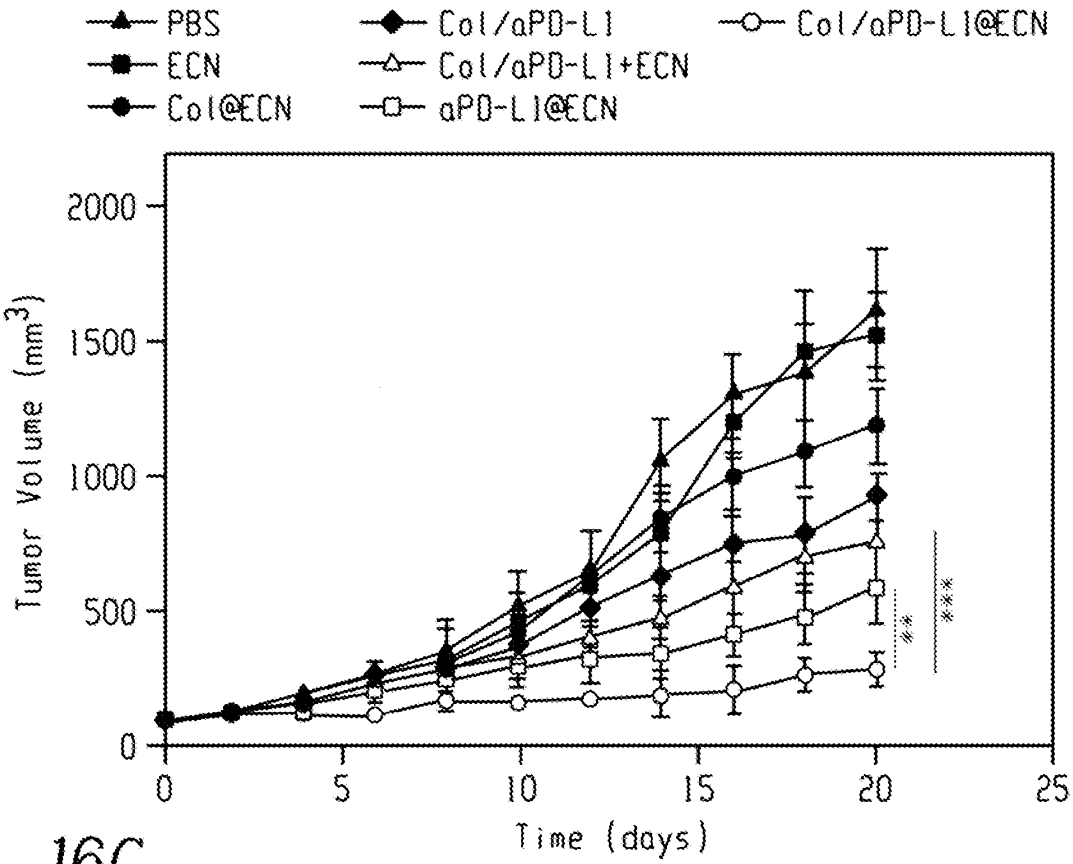

Fig. 16C

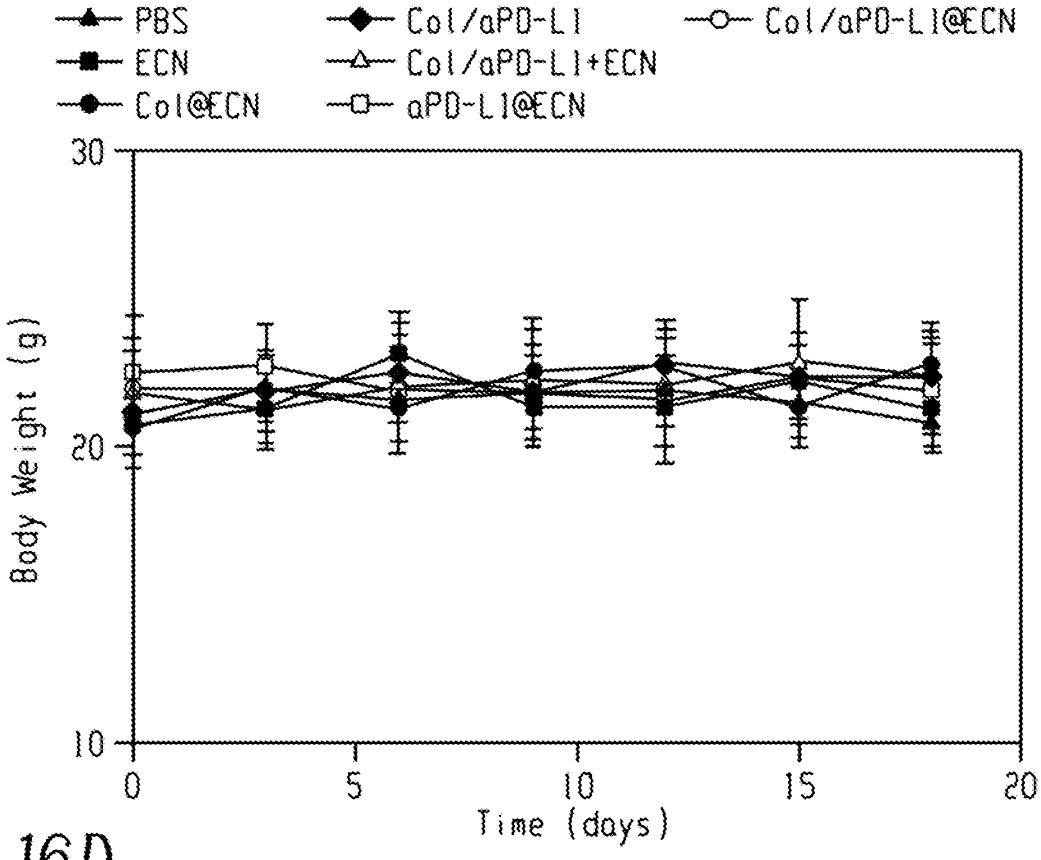

Fig. 16D

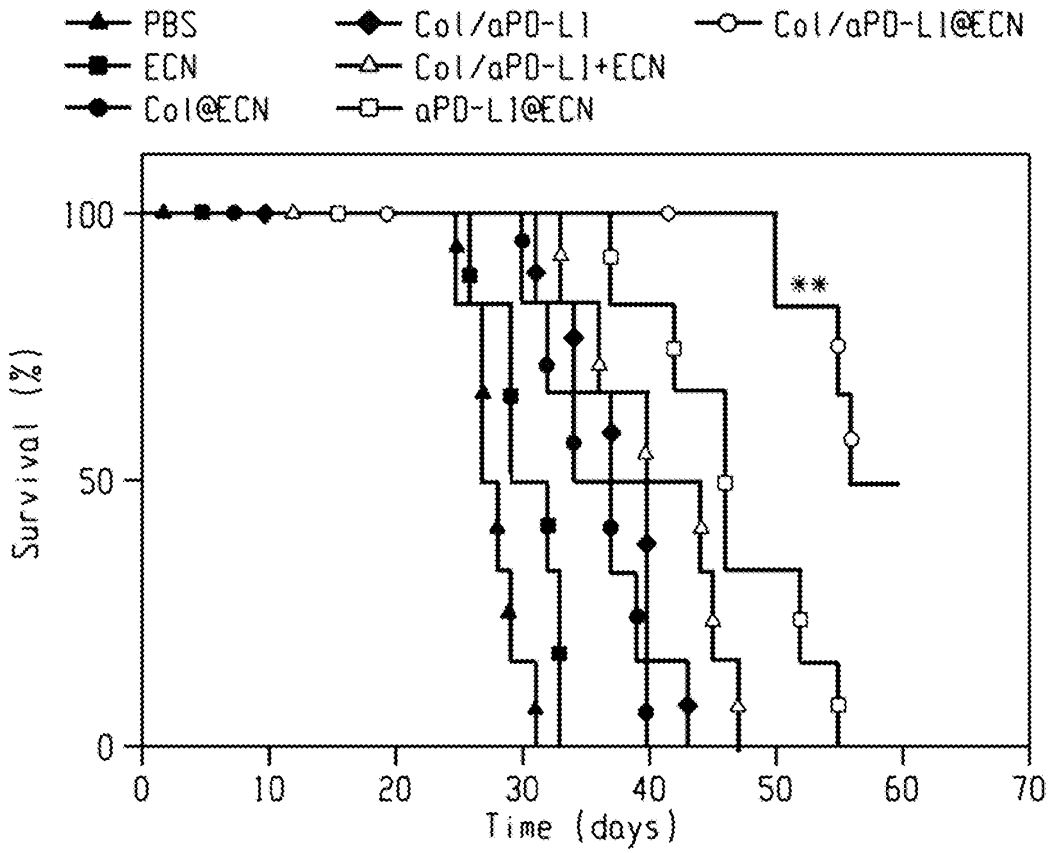

Fig. 16E

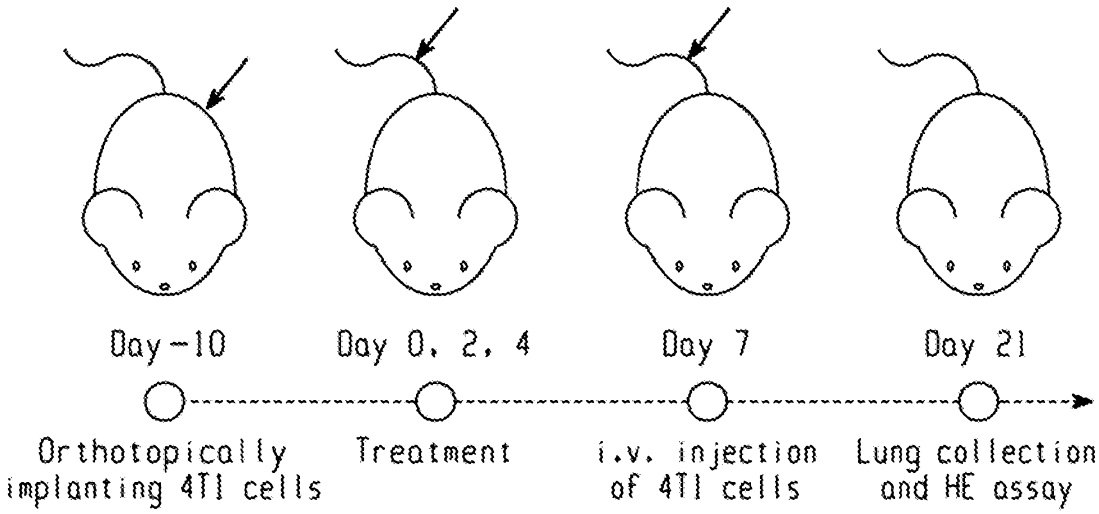

Fig. 16F

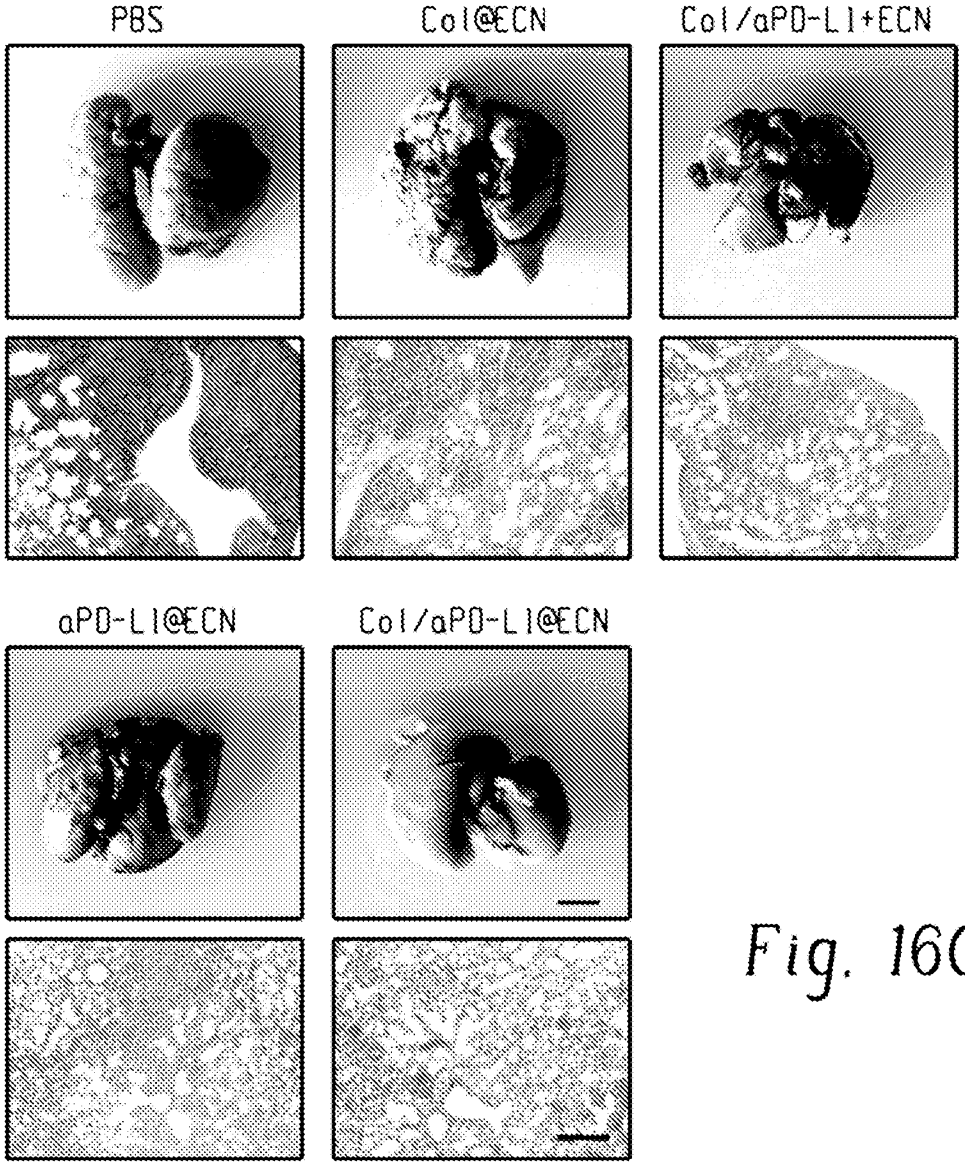

Fig. 16G

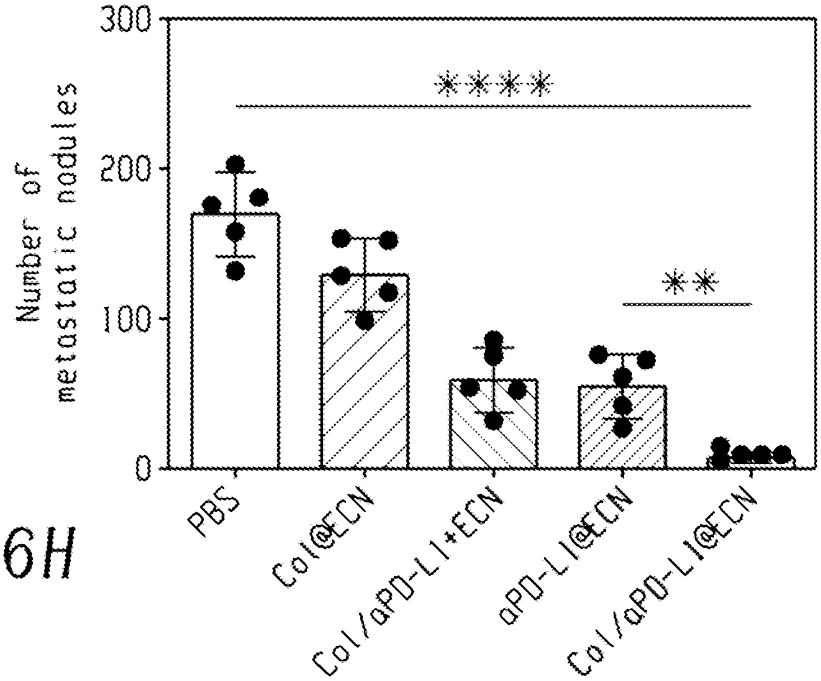

Fig. 16H